Syntheses of High Performance Bio-based Polybenzimidazoles and their Electrical Applications

Aniruddha Nag

Japan Advanced Institute of Science and Technology

Doctoral Dissertation

Syntheses of High Performance Bio-based Polybenzimidazoles and their Electrical Applications

Aniruddha Nag

Supervisor: Professor Tatsuo Kaneko

Graduate School of Advanced Science and Technology

Japan Advanced Institute of Science and Technology

Materials Science

June 2019

Preface

The present dissertation is submitted for the degree of Doctor of Philosophy at Graduate School of Advanced Science and Technology, Japan Advanced Institute of Science and Technology (JAIST). The dissertation is consolidation of results of the research work on the topic entitled, "Syntheses of High Performance Bio-based Polybenzimidazoles and their Electrical Applications" under the supervision of Prof. Tatsuo Kaneko during July 2016-June 2019 at Energy and Environment area, JAIST.

Renewable resources can provide a sustainable platform to substitute petroleum-based polymers through the design of bio-based polymers with a positive environmental impact. However, conventional bio-based plastics are usually low performance plastics in terms of thermo-mechanical properties. Here we have successfully synthesized aromatic back-bone based bio-plastics consist of high thermo-mechanical properties comparable with engineering plastics. Polybenzimidazoles (PBIs) are a series of super high performance polymers attracting researchers' attention because they consists of rigid structure of aromatic and hetero rings in their backbone to induce a good stability. Also, PBIs have active imidazole hydrogen (-NH) to receive chemical modification. The author's focus is mainly synthesizing high-performance bio-based polymers along with their various applications depending on their structure property relationships.

The work presented here covers synthesis and characterization of high-performance bio-based polybenzimidazoles and their structural modifications towards electrical applications such as; Polymer dielectrics, solid polymer electrolyte for Li-ion battery. To the best of my knowledge, the work is original and no part of this thesis is plagiarized.

Energy and Environment Area Aniruddha Nag

Graduate School of Advanced Science and Technology

Japan Advanced Institute of Science and Technology

Syntheses of High Performance Bio-based Polybenzimidazoles and their Electrical Applications

Abstract

Due to limitation of petroleum-based resources, bio-based materials are important to establish sustainable society. Research in this thesis described the syntheses of high-performance polybenzimidazoles using biomass and various applications depending on their structure-property relationships.

In chapter 2, various monomer syntheses were described such as; 3-amino-4-hydroxybenzoic acid (3, 4-AHBA) using *Streptomyces sp.* and also 3, 4-diaminobenzoic acid (3, 4-DABA) was prepared using chemical conversion of aromatic hydroxyl into aromatic amine starting from 3, 4-AHBA. Each step was optimized and detailed synthetic procedures were described along with their ^{1}H and ^{13}C-NMR characterizations. Another monomer *p*-aminobenzoic acid (PABA) was also introduced which can be derived using biomass. Furthermore, in this chapter we have described homopolymer preparations of poly(2, 5-benzoxazole) (PBI) using 3, 4-AHBA and poly(2, 5-benzimidazole) (PBO) using 3, 4-DABA. Those structures were characterized using FT-IR and solid-state NMR analysis. Thermal stability of the aforesaid polymers were found with 10% weight-loss temperatures (T_{d10}) of 622 °C and 700 °C for PBO and PBI respectively, which are enough high comparable with super-engineering plastics and even higher than few of the metals. Mechanical analysis was also performed and tensile strength of PBI and PBO copolymers were found to be 75 MPa and 53 MPa with Young's modulus values of 3.6 and 2.8 GPa respectively.

In chapter 3, author focused on various copolymer syntheses using bio-based monomers. Both PBI and PBO homopolymers are very reluctant to get soluble in any of the conventional solvents due to their rigid ring structures, thus flexible chain was introduced with PBI moiety using PABA homopolymer to prepare PBI-*co*-PA (PBI-*co*-PA). PBO homopolymer was found to have high thermo-mechanical stability and superior insulating properties (low dielectric constant, high resistivity etc.) comparable with commercial dielectric materials. On the contrary, PBI homopolymer was already established with ultra-high thermal stability but consisting of conducting imidazole proton. After considering, another series of novel copolymer PBO-*co*-PBIs were made to control balance between thermo-mechanical stability and insulating properties. PBI-*co*-PA with very low amount of PA incorporation showed highest thermal stability (T_{d10}= 743°C) among all the existing polymers in the world so far, and they can be used to prepare hybrid materials with metals at a temperature over the melting temperatures of the metals. Another copolymer PBO-*co*-PBI shows dielectric constant very low (ε_r=2.0) when consist of higher PBO content and the values are comparable with commercial ultra-low *k* materials such as; PE or PP.

In chapter 4, research focus was shifted towards structure modification of the prepared bio-based polybenzimidazoles for specific application. It was reported by many other groups that, imidazole proton on PBI polymer chain can be substituted with alkyl chains, metals etc. But for the first time we have prepared organoborane moiety by substituting PBI imidazole protons and tried to incorporate conducting lithium ion loosely bound to the polymer chain. Modified PBI structure was further hybridized with different amount of ionic liquid BMImTFSI to prepare various pseudo solid polymer electrolyte and application of those in secondary Li-ion battery were also checked. Due to innovative molecular designing ultra-high ionic conductivity was observed (~10^{-2} S cm^{-1}) even higher than most of the reported solid polymer electrolytes so far. Anodic half-cell produced higher discharge capacity of 1300 mAh g^{-1} and stable coulombic efficiency for long cycling. Also, comparatively new technique of interfacial study (dynamic electrochemical impedance spectroscopy, DEIS) was performed to check the solid electrolyte interface (SEI) layer stability.

Hence, in this research theme, we have successfully synthesized various high-performance benzazole polymers using bio-derived and bio-based monomers, which are comparable with engineering grade plastics. Also, copolymerization between various bio-based monomers and depending upon their structural compatibility various properties were established. Side chain modification of the polymer was done for specific applications such as; pseudo-solid polymer electrolyte in Li-ion battery.

Keywords: polybenzimidazole, polybenzoxazole, copolymer, dielectric, conductivity, Li-ion battery

Table of Contents

Chapter 2

Syntheses and characterization of bio-derived monomers using naturally obtained starting materials and their homopolymer syntheses

Chapter 3

Syntheses and characterization of various high-performance copolymers using bio-based monomers and property analysis for their various applications

Chapter 4

Modification of bio-based polybenzimidazole structure to prepare pseudo-solid polymer electrolyte to apply in lithium ion batteries

Chapter 1:

General Introduction

1.1 Introduction:

Since last few decades our society is demanding exponential increasing rate of production and application of synthetic polymers. Presently our beloved mother nature is already facing the consequences of uncontrolled use of petroleum based plastics such as: global warming, depletion of fossil fuel resources etc (31-32). Recent focus of research is mainly on using plant resources both for energy such as-biodiesel also for sustainable, nature friendly plastics. Bio-based and sustainable polymers can be obtained from naturally existing polymers such as-lignin, cellulose; starch etc. or several monomers can be obtained as starting materials using biomass (33-38). The organic material that stores sunlight in the form of chemical energy together with matter that makes up the Earth's living organisms is referred as Biomass. The biomass derived products provide an alternate to petroleum derived products and make human less dependent on fossil fuel and its corresponding rising cost. Hydrothermal carbonization is one of the famous methods to convert biomass into functional carbon materials for various purposes, which is termed as "*chimie douce*" (39). Bioenergy, which is an alternative energy source, is supplying 10% global energy as biofuel in USA, wood and charcoal in Asia and Africa and as combined heat and power source in Europe (Figure 1.1) (40).

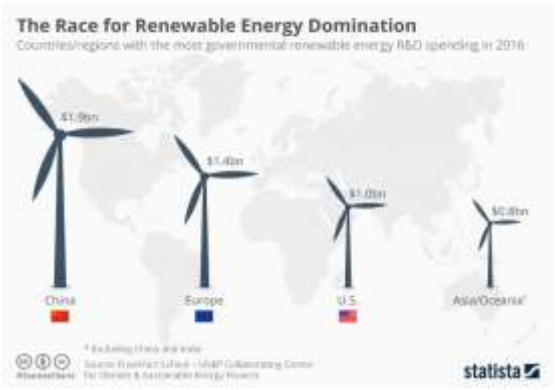

https://www.statista.com/chart/9284/the-race-for-renewable-energy-domination/

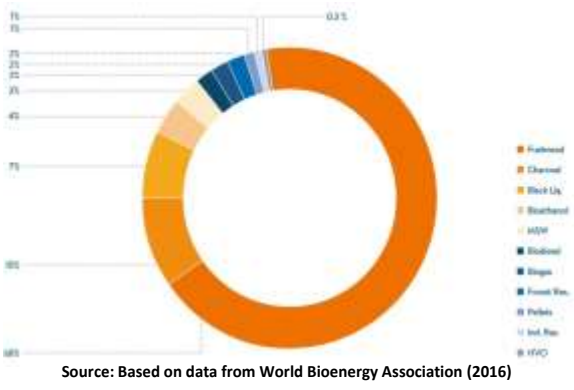

https://www.worldenergy.org/wp-content/uploads/2017/03/WEResources_Bioenergy_2016.pdf

Figure 1.1 Renewable energy contribution and resources around the globe as per 2016

Nearly 95% of the precursor monomers and chemical starting materials which are being used globally based on petroleum derived products, and to reserve the fossilized resources focus

should be shifted towards natural resources such as- agricultural waste, fruits, wood, bacteria, microbes etc. to obtain phenolic derivatives starting materials. Lactic acid, linoleic acid, oleic acid etc. can be obtained as monomers or starting materials from biomass (41-43).

1.1.1 *Bio-plastics and their necessity:*

Major contribution of our daily usage commodity plastics are coming from petroleum-based polyolefin, polypropylene, polystyrene and poly(ethylene terephthalate) etc. Replacing bio-sourced materials over the existing fossil-fuel based plastics are the prime focus of recent research. Research and development in the field of materials science over the past two decades has dramatically increased the production of synthetic or bio-based polymers each

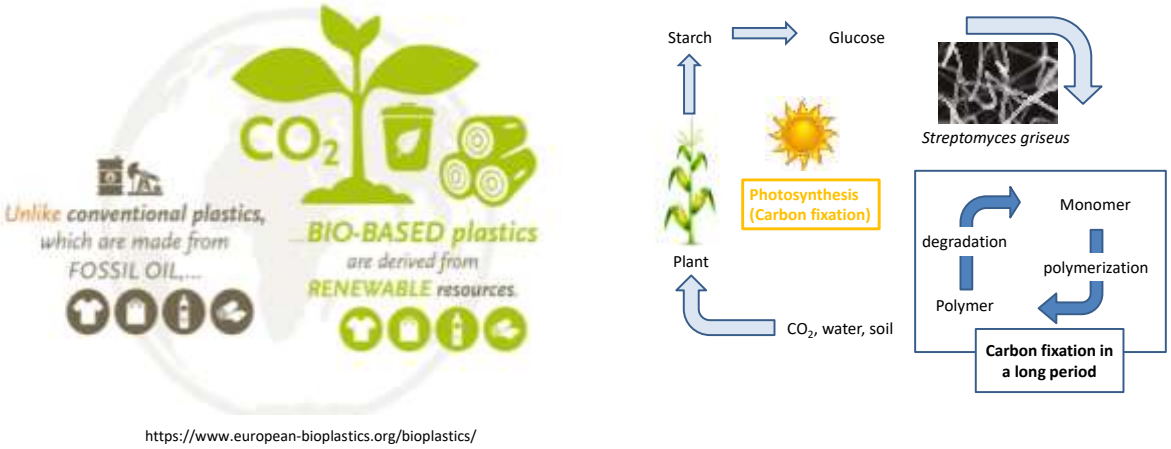

Figure 1.2 Bio-plastic production and cycle for carbon fixation

year (3, 4). Naturally occurring polymers, bio-derived plastics, synthetic bio-based plastics from renewable resources are the present base of establishing the sustainable society. Furthermore, development of high-performance aromatic polymers is prerequisite to surpass the increasing demand of engineering grade plastics. Finally, recycling of those plastics by using natural powers (water, sunlight etc.) or microbes available can be more advantageous in terms of establishing sustainable society (Figure 1.2). Poly(lactic acid) (PLA) is very well-known bioplastic can be produced using agricultural waste and microorganisms. PLA shows

promising mechanical strength (2) however thermal stability can't meet the requirement of high thermal stability. Bio-based polyesters such as poly(hydroxyalkanoate)s, polyamides (PA 11 and PA 66) and poly(butylene succinate) can't match the super-engineering grade plastics such as Zylon™, Kapton™ etc. and they can hardly substitute fossil-fuel based plastics. Syntheses of high-performance bio-based plastics with rigid backbone and inter-chain interactions derived from naturally occurring biomass can be advantageous to manage environmental problems.

1.1.2 *Bioplastic applications in commercial purpose:*

Nowadays, various companies around the globe are already manufacturing bioplastic based commodity products (Figure 1.3). Companies such as, Metabolix Inc. (USA), BASF (Germany), NatureWorks LLC (USA) controls the majority biodegradable plastic production in the world. 62% biopolymers are used in Europe are starch-based followed by PLA 24% (5). Packaging, compostable bags for single use, disposable housewares, and medical devices, automotive parts are the areas where biodegradable plastics can be used. Resins such as Solaplast1723 and Solaplast 1223 (Figure 1.3 (a)) were found their use in packaging industry with low cost maintenance and processing. (6,7). Bags which can achieve the ASTM standard of compostable bags Figure 1.3 (c)) has been prepared with the combination of starch based and PLA under the commercial name of EcoFlex (8), on the other hand oxobiodegradable TDPA™ bags can be used for faster degradability (9, 10). Cutlery has been already prepared as a compostable plastic under the brand name Nat-Ur, using starch based Cereplast which is biodegradable in nature (11). Lactic and glycolic acid made medical sutures are compostable in nature such as- medical screws, dental implants etc. and useful for reconstructive surgeries on ankles, knees Figure 1.3 (d)) (12, 13). SUPLA and Taiwanese company OEM/ODM

collaborative development has made PLA based touchscreen computer Figure 1.3 (e)) (14). Toyota SAI and Toyota Prius models are using 60% bioplastics for their interiors including DuPont's Sorona EP PTT polyester vent louver vanes (15).

1.1.3 *Bio-based and biodegradable plastic:*

Figure 1.3 Different bioplastics for commodity purpose, (a) Solaplast resins used for biodegradable packaging, (b) disposable housewares, (c) biodegradable plastic bag, (d) medical screws made of bioplastic, (e) computer touch screen using bioplastic, (f) Toyota Prius vent louver made of bioplastic, (g) biodegradable iPhone cases.

Packaging industry evolves very fast and in terms of usage of bioplastics in this sector can be either bio-based or biodegradable or both at the same time. Recently, bio-based plastic production exceeds the bio-degradable plastics as plastics like-PET bottles can be biodegradable both if produced from petroleum based or bio-based, so high-performance bio-based plastics are important rather than biodegradability. 'The institute for Bioplastics and Biocomposites' report 2016 says that, 37% of new economy bio-plastics were biodegradable, whether rest of the 63% was bio-based only. By 2020, bio-based non-biodegradable bioplastic will surpass their biodegradable counterpart with a ratio of 4:1 (Figure 1.4). However, the allover usage and production of new economy bio-based plastics has increased several folds in last five years. France already announced prohibition of single-use food service ware made of conventional plastics in 2016 and PepsiCo has committed to use

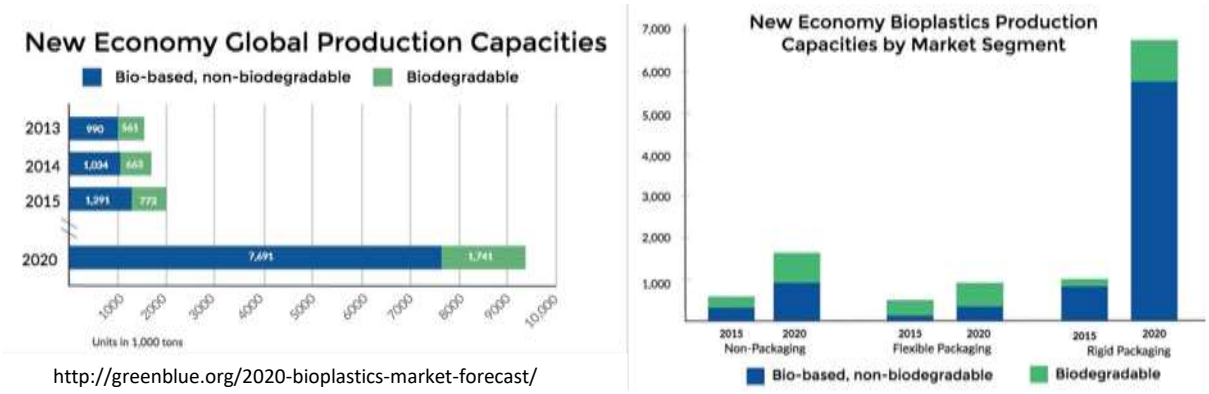

http://greenblue.org/2020-bioplastics-market-forecast/

Figure 1.4 Bio-plastic productions in terms of non-biodegradability and biodegrability

bioplastics in their packaging showing concerns on 'Green-house effect'. After extensive four years research Spanish company Ainia technology developed compostable PHB bottle using wastewater from juice industries (1). The rising usage of bioplastics as a whole dominates fossil-b ased plastics and research in this field can renew emphasis on sustainability with new varieties bioplastic feedstock.

1.2 High-performance bioplastics:

High performance polymers are the group of polymers which can retain their high thermo-mechanical as well as chemical stability against harsh conditions or environments, along with these they can show high electrical conductivity, dielectric strength or insulation and superior flame resistance depending upon their structures (16). High thermal stability can be enhanced using the resonance stabilization of heterocyclic structures. High softening temperature can be achieved by introducing crystallization, chain stiffening and crosslinking (17). Heterocyclic backbones are important for high performance polymers and along with the timeline 1960-70 s were most important in terms of high performance polymers such as- Kapton™, Vespel™, Pyre-ML™ also polysulfones etc. Upilex™ is a new example of processable polymer with low coefficient of thermal expansion has been developed in 1980s (18). Polybenzazole derived from fossil fuel resources and can be cited as the most powerful polymer derived from fossil fuels. Polybenzazole is the structure having one N- atom in 1 or 3 position of the five-membered ring attached to the aromatic ring and when we have one O-atom in 3 positions of the five membered rings it is known as polybenzoxazoles. Polybenzoxazole has a rigid cyclic structure of high strength because of π-π stacking. It shows high heat resistance and can be used for harsh environment like- protective apparels and satellite making instruments

1.2.1 *Polybenzoxazole (PBO):*

Polybenzoxazole(PBOs) are kind of polymers which represent high thermally stable polymer series due to the presence of alternative phenylene ring and heterocyclic rings. They can be the most suitable alternative substitute of the polyimides in terms of thermo-mechanical stability, low flammability, and superior chemical resistance (19). Zylon™ is the most popular commercial kind of PBO with IUPAC name of poly(*p*-phenylene-2, 6-benzoxazole)

with high mechanical strength and excellent thermal property. Being highly durable, mechanically strong and with excellent thermal property Zylon^{TM} can be used for bullet-proof vests, conductive textiles, space research etc. In our laboratory we have already prepared bio-based PBOs with various structures using bio-derived starting materials (20). Significantly low dielectric constant (low-*k*) of PBO series of polymers are also point of attention for synthesizing insulating plastics, because of their non-polar structural configuration (21).

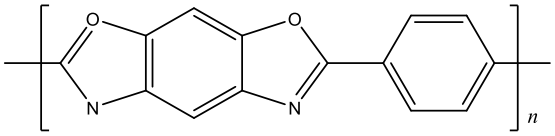

Figure 1.5 Representative structure of Zylon^{TM} [poly(*p*-phenylene-2, 6-benzoxazole)]

1.2.2 *Polybenzimidazole (PBI):*

Vogel and Marvel are considered to be the inventor of aromatic polybenzimidazoles and later by DuPont as high performance polymer and well known for its unique thermal property (22, 23). However research on polybenzimidazole became saturated because of its substitutes such as PEEK, polyimides etc., also because of high water absorbing nature and expensive properties. Recently most of the research on PBI is going on regarding low-cost polymerization, composite or blend preparation and most extensively modification of the PBI for various applications (24).

Several different structures of polybenzimidazoles (Figure 1.6) were already been developed using various monomers such as aromatic diamine-carboxylic acid, aromatic tetraamines etc. Poly (2,2'-(*m*-phenylene)-5,5' bibenzimidazole) (PBI) or commercial Celazole^{TM} shows combination of high thermal stability and processability both at the same time.

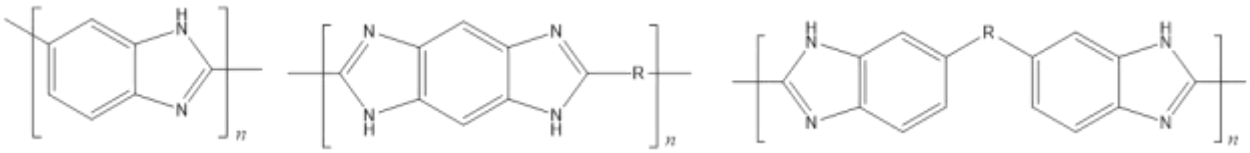

Figure 1.6 Various polybenzimidazole structures

Several blending of PBI has already been discovered such as blend with polyimides, polyarylate, polyamideimide, aramids etc. The well miscibility was found in case of PBI is due to hydrogen bonding effect and interaction between –NH to C=O group of other polymers, which can result in enhancing polymer properties with several folds such as PBI/PA or PBI/HMAs (25-27).

1.2.3 *Polyamide (PA):*

Polyamides are materials containing intermittent amide linkages between polymer units and can be aliphatic, partially or whole aromatic types (Figure 1.7). Aromatic polyamides (also known as Nylon) can be developed consisting of high mechanical strength, abrasion resistance etc. (16). Aromatic polyamides can be used as film, fiber and fillers suitable for various applications due to their high thermal resistance (28-29). Natural polyamides such as wool, silk and artificially prepared polyamides through solid-solid and step growth synthesis. Nylon™, Kevlar™ and Nomex™ from DuPont, Rilsan™ and Rilsamid™ from Arkema, Teijinconex™ and Technora™ from Teijin are few of the famous commercial polyamides and they can be used for various purposes such as textiles, automobile industry, sportswear etc (30). Physico-chemical properties of the polyamides can be variable depending on their polymer backbone structure, chain length and molecular weight. They can be synthesized by using both melt and solution polycondensation methods depending on the requirements of polymer nature.

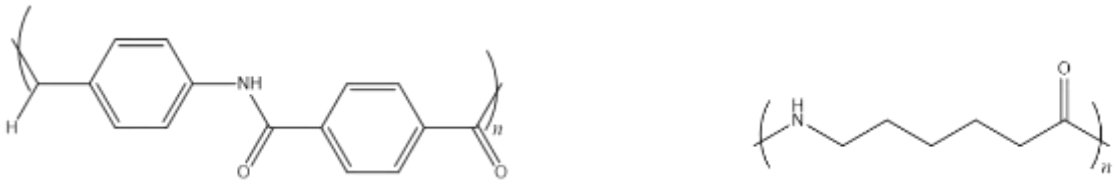

Kevlar (aromatic) Nylon 6 (aliphatic)

Figure 1.7 Various polyamide structures

1.3 Polymer applications in various fields:

The inevitable situations of ever increasing demands for energy along with depleting fossil resources and environmental concern provides motivation to scientific community to discover alternative sources.

Battery:

Primary requirements which are essential for any kind of battery are:

(a) Energy output over long period of time,

(b) Energy storage capacity,

(c) Safety,

(d) Stability and for high-performance usage purpose.

Lithium ion batteries are advantageous over other conventional secondary energy sources in terms of all the factors shown above (Figure 1.8). In 2001, Tarascon and Armand introduced prospective lithium-ion batteries in 2001 for the first time in their *Nature* manuscript (44). Furthermore few other advantages of li-ion batteries as listed by Kurzweil *et al.* (45) and those are:

- Higher energy density,
- Higher operating potential,

- Lower self-discharge,
- Wide operational window,
- Rapid charging ability etc.

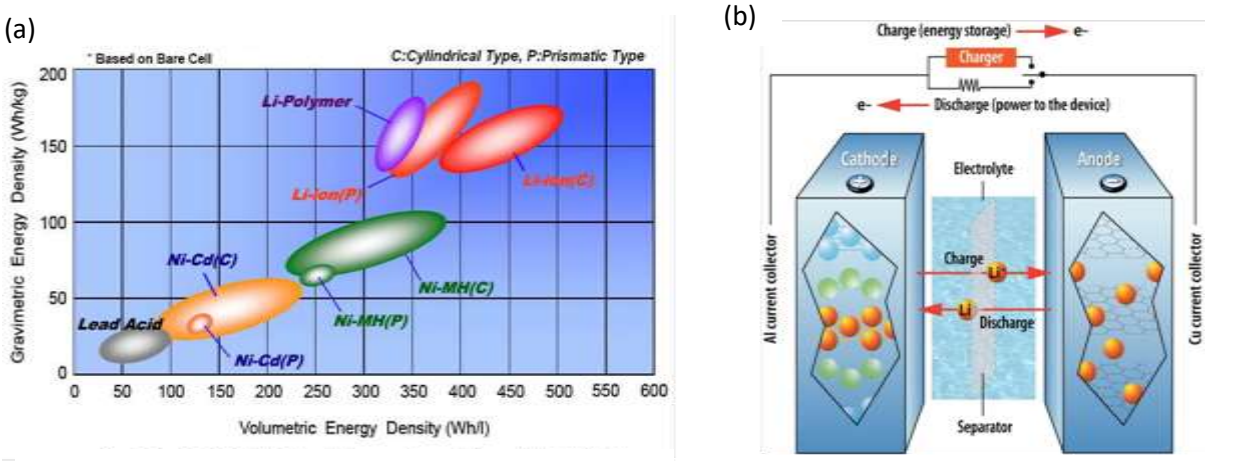

Photo credit: Nasa-National Aeronautics and Space Administration
https://www.epectec.com/batteries/cell-comparison.html

Brahim Mebarki *et al.*, Modelling and Simulation in Engineering, 2013, Article ID 935784, 1-6

Figure 1.8(a) Various battery energy density (gravimetric) profiles, **(b)** Schematic representation of the lithium-ion battery during charge-discharge

Although this emerging alternative energy source still faces shortcomings in terms of commercialization such as, longevity, and safety and cost effective.

1.3.1 *Polymer electrolyte*

Armand *et al.*, working since the very beginning of this technology, discovered solid state polymer electrolyte by coordinating polymer and a lithium salt. Polymer electrolyte can be classified mainly in following categories; (a) Salt in polymer matrix, (b) Liquid in polymer matrix: Plasticized electrolyte, (c) Salt-in polar liquid: with plasticizing polymer, (d) Ionic rubber electrolyte with ionic liquid and high molecular weight polymers. In this thesis our focus mainly will be surrounding solvent-free salt in polymer matrix. Anion receptors in

electrolyte matrix are often significant due to increasing localized lithium ion concentration in the electrolyte by binding with counter anion. Anion of lithium salt binds with lewis acid moiety thereby helping in facile lithium salt dissociation. The resulting free Li-ions will enhance transference number as well as ionic conductivity. Boron-based anion receptors have been well studied in recent past due to their excellent lewis acidic nature along the electrochemical stability. Empty *p*-orbital in boron atom plays the key role in electron attraction process, which is well-known as 'anion-trapping effect' of boron moiety. Fujinami *et al.* [59] reported for the first time about boroxine ring receptor, as a result increases ionic conductivity. Watanabe *et al.*, Aihara *et al.* [60-61] reported about different types of polymerizable novel boric esters exploiting lewis acidic nature of boron compounds. Matsumi *et al.* [62] reported organic-inorganic boron hybrid preparation by synthesizing an interpenetrating network of an ionic liquid network and boro-silicate/silicate network. Borosilicate type hybrids with incorporated ionic liquids were prepared using *in-situ* condensation technique, which provides both thermo-mechanical stability and high ionic conductivity.

The coordination of lithium ions through columbic attraction with the negatively charged oxygen atoms on the PEO chains led to their facile dissociation of lithium salts and further dissolution in the PEO matrix. PEO chain flexibility helps lithium ions to move in coordinated manner (46). R&D is rapidly moving towards organic electrolyte preparation to substitute conventional liquid electrolytes which can be superior in terms of solidity nature and thermally stable (48). Ionic liquids, eutectic solvents, most importantly biopolymers with proper functionalization such as polyelectrolytes, they appeared as promising candidates over their liquid variants being greener substitute to their environmentally toxic existing electrolytes (52). Cellulose being a renewable natural fiber, thermally stable, high dielectric constant has been used for lithium ion battery applications since long time (49-51).

Polyhydroxyalkanoates (PHAs) being bio-derived and biodegradable thermoplastic are still not explored properly in the application field of li-ion batteries with few literatures available (47). Several many other biopolymers are still unexplored in the field of solid polymer electrolyte and in my research I have introduced bio-based polybenzimidazole for the first time in electrolyte syntheses and applied to lithium ion batteries.

1.3.2 *Dielectric polymers:*

The definition of the dielectric constant or permittivity (ε) is the ability of a material to polarize in response to an applied field. Conventional dielectric materials such as: mica and silica are consists of low dielectric constant, polymer dielectric materials are advantageous over conventional inorganic ones in terms of processibility and flexibility. Both high and low dielectric constant can be important depending on various purposes; polymer-based dielectric materials with low dielectric constant are known as passivation materials useful for insulators, interlayer dielectrics in electronic packaging, miniature microprocessors to reduce crosstalk noise, power dissipation etc. On the other hand high dielectric constant materials are useful as polarizable media for capacitors, piezoelectric transducers, amplifiers etc. (54) Most of the available polymer dielectrics face shortcomings in terms of attaining high thermal stability, to attain extreme condition polymer dielectric materials to apply in hybrid vehicles, aerospace engineering etc.(53) Minimizing the polarizability in the aromatic polymer dielectric materials can reduce dielectric constant significantly and aromaticity gives them high thermo-mechanical stability (55). Incorporating high degree of free volume and fluorine atoms into the molecular structure can reduce dielectric constants (56-58). In my research I have tried to investigate this structure-property relationship to develop low dielectric constant polymer with high thermo-mechanical stability.

1.4 Aromatic amino acid monomers:

1.4.1 *3-amino-4-hydroxybenzoic acid (3, 4-AHBA):*

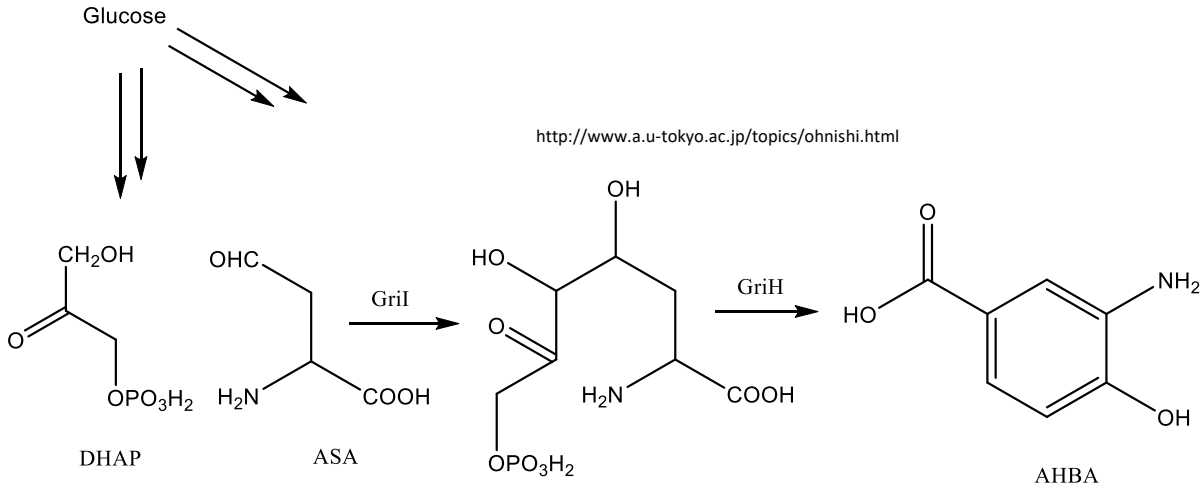

Scheme 1.1 Biosynthesis pathway of 3-amino-4-hydroxybenzoic acid (3, 4-AHBA) pathway, this novel simple enzyme system is useful for the synthesis of benzene ring from C_3 and C_4 primary metabolites.

Collaboration with our research group has found two enzymes that facilitate the production of AHBA from the bacterium *Streptomyces griseus* and generated the recombinant *Corynebacterium glutamicum* strain KT01 for the production of AHBA (Scheme 1.1). The Shikimate pathway which includes seven enzymetic steps to produce chorismate via shikimate is common in various organisms for biosynthesis of aromatic amino acids. We fermentatively produced 3, 4-AHBA and ABA using kraft pulp as the starting material. Kraft pulp, which is recovered by fractionation processes in the paper industry, is a model cellulosic biomass and represents woods, energy crops, and agricultural residue. 3, 4-AHBA came as a benzene derivative which can be biosynthesized by using comparatively simpler enzyme system. *griI* and *griH* are two genes reportedly found to be responsible for the

biosynthesis of 3,4-AHBA; and they can produce 3,4-AHBA *in vitro* even on *Escherichia coli*. *In vitro* analysis showed that *griI* catalyzes aldol condensation between primary metabolites, L-aspartate-4-semialdehyde and dihydroxyacetone phosphate, to form a C_7 product, 2-amino-4, 5-dihydroxy-6-one-heptanoic aicd-7-phosphate, which is subsequently converted to 3, 4-AHBA by *griH* (28). Three functional group attached to a single benzene ring can introduce various significant properties; can be a precursor to various benzazole kind of polymers. 3, 4-AHBA has been already used to produce polybenzoxazole and can be converted in 3,4-diaminobenzoic acid, another monomer.

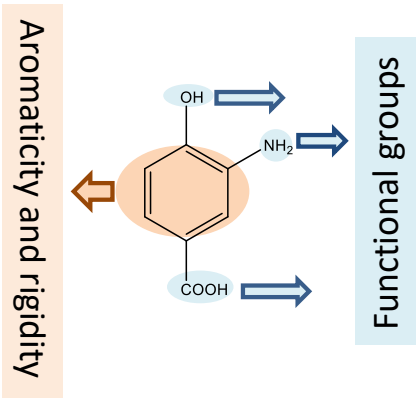

Figure 1.9 Structure and property relationship of 3, 4-AHBA

1.4.2 *4-aminobenzoic acid (PABA):*

In this study, I have introduced another biologically available monomer 4-aminobenzoic acid (PABA). PABA is an intermediate in the synthesis of foliate by bacteria, plants etc., such as *E.coli* generates PABA from the chorismate with the help of the enzymes 4-amino-4-dehydroxychorismate synthase and 4-amino-4-dehydroxychorismate lyase. Plants produce and store PABA in their tissues as glucose esters in adequate amount. Bio-derived crude sample was kindly donated by our collaborator Prof. Naoki Takaya, University of Tsukuba.

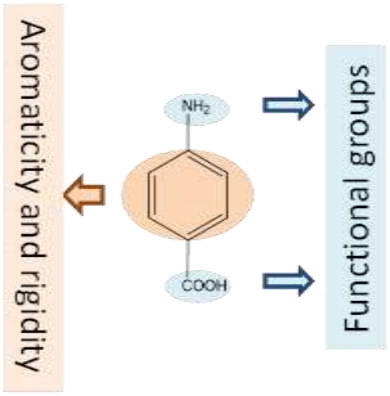

Figure 1.10 Structure and property relationship of PABA

1.4.3. *3, 4-diaminobenzoic acid (3, 4-DABA):*

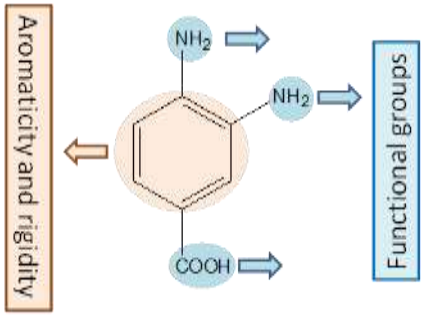

Figure 1.11 Structure and property relationship of 3, 4-DABA

Chemical conversion of the bio-derived monomer 3, 4-AHBA into another monomer 3, 4-diaminobenzoic acid (3, 4-DABA) using chemical conversion method via several easy steps. This new monomer can form another new kind of polymer i.e. polybenzimidazoles (PBIs) which are thermally more stable as compared with polybenzoxazoles (PBOs) because of the presence of H-bonding.

I will use these bio-derived and bio-based monomers throughout the research to prepare several bio-based high-performance polymers for various applications.

1.5 References:

1. <https://www.plasticsnewseurope.com/article/20160823/PNE/160829966/recovering-sugar-from-juice-industry-to-make-bioplastics>.
2. Chow, A. W., Bitler, S. P., Penwell, P. E., Osborne, D. J. Wolfe, J. F. *Macromolecules*, 1989, 22, 3514.
3. Thakur, V.K. and Thakur, M.K., Handbook of polymers for pharmaceutical technologies: structure and chemistry, Volume 3, *Wiley-Scrivener*, 2015.
4. Lendlein, A. and Sisson, A., Handbook of Biodegradable Polymers: Isolation, Synthesis, Characterization and Applications, *Wiley-VCH: Weinheim*, Germany, 2011.
5. Ashter, S. A. 'Introduction to bioplastic engineering: Commercial applications of bioplastics', *Elsevier*, 2016.
6. Solaplast, Target Markets and Applications, ,http://algix.com/solaplastapplications/.
7. Solaplast, Solaplast Resin Grades, <http://algix.com/products-services/solaplast-resin-grades/>.
8. Narayan, R., Mojo, S. Summary of ASTM D6400 Test Method and Specifications and Correlation of Test Methods to Real World Composting Results, International Biodegradable Products Institute, 2002.
9. EPI Environmental Technologies Inc., EPI-Global, <http://www.epiglobal.com/en/Index-e.htm>, 2005.
10. TDPA®: Totally Degradable Plastic Additive, EPI Environmental Technologies Inc., <http://www.epi-global.com/en/about-tdpa.php>.

11. Thomas, J. Compostable cutlery made from Cereplast, <http://www.treehugger.com/clean-technology/compostable-cutlery-made-from-cereplast.html>.

12. Fox, S. A new breed of medical screws dissolve in body and promote bone growth, <http://www.popsci.com/science/article/2010-03/biodegradable-medical-screws-disolve-body-and-promote-bone-growth>.

13. Euroscrews TCP, Teknimed, <http://www.medicalexpo.com/prod/teknimed/product-70291-499892.html.>

14. Moore, S. PLA bioplastic debuts in touchscreen computer housing, Plastics Today, <http://www.plasticstoday.com/articles/k-2013-pla-bioplastic-debuts-touchscreen-computer-housing> October 2013.

15. Bio-based resins score in auto applications, Plastics Technology, <http://www.ptonline.com/articles/biobased-resins-score-in-auto-applications>January 2012.

16. Garcia, J. M.; Garcia, F. C.; Serna, F. and Pena, D. L., J. *Prog. Polym. Sci.* 2010, 35, 623.

17. Arnold, C. Jr. Stability of high-temperature polymers, *J. Polym Sci.: Macromolecular review*, 1979, 14(1), 265.

18. Hergenrother, P. M. The use, design, synthesis, and properties of high performance/high temperature polymers: an overview, High Perform. Polym. 2003, 15(1), 3.

19. Furukawa, K., Ueda, M. *Polym. J.* 2006, 38(5), 405.

20. Ali, M. A., Shimosegawa, H., Nag, A., Takada, K., Kaneko, T. *J. Polym. Res.* 2017, 24:214, 1-7.

21. Krause, B., Koops, G.-H., van der Vegt, N. F. A., Wübbenhorst, M., Turnhout, J-V. *Adv. Mater.* 2002, 14(15), 1041.

22. Vogel, H. A., Marvel, C. S. *J. Polym. Sci.* 1961, 50, 511.

23. Vogel, H. A., Marvel, C. S. *Polym. Sci. Part A.* 1963, 1, 1531.

24. Chung, T. S., *Macromol. Sci., Part C: Polym. Rev.* 1997, 37(2), 277.

25. Chung, T. S., Chen, P. N. *J. Appl. Polym. Sc*i. 1990, 40, 1209.

26. Chung, T. S., Herold, F. K. *Polym. Eng. Sci.* 1991, 31, 1950.

27. Chung, T. S., Chen, P. N. *Polym. Eng. Sci.* 1990, 30, 1.

28. Morgan, P. W. *Macromolecules* 1977, 10, 1381.

29. Lin, J.; Sherrington, D. C. *Adv. Polym. Sci.* 1994, 111, 176.

30. Lim, J. G.; Gupta, B. S. and George, W., *Prog. Polym. Sci*. 1989, 14, 763.

31. Papageorgiou, G. Z. *Polymers* 2018, 10, 952.

32. Pathak, S., Sneha, CLR., Mathew, B. B. *Journal of Polymer and Biopolymer Physics Chemistry*, 2014, 2(4), 84.

33. Schneiderman, D.K.; Hillmyer, M.A. *Macromolecules* 2017, 50, 3733.

34. Zhu,Y., Romain,C., Williams, C.K. *Nature* 2016, 540, 354.

35. Storz, H., Vorlop, K.-D. *Landbauforsch.-Ger.* 2013, 63, 321.

36. Upton, B.M., Kasko, A.M. *Chem. Rev.* 2015, 116, 2275.

37. Isikgor, F.H., Becer, C.R. *Polym. Chem.* 2015, 6, 4497.

38. Zhang, C., Garrison, T.F., Madbouly, S.A., Kessler, M. R. *Prog. Polym. Sci.* 2017, 71, 91.

39. Falco, C., Baccile N., Titirici, M-M. *Green Chem.*, 2011, 13, 3273.

40. World Energy Resources Bioenergy/ 2016-World Energy Council. <https://www.worldenergy.org/wp-content/uploads/2017/03/WEResources_Bioenergy_2016.pdf>

41. Lochab, B., Varma, I. K., Bijwe, *J. Adv. Mater. Phys. Chem.*, 2012, 2, 221.

42. Kawser, J. M., Nash, A. F. *J. Oil Palm Res.*, 2000, 12, 86.

43. Leal, E. R., Vaquez R. R., Galindo, T. *J. Wood Chem. Tech.*, 1994, 14, 369.

44. Tarascon, J.-M. Armand, M. *Nature*, 2001, 414, 359.

45. Kurzweil, P. *J. Power Sources*, 2010, 195, 4424.

46. Scrosati, B., Abraham, K.M., van Schalkwik W. Hassoun, J. Eds., in Lithium Batteries- Advanced Technologies and Applications, 2013, Wiley.

47. Reusch, R. N., Reusch, W. H. US005266422, 1993.

48. Dall'Asta, V., Berbenni, V., Mustarelli, P., Ravelli, D., Samori, C., Quartrone, E. *Electrochim. Acta*, 2017, 247, 63.

49. Jabbour, L., Bongiovanni, R., Chaussy, D., Gerbaldi, C., Beneventi, D. *Cellulose*, 2013, 20, 1523.

50. Sabo, R., Yermakov, A., Law, C. T., Elhajjar, R. *J. Renew Mater*. 2016, 4, 297.

51. Sharifi, F., Ghobadian, S., Cavalcanti, F. R., Hashemi, N., *Renew. Sust. Energ. Rev.*, 2015, 52, 1453.

52. Smith, E. L., Abbott, A. P., Ryder, K. S., *Chem. Rev*. 2014, 114, 11060.

53. Li, Q., Chen,L., Gadinski, M. R., Zhang, S., Zhang, G., Li, H. U., Iagodkine, E., Haque, A., Chen, L-Q., Jackson, T. N., Wang, Q. *Nature*, 2015, 523, 576.

54. Ahmed, Z. Polymer dielectric materials, Dielectric material, InTech Open, 2012.

55. DuPont Co., Kapton Polyimide Film-Summary of Properties, Polymer Products Department, Industrial Films Division, Wilmington, DE 1989.

56. Singh, J. J., St. Clair, T. L., Holt, W. H., Mock, W. NASA Tech. Memo. No. 86431 (1985).

57. Hougham, G., Tesoro G., Viehbeck, A. *Macromolecules*, 1996, 29, 3453.

58. Hougham, G., Tesoro G., Viehbeck, A., Chapple-Sokol, J. D. *Macromolecules*, 1994, 27, 5964.

59. Fujinami, T.; Mehta, M. A.; Sugie, K.; Mori, K. *Electrochim. Acta*, 2000, 45, 1181.

60. Aihara, Y.; Kuratomi, J.; Bando, T.; Iguchi, T.; Yoshida, H.; Ono, T.; Kuwana, K. *J. Power Sources*, 2003, 114, 96.

61. Tabata, S.; Hirakimoto, T.; Tokuda, H.; Susan, M. A. B.; Watanabe, M. *J. Phys. Chem. B*, 2004, 108, 19518.

62. Matsumi, N.; Miyake, M.; Ohno, H. *Chem. Commun*., 2004, 2852.

Chapter 2:

Syntheses and characterization of bio-derived monomers using naturally obtained starting materials and their homo-polymer syntheses

2.1 Introduction:

Rising demand for plastic and polymer based products in daily life and almost in every field caused serious damage to the environment in terms of non-renewability and bio-degradability. However, apart from these two main problems, depletion of petroleum based resources which is also limited in nature and increasing cost of the available resources has diverted researchers' to think about alternative resources as substitute. There are several bio-available resources for different polymers and they are better known as 'biomasses' which can be less-toxic to the environment and as well as cost-effective in nature. Recently, since past few decades biomass derived or bio-based plastic industry is growing for making different products and packaging. Proteins, fat, carbohydrates, nucleic acid and their metabolites including amino acids, lactates, alkaloids, cinnamates etc. are well-known as biomass to contribute in polymer industry. These bio-based monomers are useful and already used for preparing polymers, but their applications are limited due to their poor thermo-mechanical properties as compared with super-engineering plastics (1-3).

Polyamides such as Kevlar™, polybenzoxazoles such as-Zylon™, polybenzimidazole such as Celazole® are well known to be used as super-engineering plastics (4-5). All of the monomers which were used to syntheses these polymers are from fossil- based and aromatic back-bone based. All the monomers are being used since long back as bio-based or bio-derived to synthesis their corresponding bio-plastics are poor in thermal and mechanical performances. By introducing stable functionality and aromatic moiety in the monomers and thus polymers can get stability comparable with their petroleum based alternatives (8-11). Aromatic diamine monomers of polybenzoxazole, polybenzimidazole are toxic to micro-organisms so it is better to make them chemically using bio-available starting monomers (12).

In this chapter we will focus on the syntheses of different bio-derived and bio based monomers to synthesize bio-plastics. Homopolymer preparation in every case will also be discussed in this chapter along with their characterization.

2.2 Experimental:

3, 4-AHBA, 3, 4-DABA, PABA were purchased from TCI (Tokyo, Japan); Bio-derived 3, 4-AHBA was also kindly provided by our collaborator Prof. Y. Ohnishi in Tokyo University, while bio-derived PABA has been provided by Prof. N. Takaya in Tsukuba University. N-methyl-2-pyrrolidinone (NMP, 99.5% purity), N, N-dimethylformamide (DMF, 99.8% purity), dimethyl sulfoxide (DMSO, 99.5% purity), tetrahydrofuran (THF, 99.8% purity), and concentrated sulfuric acid (H_2SO_4, 95.0% purity), trifluoroacetic acid (TFA), and methanesulfonic acid (MSA) were purchased from Wako Pure Chemical Industries, Ltd. 2-bromoisobutylamide and potassium peroxymonosulfate were purchased from TCI, and potassium carbonate (K_2CO_3), potassium hydroxide (KOH), hydrochloric acid (HCl), phosphorus pentoxide (P_2O_5) and DMSO-d_6 (NMR solvent) were purchased from Kanto Chemicals Co. Ltd. (Tokyo, Japan). Palladium-charcoal (5%) purchased from Sigma-Aldrich was used as a catalyst of hydrogen reduction. Eaton's reagent (P_2O_5/methansulfonic acid 1/10) and poly(phosphoric acid) (PPA) were purchased from TCI, and were used as polymerization solvents.

2.2.1 *Characterization:*

Proton nuclear magnetic resonance (^{1}H NMR) and carbon (^{13}C NMR) spectra of the monomers were recorded using a Bruker AVANCE III 400 NMR spectrometer operating at a proton frequency of 400 MHz using DMSO-d_6 as the solvent. The FT-IR spectra were recorded with a Perkin-Elmer Spectrum One spectrometer between 4000 and 400 cm^{-1} using a diamond-attenuated total reflection (ATR) accessory. The ^{13}C solid-state NMR (cross

polarization total side band suppression/CP-TOSS) spectra of the polymer were recorded using a standard cross-polarization pulse sequence. The samples were packed in a 7 mm diameter zirconia rotor with a Kel-F cap and spun at 10 kHz. A contact time of 2 ms was used, the period between successive accumulations was 5 s, and the total number of scans was 10000.

2.2.2 *Syntheses of 3, 4-diaminobenzoic acid from bio-derived 3-amino-4-hydroxybenzoic acid (3, 4-DABA from 3, 4-AHBA)*

As discussed in *Chapter 1* 3, 4-AHBA can be described by several biotechnological methods using Kraft pulp, which is basically cellulose biomass can be obtained from paper industry. Also, using enzymatic pathway 3, 4-AHBA can also be obtained *in vitro* on *Escherichia coli.* Bio-derived 3, 4-AHBA was kindly donated by our collaborator Prof. Yasuo Ohnishi, University of Tokyo. However, we have purchased commercial 3, 4-AHBA as well and

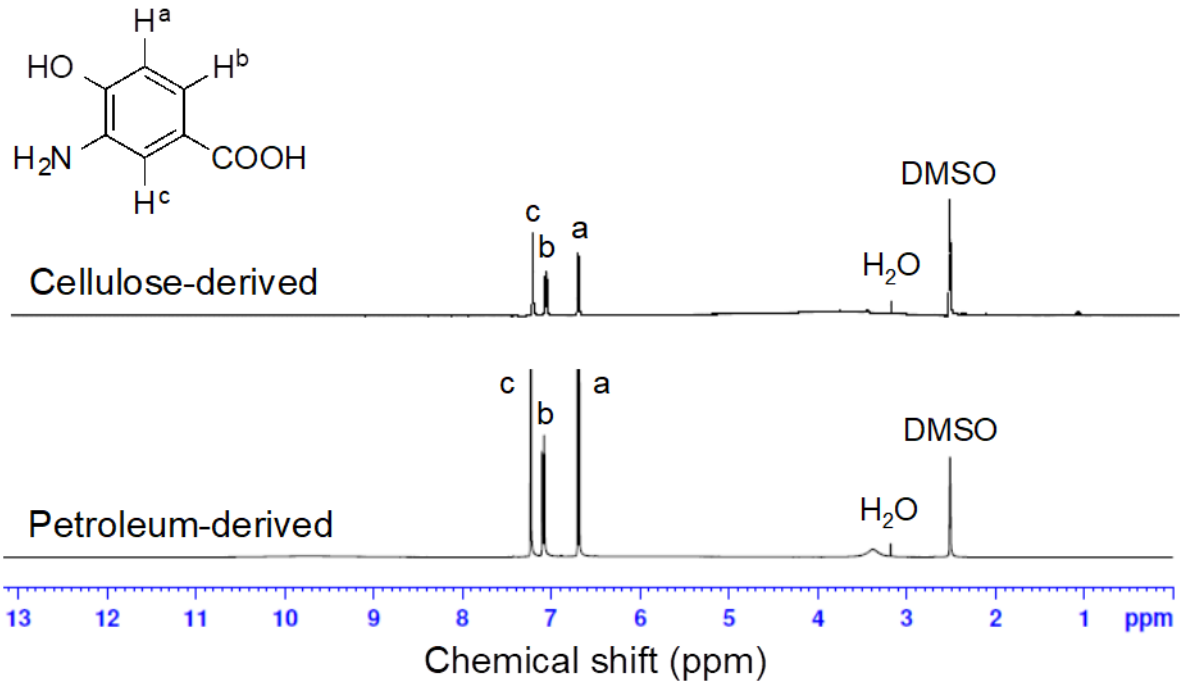

Figure 2.1 ^{1}H-NMR spectrum of commercial and cellulose-derived 3, 4-AHBA

below are the ^{1}H-NMR comparison between them.

The most challenging step is converting aromatic –OH to aromatic –NH_2 by following Smiles rearrangement (6-7). Our first attempt got failed to go through as a successful smiles rearrangement.

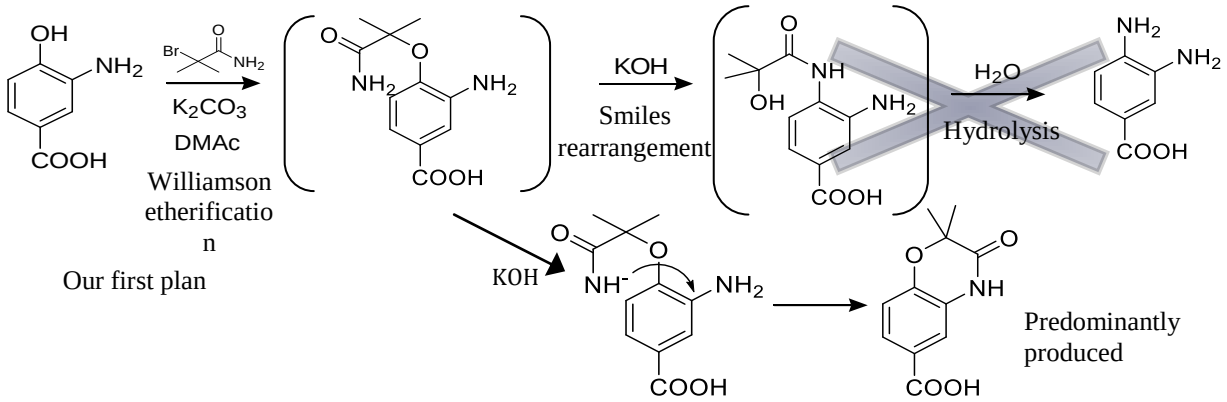

Scheme 2.1 Expected and actual schematic pathway of 3, 4-AHBA through Smiles rearrangement

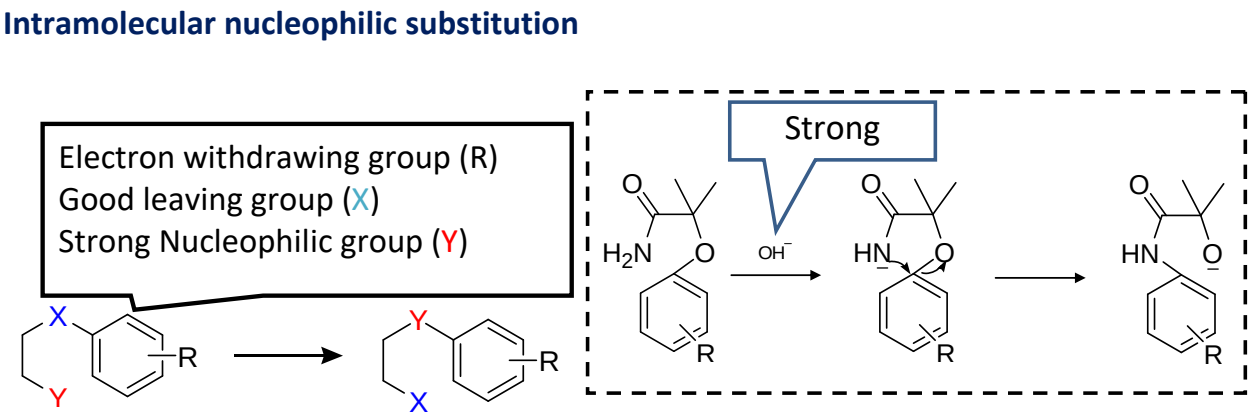

Scheme 2.2 Plausible mechanism and substituents to occur Smiles rearrangements successfully

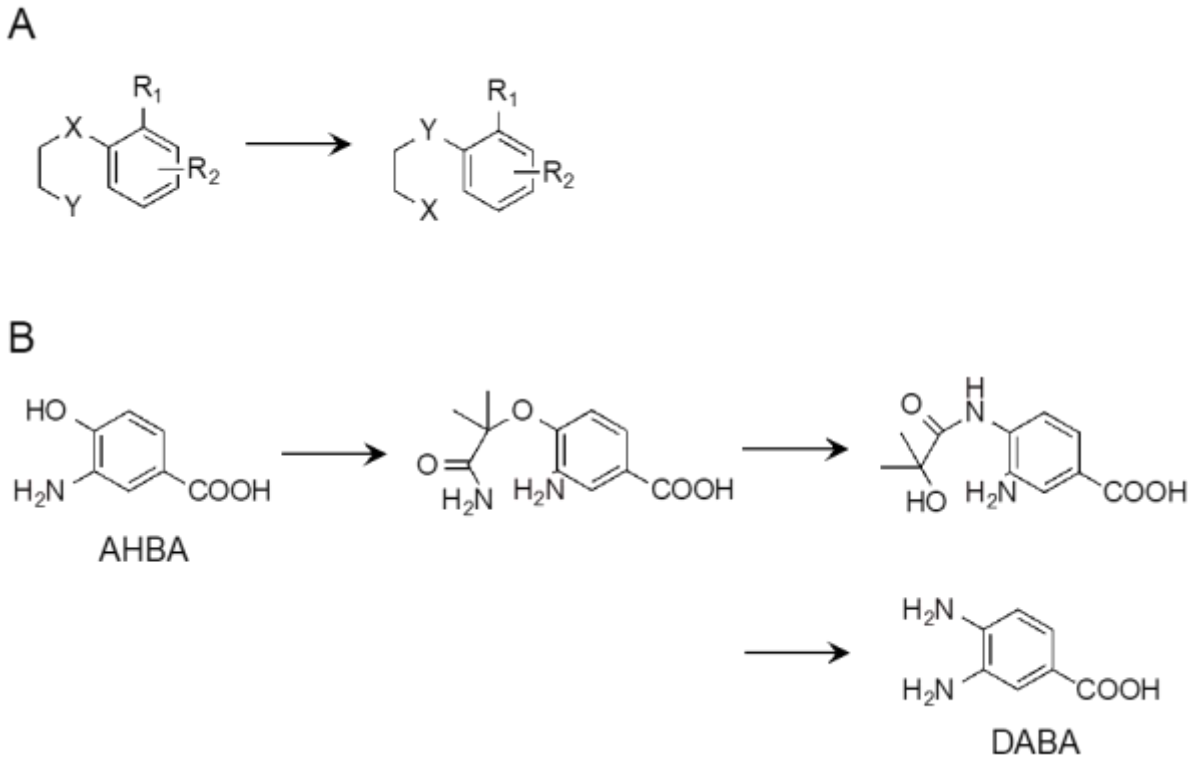

Scheme 2.3 Possible chemical conversion of 3-amino-4-hydroxybenzoic acid (AHBA) to 3,4-diaminobenzoic acid (DABA) by the Smiles rearrangement

General scheme of the Smiles rearrangement, which is an intramolecular nucleophilic aromatic substitution are shown above. 'X' is a functional group (*e.g.*, sulfone, sulfide, and ether) that is capable of dislodging from the arene carrying a negative charge. 'Y' is a functional group (*e.g.*, alcohol, amine, and thiol) that is able to act as a strong nucleophile. Possible chemical conversion of AHBA to DABA can be done by modifying the hydroxyl group of AHBA with 2-bromoisobutylamide, resulting in a compound applicable to the Smiles rearrangement to yield DABA.

Oxidization of the amine group of AHBA into a nitro group was essential for the following Smiles rearrangement, because strong electron-withdrawing property of the nitro group facilitated the Smiles rearrangement. Before the Smiles rearrangement, 4-hydroxy-3-nitrobenzoic acid (HNBA) was converted to its methyl ester (HNBAm) to increase the solubility. After the Smiles rearrangement, the nitro group was reduced in the presence of Pd/C (5%) to produce DABA. In the final step, DABA was neutralized by HCl to prevent oxidation of amine groups during storing and heating at the beginning of polymerization.

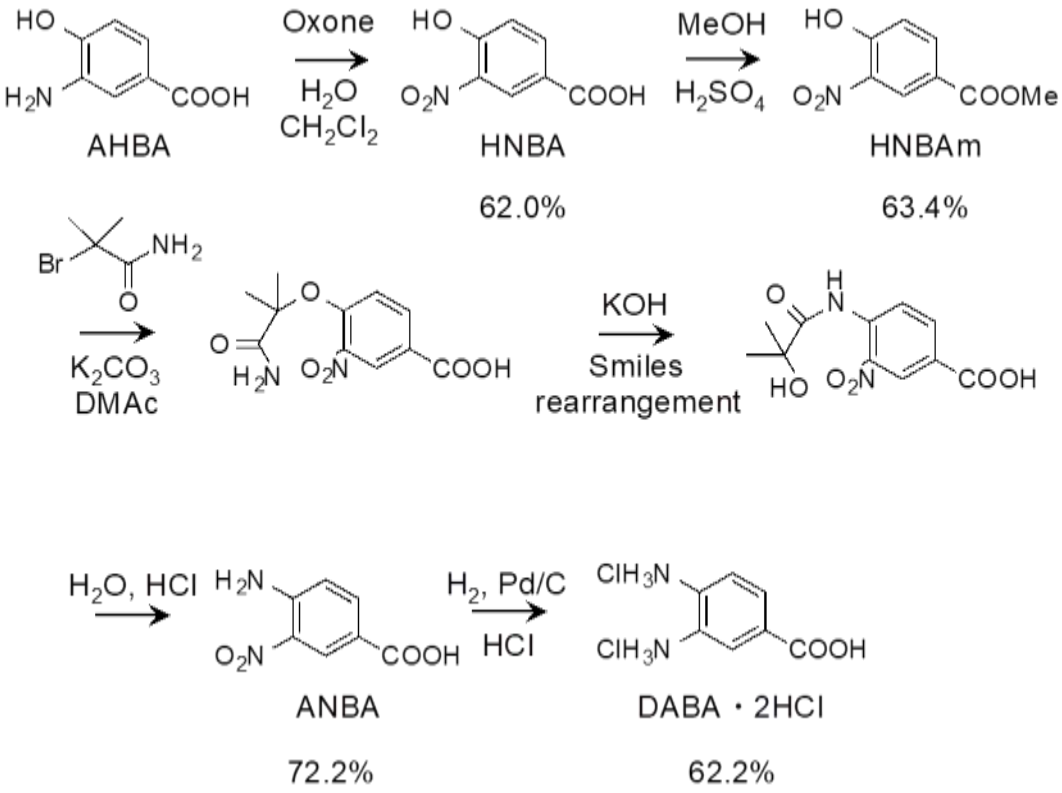

Scheme 2.4 Syntheses of 3, 4-diaminobenzoic acid from 3-amino-4-hydroxybenzoic acid (3, 4-AHBA) via Smiles rearrangement along with the yield for each step

2.2.3 *Synthesis of 4-hydroxy-3-nitrobenzoic acid (HNBA):*

Potassium peroxymonosulfate (6.16 g, 10 mmol) was dissolved in pure water (32 mL) at room temperature, and AHBA (0.77 g, 5 mmol) and dichloromethane (8 mL) were added to the resulting solution. The mixture was kept under continuous stirring for 1 day. The reaction solution was filtered, and the resulting solids were washed with water and dried under vacuum to obtain pure 4-hydroxy-3-nitrobenzoic acid (HNBA) (yield; 0.57 g, 62.0%). ^{1}H-NMR (400 MHz, DMSO-d_6, δ, ppm): 7.27 (dd, 1H, J = 8.4 Hz), 8.35 (s, 1H), ^{13}C-NMR (400 MHz, DMSO-d_6, δ, ppm): 40.4, 120.2, 122.5, 128.5, 138.1, 138.6, 157, 167.2.

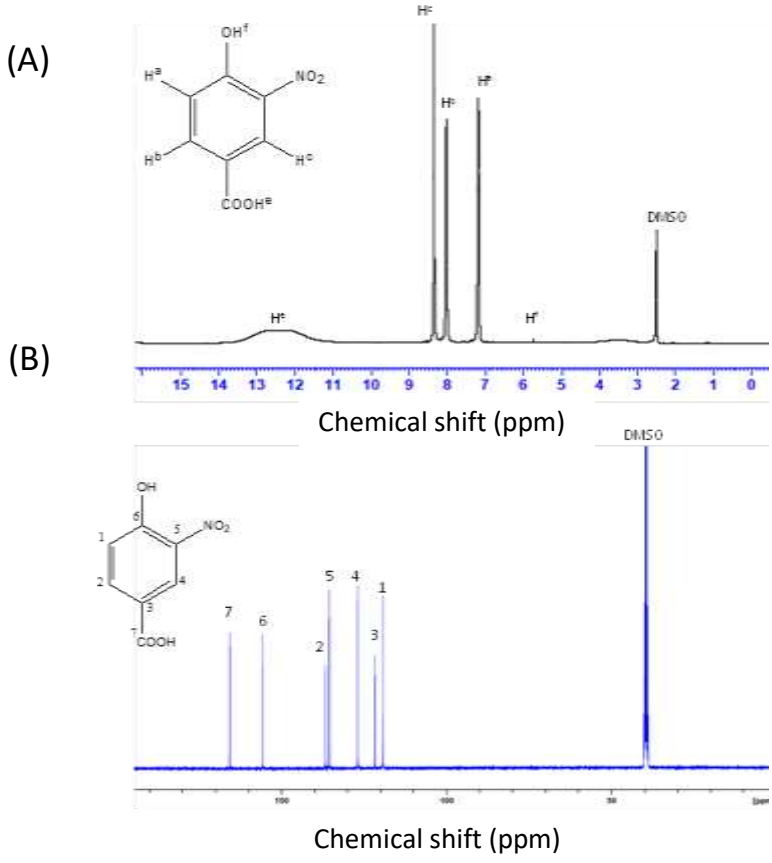

Figure 2.2 NMR spectra of 4-hydroxy-3-nitrobenzoic acid (HNBA). (A) ^{1}H NMR, (B) ^{13}C NMR

.

2.2.4 *Synthesis of 4-hydroxy-3-nitrobenzoic acid methyl ester (HNBAm):*

A catalytic amount of conc. sulfuric acid was added to methanol solution (10 mL) of HNBA (0.66 g, 3.6 mmol). The reaction solution was refluxed for 24 h and evaporated. The resulting solids were washed with pure water and dried under vacuum to obtain HNBA methyl ester (HNBAm; yield 0.45 g, 63.4%). ^{1}H-NMR (400 MHz, DMSO-d_6, δ, ppm): 3.88 (s, 3H), 7.96 (dd, 1H, J = 8.8 Hz), 7.16 (dd, 1H, *J* = 8.8 Hz), 8.35 (s, 1H); ^{13}C-NMR (400 MHz, DMSO-d_6, δ, ppm): 39.8,51.7, 119.8,121.5, 128.5, 137.2, 138.3, 157, 165.4.

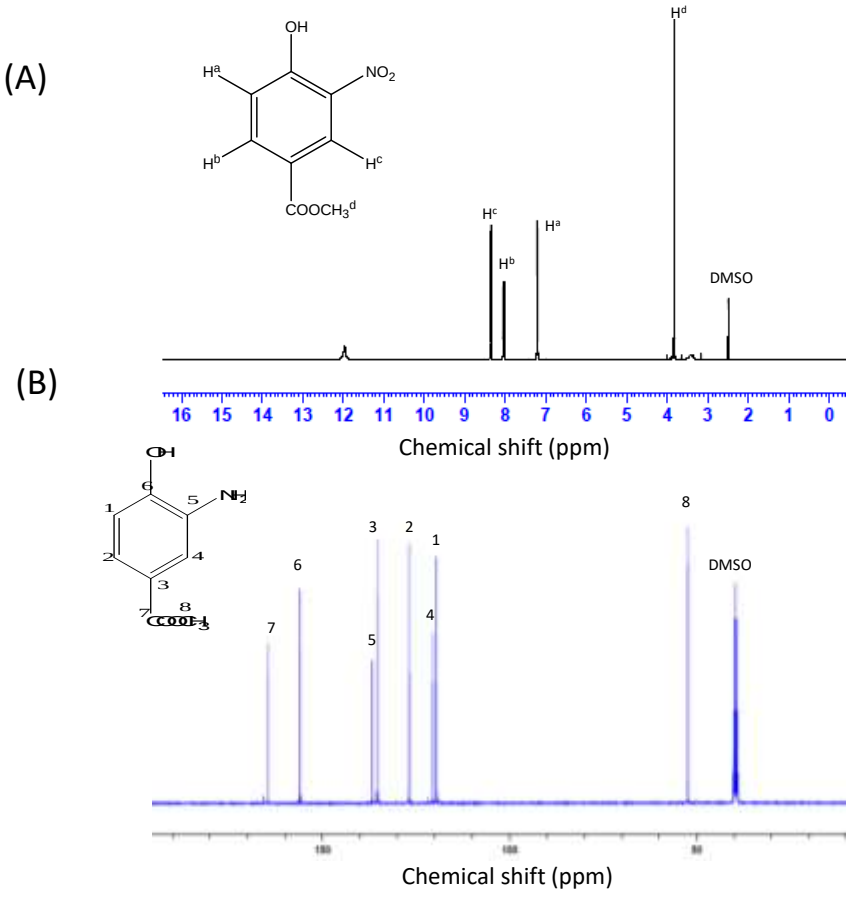

Figure 2.3 NMR spectra of 4-hydroxy-3-nitrobenzoic acid methyl ester (HNBAm). (A) ^{1}H NMR, (B) ^{13}C NMR

2.2.5 *Synthesis of 4-amino-3-nitrobenzoic acid (ANBA):*

HNBAm (0.39 g, 2 mmol) was dissolved in *N*,*N*-dimethylacetamide (12 mL) and the solution was stirred for 1.5 h at room temperature, then potassium carbonate (0.84 g, 6 mmol) was added. 2-Bromoisobutylamide (1.00 g, 6 mmol) was added to the solution, which was stirred for 48 h at 60°C, then KOH (1.00 g, 18 mmol) was added and the reaction solution was stirred overnight. After HCl was added to the reaction solution, the solution was evaporated. The resulting solid was washed with hexane and water, and dried under vacuum to obtain 4-amino-3-nitrobenzoic acid (ANBA, yield; 0.26 g, 72.2%). ^{1}H-NMR (400 MHz, DMSO- d_6, δ, ppm): 7.03 (dd, 1H, J = 8.0 Hz), 7.82 (dd, 1H J = 8.2 Hz), 8.52 (s, 1H), 12.82 (s, 1H); ^{13}C-NMR (400 MHz, DMSO- d_6, δ, ppm): 39.8, 117.2, 120.7, 122.1, 128.5, 131.5, 133.8, 143.2, 148.7, 169.2.

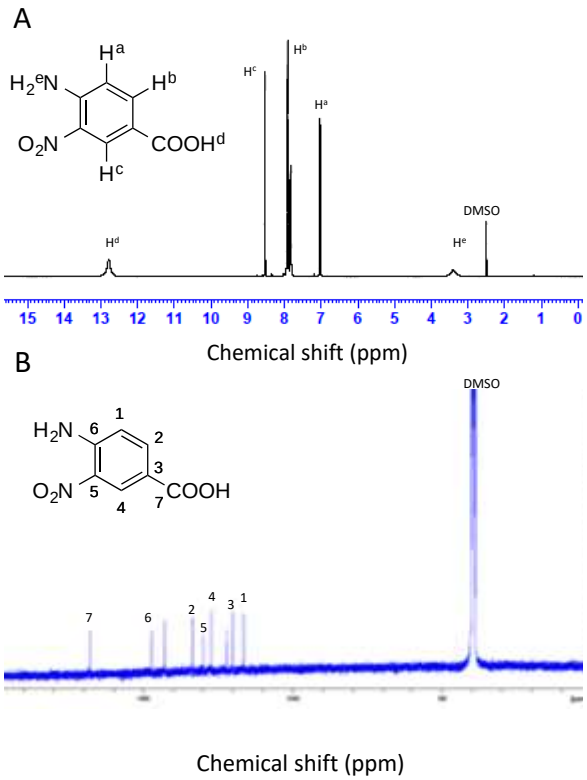

Figure 2.4 NMR spectra of 3-nitro-4-aminobenzoic acid methyl ester (ANBA). (A) ^{1}H NMR, (B) ^{13}C NMR

2.2.6 *Synthesis of 3, 4-diaminobenzoic acid hydrochloride (DABA.2HCl):*

ANBA (0.36 g, 2 mmol) was dissolved in methanol (20 mL), to which palladium-charcoal (0.21 g, Pd content: 5%) was added. The reaction mixture was stirred for 2 h with a continuous hydrogen supply at room temperature. After the palladium-charcoal catalysts were removed by filtration, HCl was added to the filtrate to precipitate 3,4-diaminobenzoic acid hydrochloride (DABA•2HCl). After vacuum drying, 0.28 g (62.2% yield) of DABA•2HCl was obtained. 1H-NMR (400 MHz, DMSO-d_6, δ, ppm): 6.84 (dd, 1H, J = 9.2 Hz), 7.63 (dd, 1H, J = 9.0 Hz), 7.75 (s, 1H), 10.2 (s, 1H); 13C-NMR (400 MHz, DMSO-d6, δ, ppm): 39.8, 117.2, 118.1, 119.5, 126.5, 130.2, 140.2, 167.1.

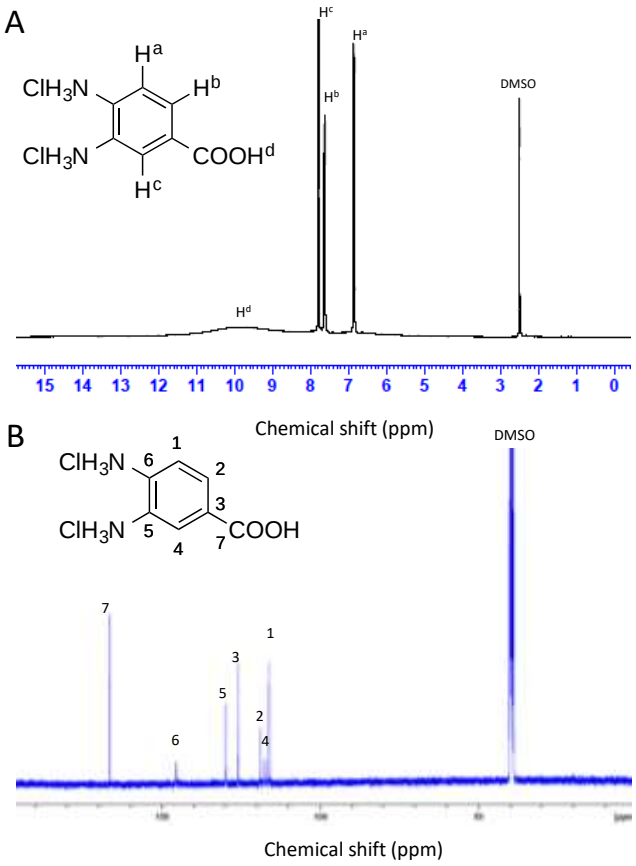

Figure 2.5 NMR spectra of 3, 4-diaminobenzoic acid. Hydrochloride salt (DABA.2HCl) (A) ^{1}H NMR, (B) ^{13}C NMR

2.2.7 *4-aminobenzoic acid (PABA):*

Previous in *chapter 1* we have already described regarding the bio-availability of 4-aminobenzoic acid (PABA) from various natural sources. The aminodeoxychorismate synthase PabAB converts chorismate to 4-amino-4-deoxychorismate. Subsequently, the 4-amino-4-deoxychorismate lyase PabC converts 4-amino-4-deoxychorismate to ABA (Scheme 2.5). Bio-derived PABA was kindly donated by our collaborator Prof. Naoki Takaya, University of Tsukuba.

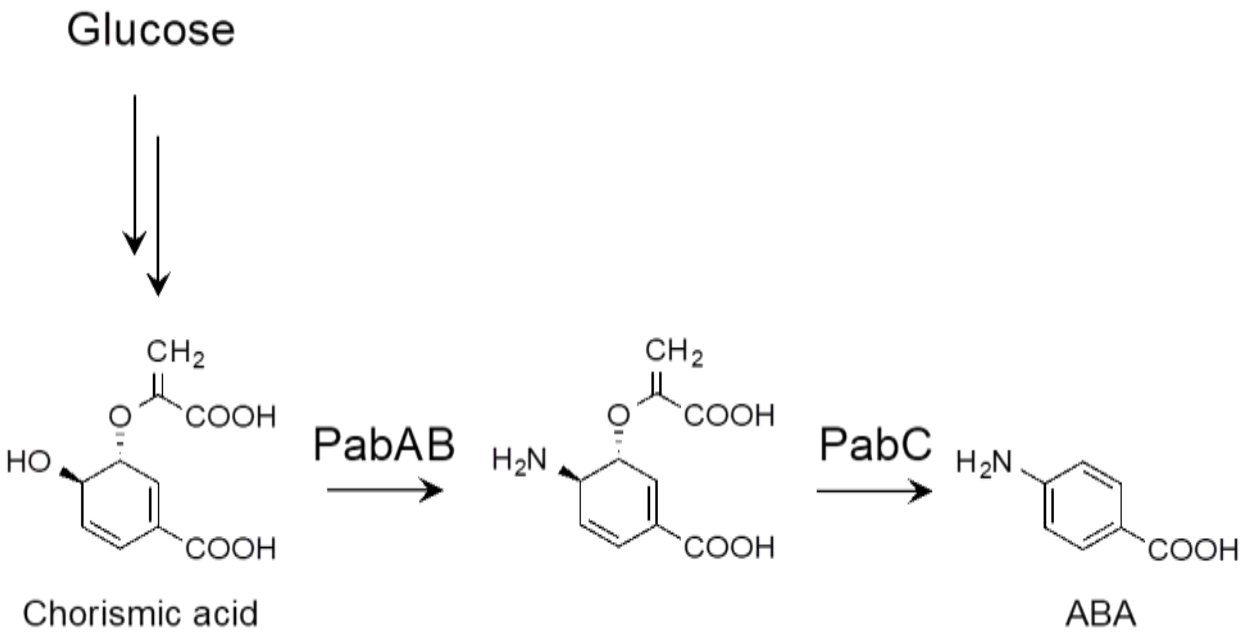

Scheme 2.5 Biosynthesis of 4-aminobenzoic acid (ABA)

However, we have purchased commercial PABA as well and below are the ^{1}H-NMR comparison between them (Figure 2.6).

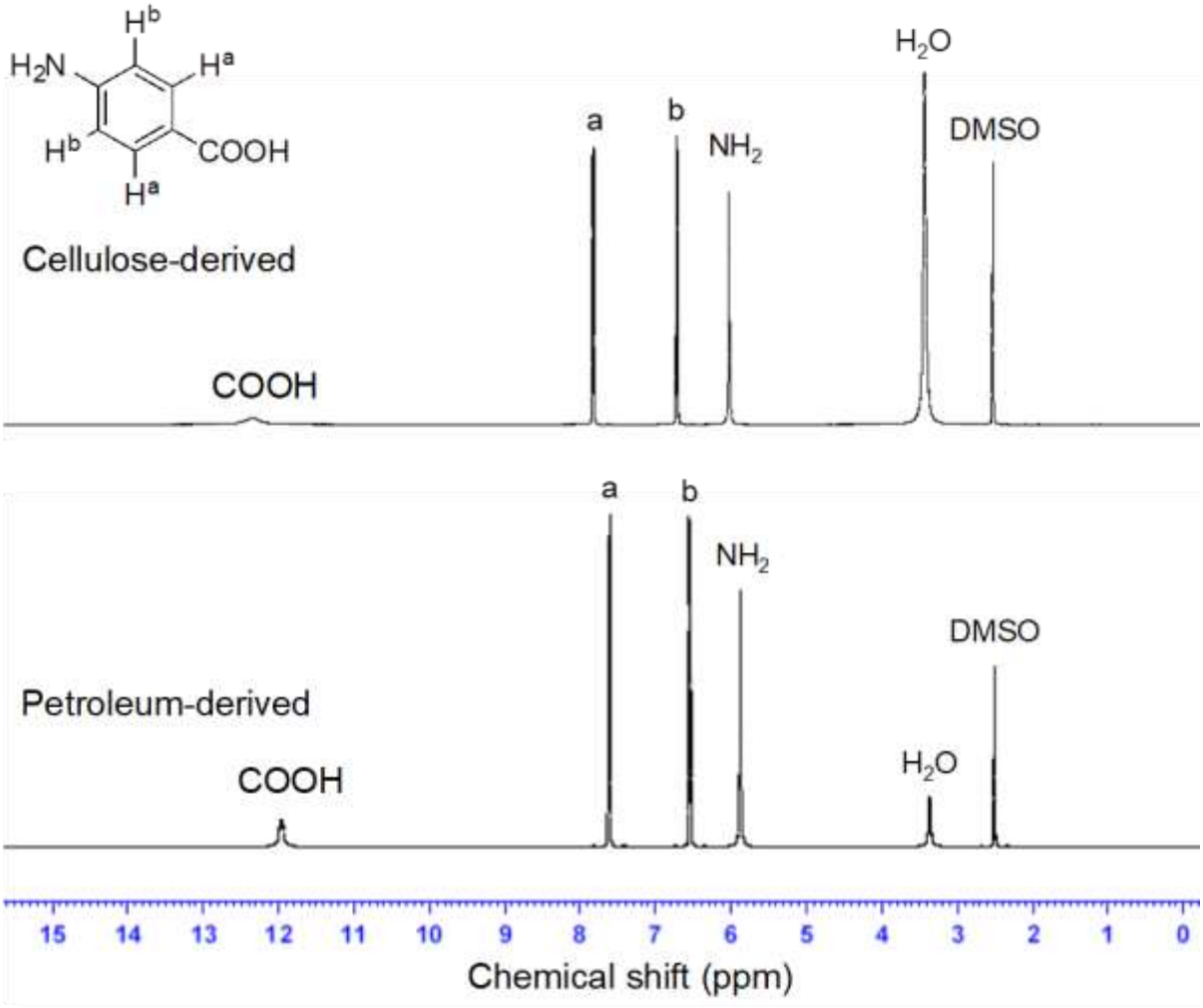

Figure 2.6 ^{1}H NMR spectra of cellulose and petroleum-derived ABA

Bio-derived 3,4-AHBA and PABA attained the purity level of their commercial alternatives, bio-based 3,4-DABA also successfully prepared using 3, 4-AHBA as the starting material. These monomers will be used further to make various polymers including their copolymers for various purposes. Different functionalization can introduce different properties in the polymers.

2.3 High performance benzazole synthesis using bio-based monomers:

Bio-derived 3, 4-AHBA was polymerized to prepare 2, 5-polybenzoxazole (ABPBO) which is a kind of benzazole with N and O atom at 1 and 3 positions respectively. Polybenzoxazole has a rigid cyclic structure of high strength because of π-π stacking. It shows high heat resistance and can be used for harsh environment like- protective apparels and satellite making instruments. Polybenzimidazole is anather kind of polybenzazole structure having N- and O-atom at 1 & 3 positions respectively. It shows better insulating properties, high heat resistance than polybenzoxazoles. It can be used in making semiconductor equipment and electrical equipment as they have special structural properties of conductivity nature. They can be used to prepare high heat resistant, proton conductive films to be used in fuel cells (4-5).

2.3.1 *Polybenzoxazole syntheses:*

2.3.1.1 *Salt preparation:*

3, 4-AHBA (1.2 g, 6.3 mmol) was dissolved in 20 ml methanol while keeping on an ice-bath. Hydrochloric acids (12 N, approx. 0.6 ml) was added dropwise to this solution and the mixture was allowed to stir at room temperature for 4 hr. The brown colored product, 3-amino 4-hydroxybenzoic acid hydrochloride (3, 4-AHBA.HCl) was obtained after evaporating the solvent under reduced pressure, (yield; 1.47 g, 97 %). The structure of the resulting product was confirmed by ^{1}H NMR.

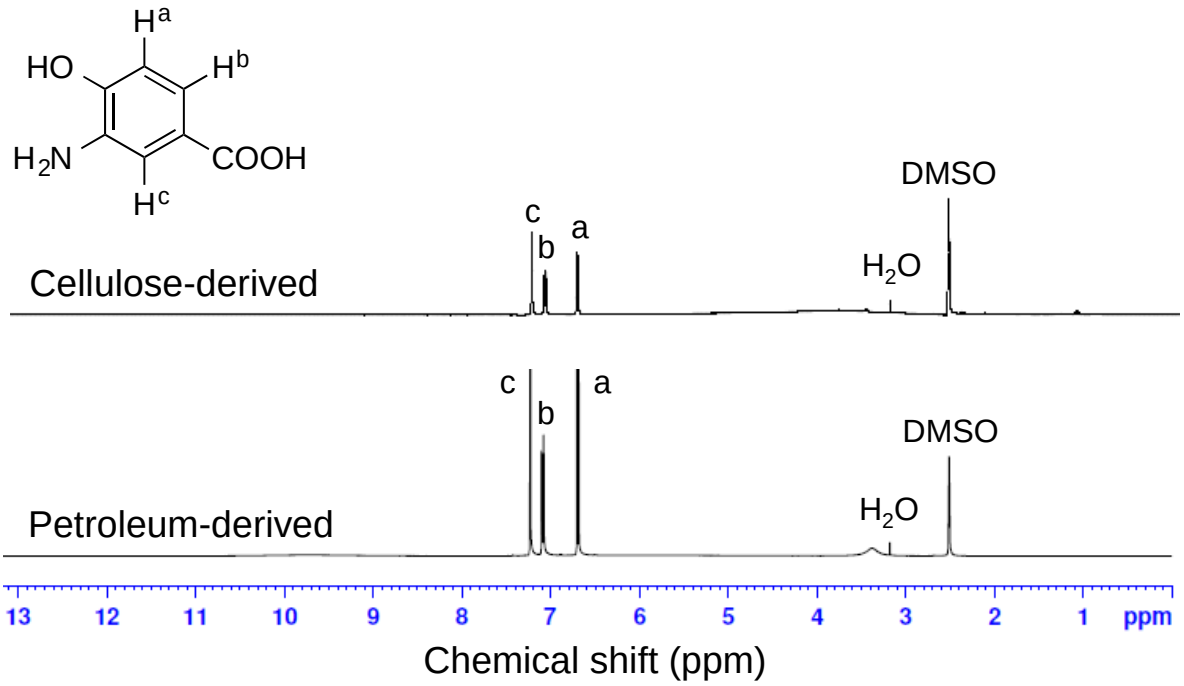

Figure 2.7 ^{1}H-NMR spectra of 3, 4-AHBA and 3,4-AHBA·HCl (salt)

2.3.1.2 *Polymerization:*

A typical procedure was followed to polymerize this salt monomer (3, 4-AHBA. HCl) by polycondensation and polyphosphoric acid (PPA) has been used as polymerization solvent. A three-necked flask fitted with a mechanical stirrer and a nitrogen inlet was charged with 30 g of PPA and dried by thermal treatment at 100 °C for 2 h. Subsequently, 1.137 g (6 mmol) of 3, 4-AHBA.HCl was added slowly into the flask with continuous nitrogen flow, the mixture was stirred at 170 °C until it became viscous and then after 4 h temperature was raised to 200 °C for 9 h for completing the polymerization. The viscosity of the reaction increased quickly with the temperature and reaction time, color changed to deep brown. The resulting viscous solution was precipitated in 200 mL of deionized water to obtain fibrils. The fibrils were filtered out and washed once with deionized water, followed by repeated washing with an aqueous solution of 1 M KOH (10%) and deionized water until the pH of the cleaning liquid reached 7 (measured using pH test paper, Macherey-Nagel GmbH & Co. KG, Düren,

Germany). The polymer powder was dried at 150 °C under vacuum to remove the water completely (yield; 90-95 wt%). The polymer powder was heated to 400 °C under vacuum for complete cyclization to get poly (2, 5-benzoxzole) (ABPBO).

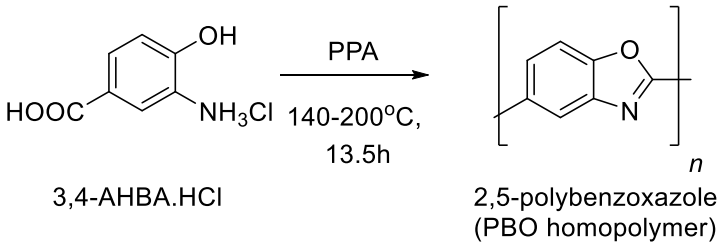

3,4-AHBA.HCl

2,5-polybenzoxazole
(PBO homopolymer)

Scheme 2.6 Polybenzoxazole preparation scheme from 3, 4-AHBA.HCl salt

2.3.2 *Polybenzimidazole syntheses:*

2.3.2.1 *Salt preparation:*

3, 4-DABA (1.5 g, 10 mmol) was dissolved in 50 ml methanol in an ice-bath. To this solution, 12 N hydrochloric acid (approx.1ml) was added dropwise until the powder was completely dissolved, and the mixture was allowed to stir at room temperature for 24 h. The white-colored salt of 3,4-diaminobenzoic acid dihydrochloride (3,4-DABA. 2HCl) was obtained via solvent evaporation (yield; 2.13 g, 96 %). The structure of the resulting product was confirmed by ^{1}H NMR.

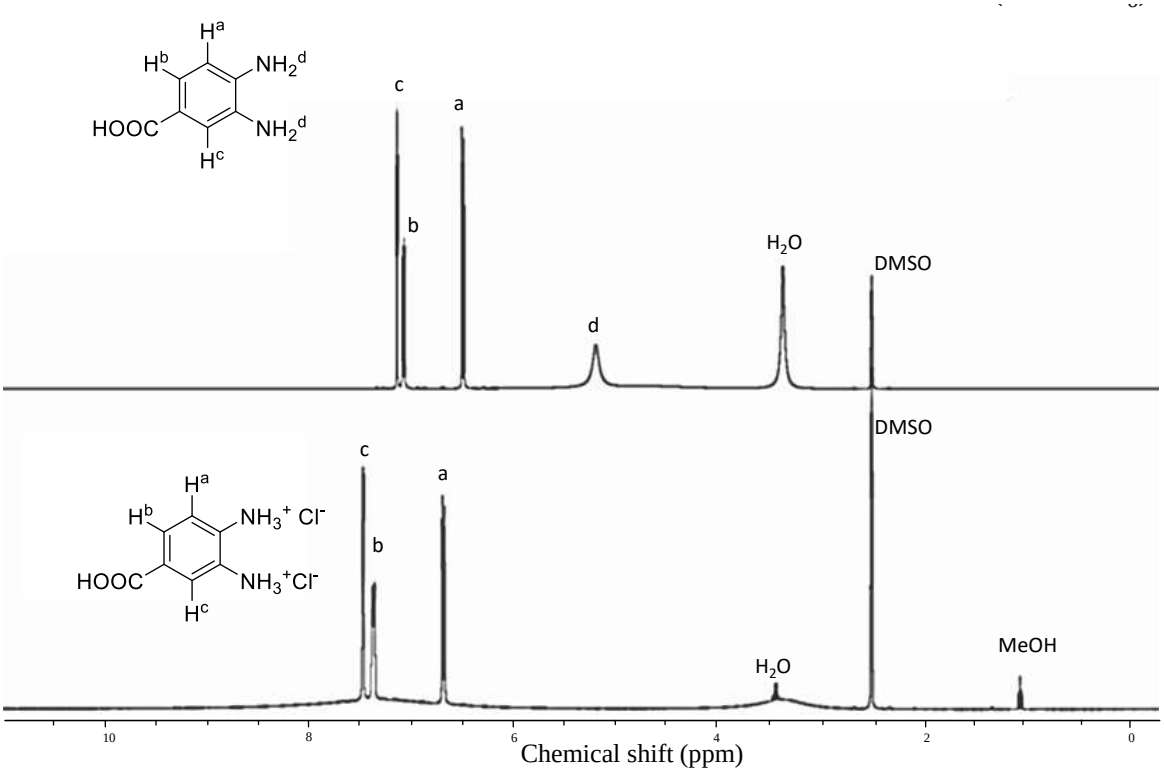

Figure 2.7 ^{1}H-NMR spectra of 3, 4-DABA and 3,4-DABA·2HCl (salt)

2.3.2.2 *Polymerization:*

DABA·2HCl (0.58 g, 2.6 mmol) and P_2O_5 (0.51 g, 3.6 mmol) were purged with nitrogen gas in a 30-mL round-bottomed flask and $MeSO_3H$ (4 mL) was added as solvent with a syringe, the polymerization mixture was stirred for 24 h at 150 °C. The resulting mixture was poured into pure water (100 mL) to form a spherical precipitate of the polyamide precursor of PBI, which was dried at 110 °C under vacuum. The resulting solids were ground into a powder with a mortar-mill, and were washed with pure water. After being dried under vacuum at 100 °C, the powder was heated stepwise at 100, 200, 300, and 400 °C (kept for 1 h at each step) under nitrogen to form poly(2,5-benzimdazole) (2,5-PBI; 0.23 g, 76.2%)

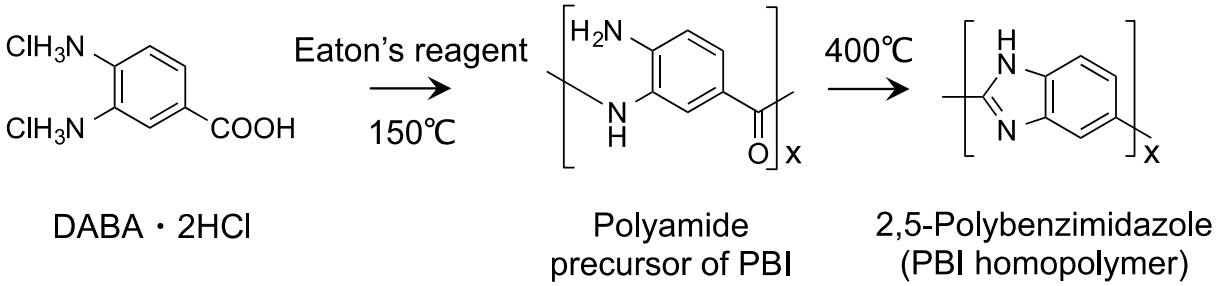

Scheme 2.7 Polybenzimidazole preparation scheme using 3, 4-DABA.2HCl salt

2.3.3 *Solubility test:*

Table 2.1 Solubility test of PBO and PBI homopolymers in various solvents

Solvent	PBI homopolymer	PBO homopolymer
DMSO	-	-
DMAc	-	-
m-cresol	-	-
1,2-dichlorobenzene	-	-
Dimethyl sulfate	-	-
NMP	-	-
TFA	-	-
TFA+MSA	+	+
MSA	+	+
H_2SO_4	++	++

+: Soluble at room temperature, ++: Highly soluble at room temperature, -: Insoluble at their boiling point

2.4 Structural characterization of polymers:

2.4.1 *^{13}C-NMR (solid state):*

Due to poor solubility to any conventional solvents available for solution state NMR we were only able to do solid state NMR evaluation, which is ^{13}C-NMR (cross polarization total side band suppression/CP-TOSS) and FT-IR analysis (Figure 2.8-2.10). The peaks of the polymers are assigned to the corresponding number. For the homopolymers PBO and PBI, five broad ^{13}C signals appeared for each (One shoulder for PBO case) between 110 and 170 ppm, and were assigned ppm appeared at a higher chemical shift value than that of the imidazole ring (155 ppm).

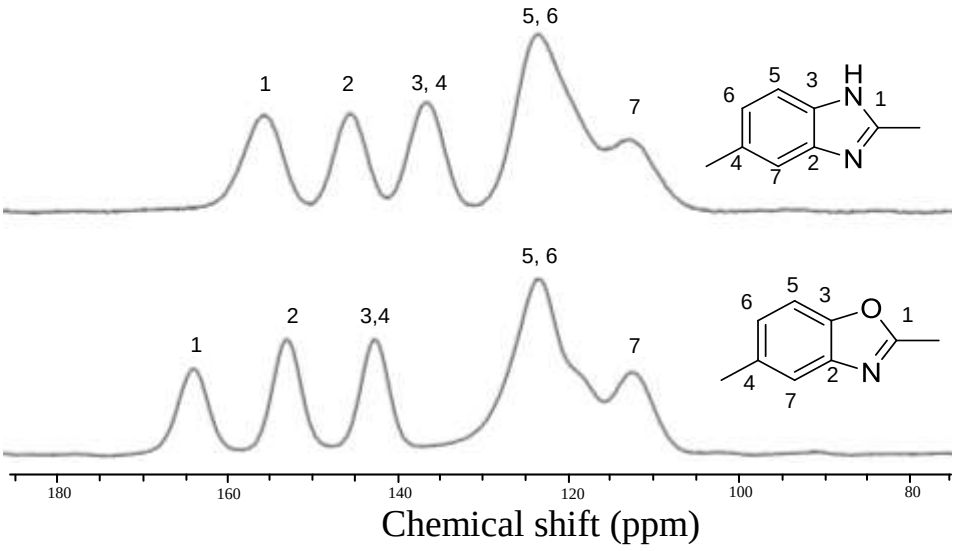

Figure 2.8 ^{13}C-NMR (CP-TOSS) spectra of polybenzimidazole and polybenzoxazole

2.4.2 *FT-IR analysis:*

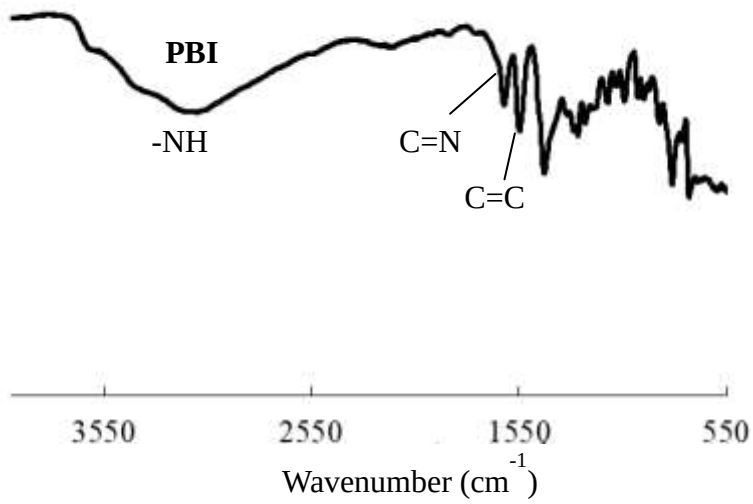

Figure 2.9 FT-IR spectrum of poly(2, 5-benzimidazole)

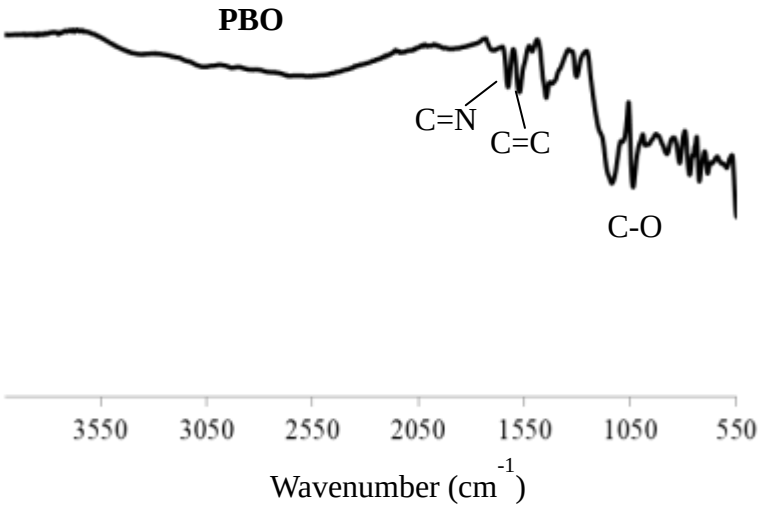

Figure 2.10 FT-IR spectrum of poly(2, 5-benzoxazole)

The stretching vibration of polybenzimidazole(PBI) spectra shows peaks for N-H, aromatic C-H and C=C and they were detected at 3100, 1450 and 1000 cm^{-1} along with the characterized C=N peak appears at 1690 cm^{-1}. For polybenzoxazole (PBO) the aromatic alkene (C=C) at 1637 cm^{-1} and for imine (C=N) at 1559 cm^{-1} bands, also, carboxylic acid (C-O) stretch was observed at 1331 cm^{-1}.

2.4.3 *Film casting:*

Film casting method was almost similar in both the cases for PBI and PBO polymers. The polymer powder was dissolved in the TFA and CH_3SO_3H (2–3%) mixture to obtain a 15 wt% solution in a flask. Nitrogen was bubbled into the closed flask to expel oxygen from the solution. The solution was heated and kept at 65 °C for 15–18 h to be homogeneous. If some solids remained insoluble, they were removed by filtration. The resulting homogeneous solution was cast over a glass substrate to make a film. The film was peeled from the glass substrate and dipped in KOH aqueous solution (10%) for 12 h, followed by drying under vacuum, with the temperature increasing at a rate of 0.8–1.0 °C min^{-1} to 200 °C and keeping at 200 °C for 15 h to remove the residual solvents. After cooling spontaneously, a tough brown film was obtained.

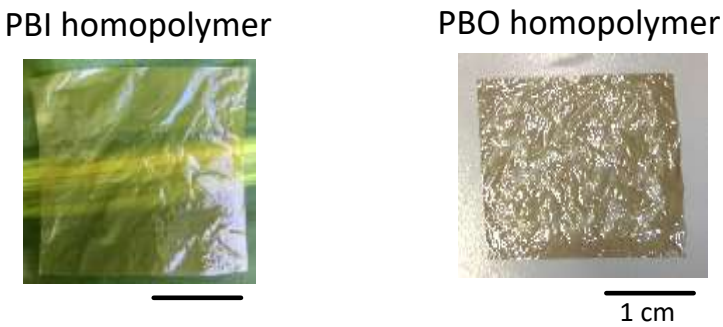

Figure 2.11 Film/membrane obtained using polymer powders for both PBI and PBO

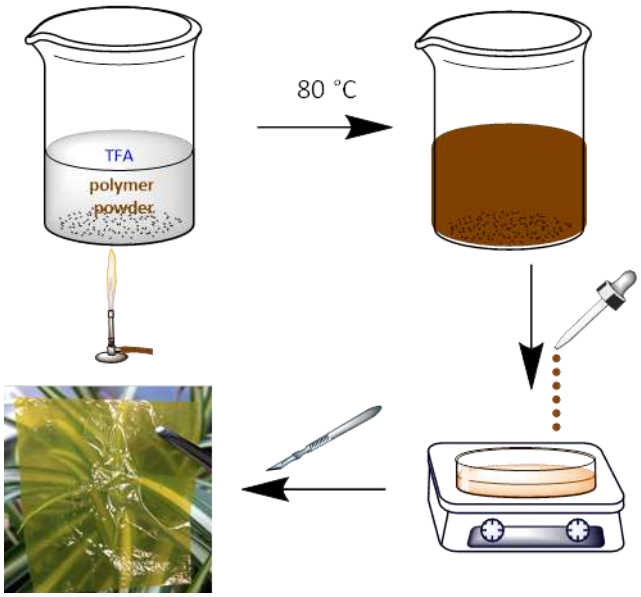

Scheme 2.7 Film casting method by using TFA: CH_3SO_3H (2-3%) as solvent

2.4.4 *Thermal and mechanical analyses:*

TGA of both the polymers polybenzimidazole (PBI) and polybenzoxazole (PBO) were analyzed. Both of these aromatic bio-based polymer structures have to be highly thermally stable. TGA was conducted using a Hitachi STA7200 as follows. Samples (< 5 mg) were placed in a platinum crucible and heated to the maximum temperature of 800°C at a rate of 5°C min^{-1} in an air and nitrogen atmosphere. The residual polymer yield (char yield) was determined, with the temperatures at the starting of degradation (T_{onset}), 1% mass loss (T_{d1}), and 10% mass loss (T_{d10}).

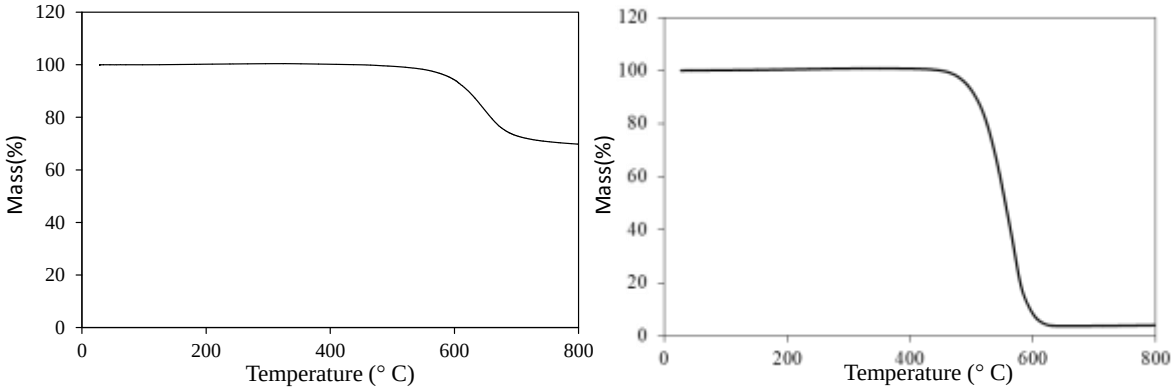

Figure 2.12 TGA curves of PBO homopolymer under air and N_2 atmosphere

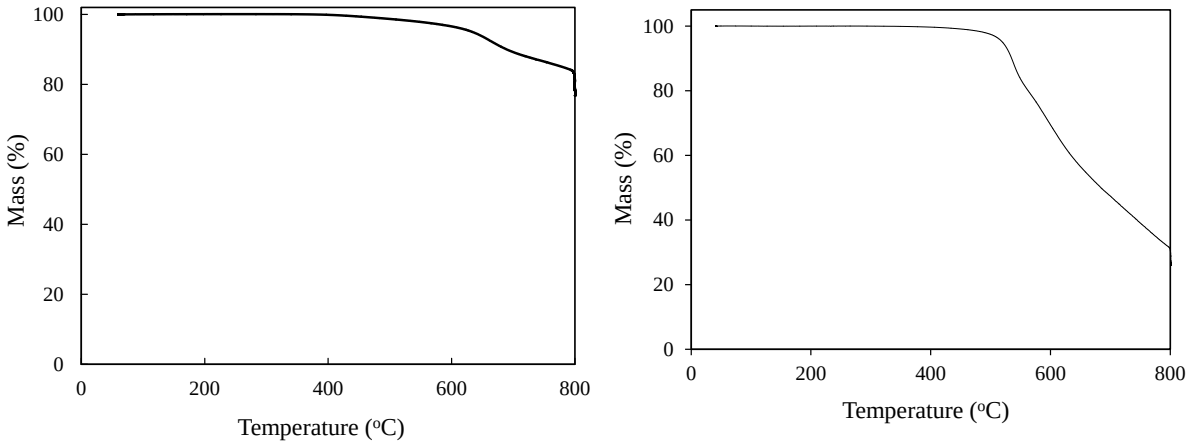

Figure 2.13 TGA curves of PBI homopolymer under air and N_2 atmosphere

Figure 2.12 and 2.13 shows thermogravimetry curve for PBI and PBO homopolymers respectively along with their 5% and 10% weight loss temperatures (T_{d5} and T_{d10}). Containing highly stable aromatic structure and benzazole moiety both PBI and PBO homopolymers show high thermal stability. In case of PBO homopolymer, 5% degradation temperature (T_{d5}) and 10% weight loss temperature (T_{d10}) were found to be 594 and 622 °C under N_2 atmosphere while those of corresponding temperatures were found to be at 421 and 449 °C under air atmosphere. In case of PBI homopolymer, 5% degradation temperature (T_{d5}) and 10% weight loss temperature (T_{d10}) were found to be at 635 and 700 °C under N_2 atmosphere

while those of corresponding temperatures were found to be at 495 and 535 °C under air atmosphere.

Stress-strain analysis of the films prepared over a 10 mm length was performed in the elongation mode with crosshead speed at 1 mm s^{-1} at room temperature using a tensile testing machine (3365-L5, INSTRON) with a load cell (5 kN). The stress-strain curves (Figure 2.14) of five specimens were averaged to obtain mean values for Young's moduli (E), tensile strength (σ), and elongation at break (ε). PBI homopolymer film showed tensile strength (75 MPa) higher than PBO homopolymer (53 MPa) and Young's modulus values are 3.6 and 2.8 GPa respectively. The value for tensile elongation at break in case of PBI homopolymer is 2.6%, on the contrary corresponding value for PBO homopolymer is more than 15%. After obtaining the above mechanical data we can conclude that PBI films are stronger as compared with the PBO film, however, PBO films are more flexible than PBI films.

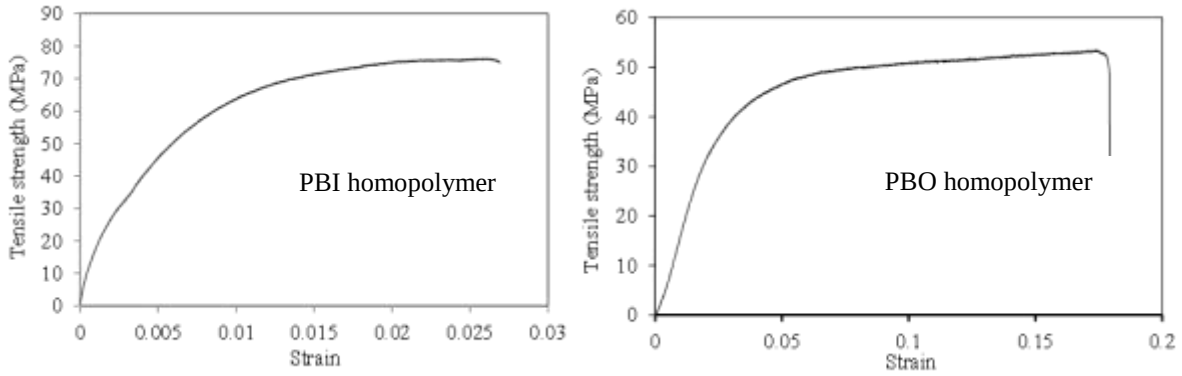

Figure 2.14 Mechanical stress-strain curve of PBI and PBO homopolymers

2.5 Conclusion:

The chapter focused on the syntheses of novel bio-derived and bio-based monomers to synthesize benzazole type of polymers. New route for the syntheses of diamine (3, 4-DABA) starting from bio-derived aromatic molecule 3, 4-AHBA through few steps. All the steps and end products were confirmed using ^{1}H-NMR and ^{13}C-NMR to optimize the reaction condition for each step. Bio-based polymers (such as: poly(2, 5-benzoxazole) from 3, 4-AHBA and poly(2, 5-benzimidazole) from 3, 4-DABA) were prepared successfully for the first time using bio-derived monomers. Polymer structures were characterized using FT-IR and ^{13}C solid-state NMR spectra and their physical properties were also analyzed. Thermal stability of the polymers were determined using TGA and both of the bio-based polymers i.e. PBI and PBO homopolymers were found to be highly thermally stable and comparable with commercial high-performance plastics such as- Kapton^{TM}, Zylon^{TM} etc. Mechanical strength was also analyzed using tensile analysis, and both the polymer films were found to be strong enough to perform as engineering plastics, however, PBO film was found to be more flexible than PBI, while PBI film was found to be stronger than PBO film.

2.6 References:

1. Koronis, G., Silva, A., Fontul, M. *Composites Part B*, 2013, 44, 120.
2. Park, H. M., Misra, M., Drzal, L. T., Mohanty, A. K. *Biomacromolecules*, 2004, 5, 2281.
3. Terzopoulou, Z. N., Papageorgiou, G. Z., Papadopoulou, E., Athanassiadou, E., Alexopoulou, E., Bikiaris, D. N., *Ind. Crop. Prod*., 2015, 68, 60.
4. Fan, J., Shi, Z., Tian, M., Yin, J. *RSC Adv.*, 2013,3, 17664.
5. Friedrich, K., Sue, H.J., Liu, P., Almajid, A. A. *Tribiol. Int.*, 2011, 44, 1032.
6. Truce, W. E., Kreider, E. M., Brand, W. W. "The Smiles and Related Rearrangements of Aromatic Systems", Organic Reactions, Inc. Published by John Wiley and Sons, Inc., 2011.
7. Xiang, J., Xie, H., Wen, D., Dang, Q., Bai, X. *J. Org. Chem*., 2008, 73 (8), 3281.
8. Lim, J. G.; Gupta, B.S.; George, W. Prog. *Polym. Sci.* 1989, 14, 763.
9. Suh, D. H.; Ju, S. Y.; Park, S. H.; Lee, J. W. J. *Macromol. Sci. Pure Appl. Chem.* 2001, 38, 751.
10. Morgan, P. W. *Macromolecules* 1977, 10, 1381.
11. Lin, J.; Sherrington, D. C. *Adv. Polym. Sci.* 1994, 111, 176.
12. Chung, H., Yang, J. E., Chae, T. U., Shin, j. H., Gustavsson, M., Lee, S. Y. *Curr. Opin. Biotechnol.* 2015, 36, 73.

Chapter 3:

Syntheses and characterization of various high-performance copolymers using bio-based monomers and property analysis for their various applications

3.1 Abstract:

Development of various bio-plastics from cellulosic biomass is a prerequisite for establishing a sustainable society. High-performance bio-based plastics can make a major contribution to environmental sustainability. Here, we developed biomass-derived, high-performance polybenzimidazole (PBI) plastics. 3-amino-4-hydroxybenzoic acid was produced from an enzymatic hydrolysate of kraft pulp (a cellulosic feedstock) by a metabolically engineered bacterium, and was chemically converted to 3, 4-diaminobenzoic acid (DABA). DABA was polymerized to form poly(2,5-benzimidazole) (2,5-PBI). Copolymerization of DABA with cellulosic biomass-derived 4-aminobenzoic acid (15 mol%) increased the 10% mass-loss temperature (an indicator of thermal stability) of the resulting polymer film to 743 °C, probably owing to more inter-chain hydrogen bonds. This ultrahigh heat-resistant bioplastic film could be used as a heat-resistant polymer composites formed in not-reported combination with light metals and/or inorganics. A series of high-performance poly(2,5-benzoxazole-*co*-2,5-benzimidazole)s (PBO-*co*-PBI) bio-based plastic films, were developed using the aromatic biomolecule 3-amino-4-hydroxybenzoic acid and the commercial product 3,4-diaminobenzoic acid. The partially bio-based PBO-*co*-PBI films exhibit higher thermal and mechanical performance than conventional bio-based polymers such as polyamide 11 or poly(lactic acid). The robust PBO-*co*-PBI films exhibit lower dielectric constants (ε_r) than conventional high-performance aromatic polymers, attaining the value comparable to those of polyethylene or polypropylene.

Keywords: bioplastics, cellulose, high performance polymers, polybenzimidazole, Polybenzoxazoles, Low-*k*.

3.2 Introduction:

Development of bio-based plastic is requisite for the establishment of low carbon and green-sustainable society. Conventional bio-based polymers known were mainly aliphatic polyesters such as poly-(lactic acid) produce low thermo-mechanical properties, and their applications are limited. In our laboratory bio-based polymers with rigid backbones has been already derived from cinnamic acid derivatives which are representative renewable aromatic resources, to develop polyarylates and polyimides. Plant-derived cellulosic feedstocks comprising cellulose, hemicellulose, and lignin are renewable, the most abundant feedstocks in the biosphere, and attractive alternatives to petroleum-derived feedstock [1, 2]. Conventional bioplastics are typically produced from edible sugars and starches, but a bio-based economy requires the development of various bioplastics from non-edible cellulosic feedstock [3]. Current bio-plastics are mainly composed of aliphatic polymers, limiting their applications owing to their low levels of thermal resistance. To overcome these limitations, bio-based aromatic compounds are promising starting materials for synthesizing thermo-resistant engineering plastics [4]. Although no thermoresistant engineering plastic has previously been developed from cellulosic biomass, aromatic polyureas, polyamides, and polyimides were recently produced from microbial fermentation products of glucose [5-7]. The thermal degradation temperatures of these three polymers (210, 273, and 425 °C, respectively) far exceed those of conventional aliphatic bioplastics, and enable their use as thermoresistant matrixes for next-generation composites with soft inorganic materials, such as oxidized indium and tin. These developments have opened new application fields for bioplastics in electronics, and subsequent improvements to bioplastics' thermoresistance could extend these fields further.

Polybenzimidazole (PBI) is the most thermostable plastic that is currently known. The benzimidazole bond responsible for the high thermostability comprises aromatic ortho-

diamines and one carboxylic acid. The simplest PBI monomer is 3, 4-diaminobenzoic acid (DABA); two DABA molecules can form a 2, 5-benzimidazole bond. Because no natural compound exists with the ortho-diaminobenzoic acid backbone, we searched for compounds that can be (i) converted to ortho-diaminobenzoic acid without employing complex chemical reactions, and (ii) produced in large amounts by a microorganism. Finally, we selected 3-amino-4-hydroxybenzoic acid (AHBA) as an ideal precursor of DABA. Members of our research group discovered two enzymes that facilitate the production of AHBA from the bacterium *Streptomyces griseus* [28] and generated the recombinant *Corynebacterium glutamicum* strain KT01 for the production of AHBA [29]. Copolymerization of DABA with a small amount of a monoaminobenzoic acid introduces amide bonds into the PBI, and may control its thermal performance [30]. We selected 4-aminobenzoic acid (ABA) as such a comonomer. ABA is a monomer of a popular high-performance polyamide, *para*-aramid, and can be produced by recombinant bacteria capable of converting chorismate to ABA [31, 32]. Here, biomass-derived, high-performance polybenzimidazole (PBI) plastics were developed using 3-Amino-4-hydroxybenzoic acid, which was produced from an enzymatic hydrolysate of kraft pulp (a cellulosic feedstock) by a metabolically engineered bacterium, and was chemically converted to 3, 4-diaminobenzoic acid (DABA). Copolymer PBO-*co*-PBI was prepared using bio-derived AHBA and DABA which is another novel structure high-performance bio-plastic.

Recently, researchers' keen interest to prepare low dielectric constant (low-*k*) polymer materials is in focus for electronic industry such as: miniaturized dimensional electronic devices that can be used in ultra-large-scale integration (ULSI) circuits [8-10]. Polyethylene (PE) and polypropylene (PP) are low-k materials, but their applications are limited by their low thermal stability (<105 °C) [11]. Various different polymer nanocomposites (e.g. SiO_2, graphene oxide etc.) were prepared to meet the expectation of low-*k* and high-performance

together. On addition, fluorine substituted side-chains, non-polar polymers [10, 13] exhibiting low dielectric constant of 2.7. Additionally incorporating porosity in the polymeric materials can also achieve ultralow-*k* values (≤ 2.0) but compromise with their thermo-mechanical stabilities. Polyimides were long been used as high-performance insulating material for microelectronics and optoelectronics [10, 14]. Our molecular design strategy for low-k polymers is the use of aromatic rings connected via non-polar ring-type linkages [10, 12, 14]. PBOs are already well-known materials for their low dielectric constant and synthesized through fluorination or trifluoromethylation by many groups [15-17], but still ultralow-*k* PBOs were not developed yet. Bio-based ABPBO structure consists of considerable thermo-oxidative stability, excellent mechanical strength, and superior chemical resistance [10, 12, 13]. Preparation of PBO-*co*-PBI for low-*k* materials and investigate the effect of polarity of benzazole rings by changing O to –NH, i.e. oxazole to imidazole.].

We have used the aromatic biomolecule 3-amino-4-hydroxybenzoic acid (3, 4-AHBA), which is produced by fermentation using Streptomyces griseus [19, 20] and as a bio-derived monomer for polyesters, polyanilines, poly(benzoxazoleamide), and poly(benzoxazolediazole) [21-24]. 3, 4-AHBA is also well known as a monomer of poly(2,5-benzoxazole) (ABPBO) [25]. Here, we report the preparation of PBO-*co*-PBI for low-k materials and investigate the effect of the polarity of benzazole rings by converting the O to NH, that is, oxazole into imidazole [26]. We found that benzazole was very effective for creating low-*k* materials, and that polarity control is significant for balancing thermo-mechanical and dielectric properties [27].

3.3 Experimental

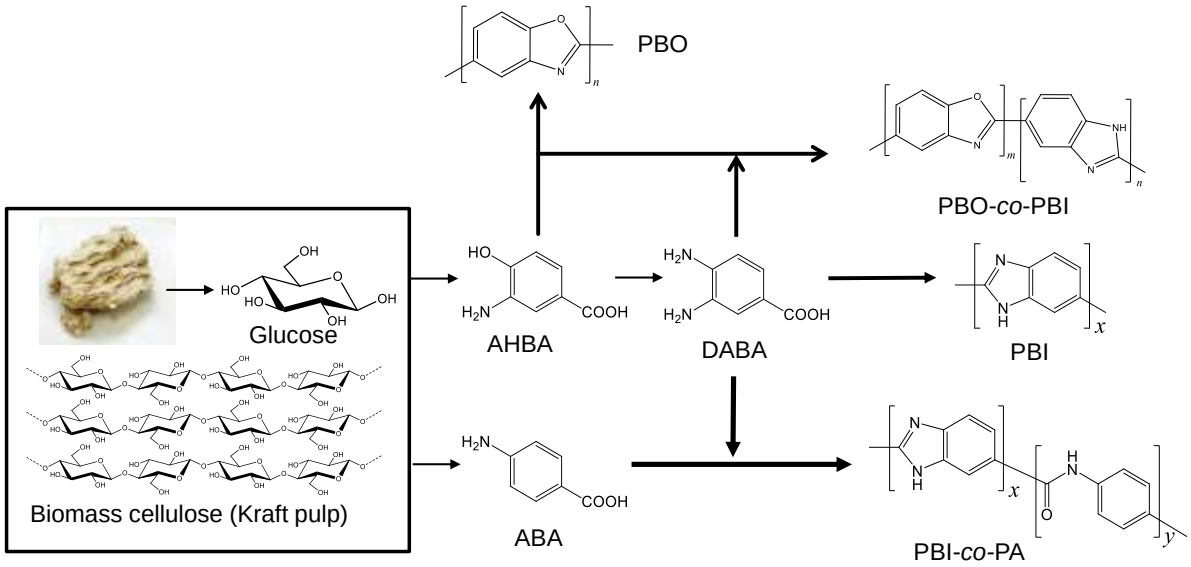

Scheme 3.1 Synthetic scheme of this chapter to synthesize various copolymers using biomaterials

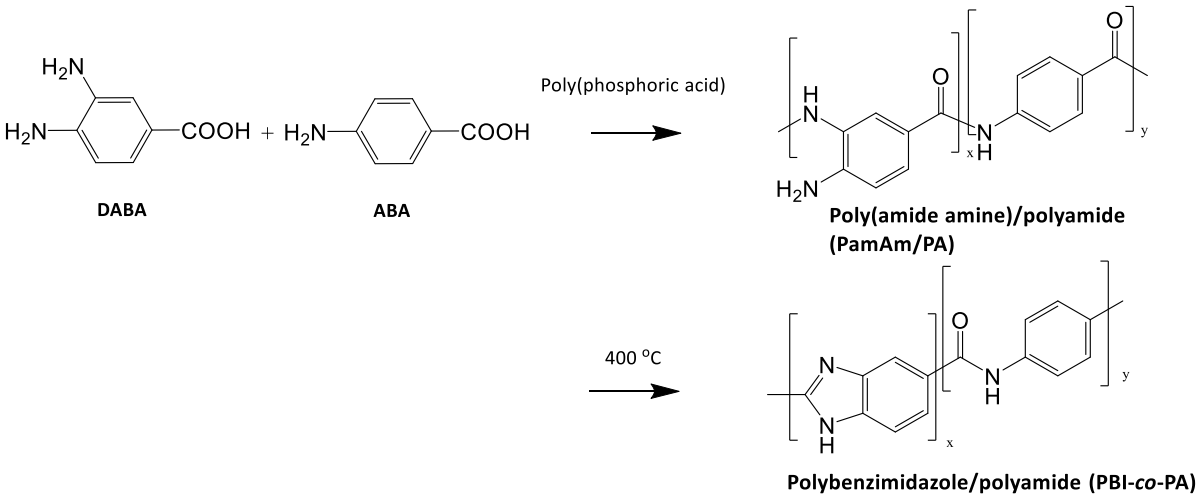

Scheme 3.2 Synthesis of copolymer poly(benzoxazole-*co*-amide) from DABA and ABA

3.3.1 *Preparaition of copolymer PBI-co-PA:*

As describe in the scheme 3.2 15 g of polyphosphoric acid (PPA) was taken in a three necked round bottom flask. To remove all the remaining moisture, the flask was heated at 120° C for 1 h under continuous N_2 flow. To prepare various copolymer compositions, amounts of two monomers i.e. 3, 4-DABA and PABA were calculated according to the desired weight %. They were mixed well and added carefully into the flask maintaining the N_2 atmosphere, the mixture was further heated for another 1 h at 120 °C. Temperature was maintained then at 160° C for next 4 h and 220 °C for next 16 h to complete the polymerization while maintaining continuous N_2 flow. Viscous brown polymeric mixture was obtained which was precipitated in 200 ml of water and polyamideamine-polyamide (PAA/PA) was formed. Sticky rubber like polymer was then dried at 110° C for 4 h and crushed to make powder which contains unreacted PPA. 10% KOH solution has been prepared and the PAA/PA powder was dissolved overnight in KOH solution. The solution was filtered and neutral pH was maintained by repetitive washing with water, dried and neutral PAA-PA was obtained. PAA/PA was further thermally cyclized by stepwise heating to 400° C under N_2 atmosphere to form imidazole ring and polybenzimidazole-polyamide (PBI-*co*-PA) was prepared. All different composition copolymers were obtained by following the same method.

3.3.2 *Preparaition of copolymer PBO-co-PBI:*

A typical synthetic procedure for PBO-*co*-PBI is given below for a PBO composition of 50% (Scheme 3.3). A three-necked flask fitted with a mechanical stirrer and a nitrogen inlet was charged with poly(phosphoric acid) (PPA) and dried by thermal treatment at 100 °C for 2 h. Subsequently, 1.13 g (5 mmol) of 3,4-DABA.2HCl and 0.947 g (5 mmol) of 3,4-AHBA.HCl were slowly added into 20 g of PPA. The mixture was stirred at 170 °C until it became completely viscous; the temperature was then maintained at 170 °C for 4 h and then raised to 200 °C for 9 h. The same temperature profile was utilized for polymers with other PBO:PBI

molar ratios. The viscosity of the reaction increased quickly with the temperature and reaction time, and the color of the solution changed from yellow to dark brown. The resulting viscous solution was precipitated in 200 mL of deionized water to obtain fibrils. The fibrils were filtered out and washed once with deionized water, followed by repeated washing with an aqueous solution of 1 M NaOH (10%) and deionized water until the pH of the cleaning liquid reached 7 (measured using pH test paper, Macherey-Nagel GmbH & Co. KG, Düren, Germany). The precursor polyamide, poly((*p*-hydroxy)-*m*-benzamide-co-(*m*-/*p*-amino)-*p*-/*m*-benzamide-) (*pre*-PBO-*co*-PBI), were dried at 150 °C under vacuum to remove the water completely (yield; 90-95 wt%). The *pre*-PBO-*co*-PBI powders were heated at 400 °C to induce conversion to PBO-*co*-PBI. Polymers with other copolymer compositions and homopolymers were synthesized using the same method, with only the amount of 3, 4-AHBA and 3, 4-DABA added being varied.

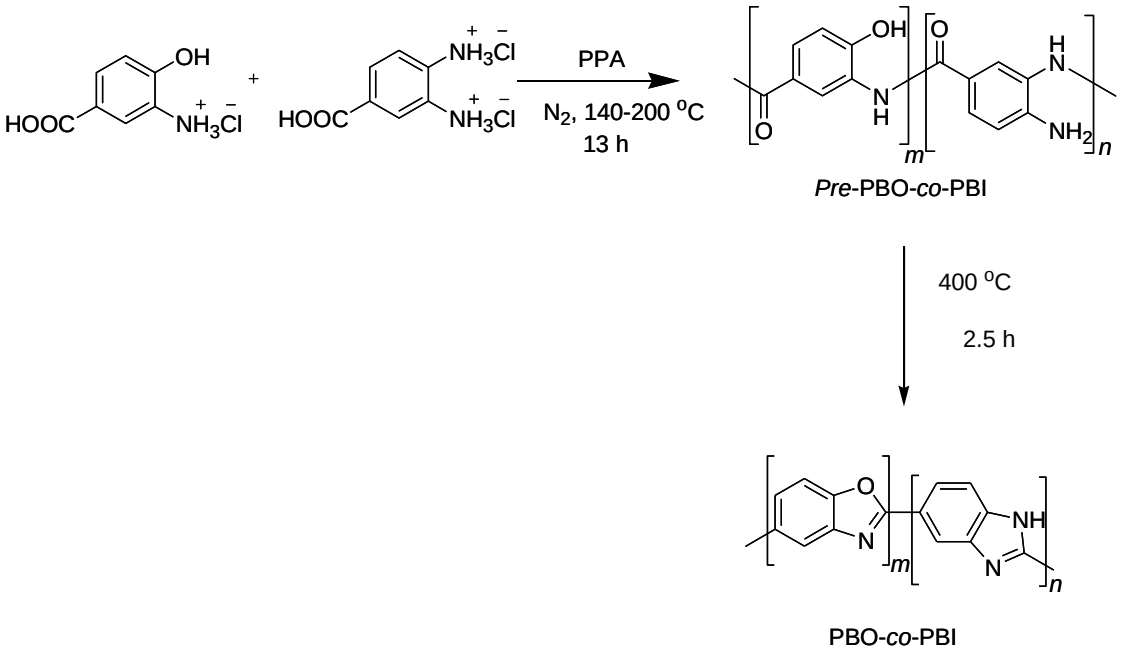

Scheme 3.3 Synthesis of copolymer poly(benzoxazole-co-benzimidazole) from DABA and AHBA

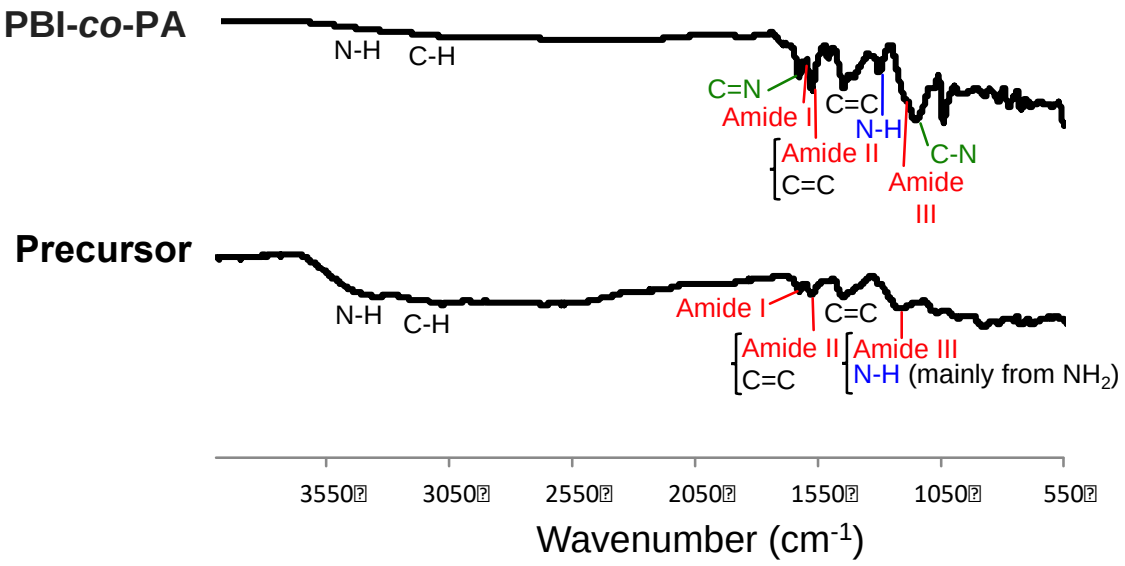

Figure 3.1 FT-IR spectra of PBI-*co*-PA and its precursor polyamide

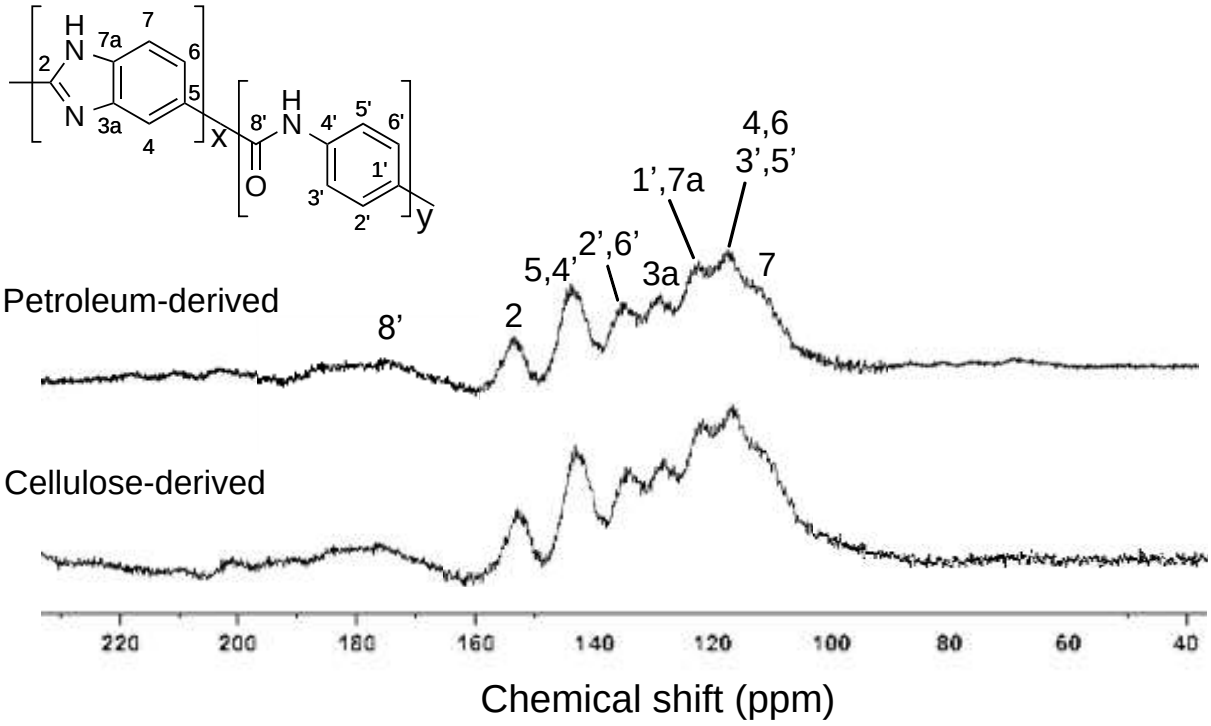

Figure 3.2 Solid-state ^{13}C-NMR spectrum (dipolar decoupled magic angle spinning; DD-MAS) of PBI-*co*-PA

3.3.3 *Structural characteristics of PBI-co-PA:*

The solid-state Fourier-transformed infrared (FT-IR) spectra of the polyamide precursors of PBI-*co*-PA were recorded on the Perkin-Elmer spectrum One spectrometer between 4,000 and 550 cm^{-1} using a diamond-attenuated total reflection accessory (Figure 3.1). The structures of cellulose-derived PBI-*co*-PA of 15 mol% ABA were further characterized by solid-state ^{13}C-NMR. In the PBI-*co*-PA of 15 mol% ABA, ^{13}C-NMR signals were detected between 110 and 190 ppm. All the carbons for benzimidazole and benzamide were assigned as shown in above Figure 3.2. In the polyamide precursor of PBI-*co*-PA, characteristic peaks of amide (amide I, amide II, and amide III) are clearly detected at 1635, 1570, and 1210 cm^{-1}, respectively. The peaks of carbon double bond (C=C) and N-H bond (mainly derived from the primary amine) overlap with those of amide II and amide III, respectively. In addition, N-H, aromatic C-H, and C=C are detected at 3360, 3060, and 1440 cm^{-1}, respectively. In the PBI-*co*-PA, which was produced by heating the precursor to 400 °C, all the amide peaks seemed to disappear. (Although some amides should remain, the amide content should not be high enough to be detected). However, a C=N peak appears at 1640 cm^{-1}, indicating that the unit consisting of an amide and a primary amine is converted into an imidazole ring.

We synthesized various PBI-*co*-PAs by a thermal cyclization reaction of the precursor polyamides having an amine group contiguous to each amide linkage. Thermogravimetric analysis (TGA) under nitrogen examined for the homopolymer of DABA and copolymers of DABA with ABA (DABA:ABA = 90:10, 85:15, and 80:20) to determine their thermal ring closing temperatures (Figure 3.3). In the temperatures ranging from 390 to 410 °C, the masses of all the PBI and PBI-*co*-PA precursors decreased by 8.1–11.7%, which agreed roughly with the theoretical mass loss by the elimination of one H_2O molecule per amide with a contiguous amine (e.g., 13.4% for the homopolymer of DABA and 11.0% for the copolymer with 20 mol% ABA) and indicated that the amide with a contiguous amine is

cyclized around these temperatures. From these results, we selected 400°C for the thermal cyclization temperature for 2, 5-PBI and all PBI-*co*-PA.

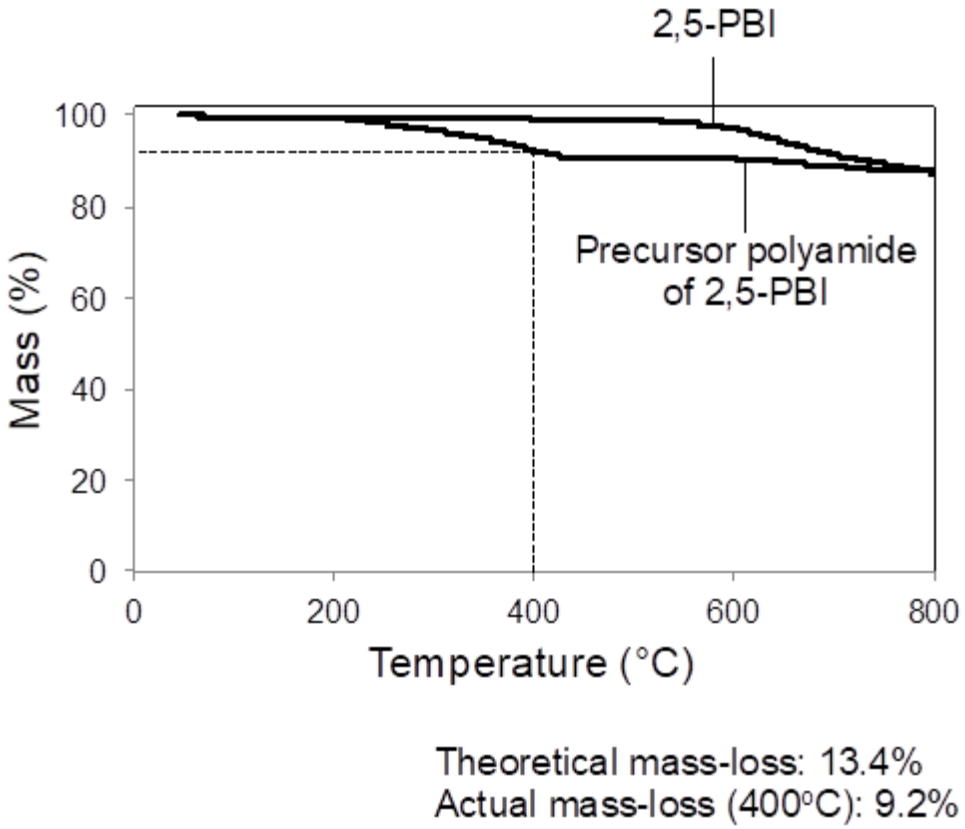

Figure 3.3 Determination of the thermal ring closing temperature of the precursor polyamide of 2, 5-PBI by thermogravimetric analysis (TGA) under nitrogen

3.3.4 *Structural characteristics of PBO-co-PBI:*

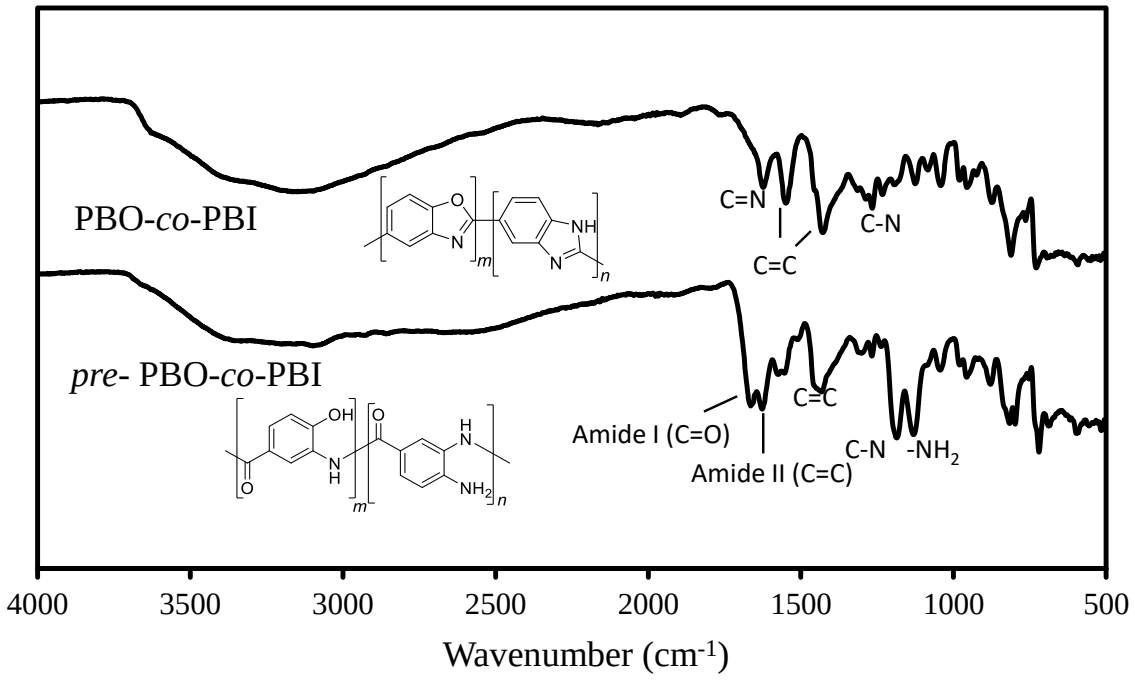

Figure 3.4 FT-IR spectra of PBO-*co*-PBI and its corresponding precursor

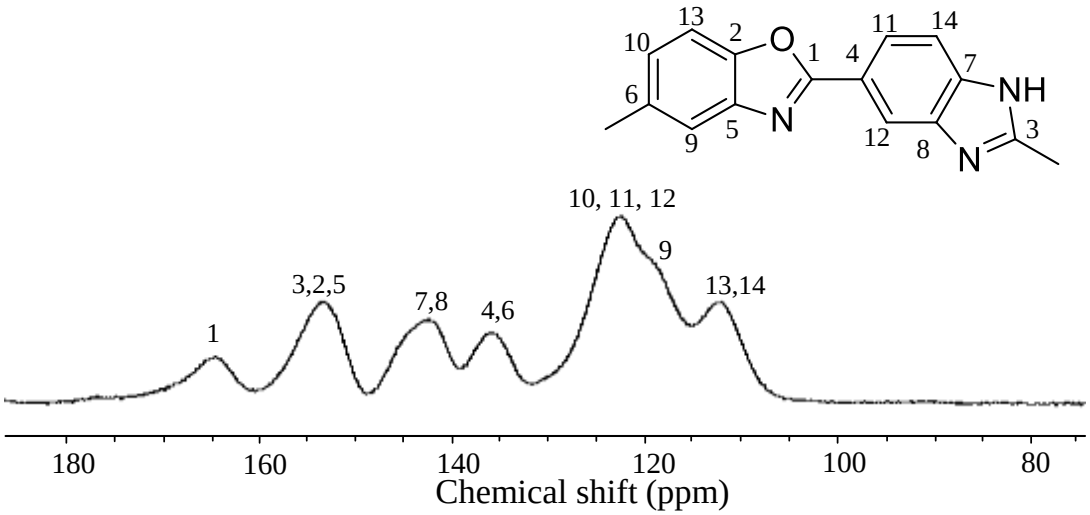

Figure 3.5 Solid state ^{13}C CP-TOSS NMR spectra of PBO-*co*-PBI

The stretching vibration of *pre*- PBO-*co*-PBI spectra shows two peaks for the carbonyl (C=O) at 1673 cm^{-1} (amide I) and 1634 cm^{-1} (amide II) bands were disappeared at 400 °C indicating that PBO-*co*-PBI has no C=O group available in the structure. Also, the absorption band at 1458 cm^{-1} was directly attributed to the characteristic C=C stretching of aromatic groups and other absorption bands observed at 1197 cm^{-1}, and 1140 cm^{-1} were attributed to the characteristic C-N bonds and -NH_2 group were disappeared. The distinct characteristic C=N and C-N absorption around 1624 cm^{-1} and 1292 cm^{-1} were associated to oxazole and imidazole ring as presented in Figure 3.4.

The structures of the PBO-*co*-PBI copolymers were further confirmed from the solid-state ^{13}C CP/MAS NMR spectra as shown in Figure 3.5, where several broad ^{13}C signals appearing between 110 and 170 ppm were assigned as oxazole, imidazole, and aromatic carbons. One can notice that 1-position carbon of oxazole ring appeared at 168 ppm lower magnetic field than corresponding carbon of imidazole ring (at 155 ppm). PBO-*co*-PBI with various PBO:PBI molar ratios were synthesized by thermal polymerization of 3-amino-4-hydroxybenzoic acid hydrochloride (3, 4-AHBA.HCl) and 3,4-diaminobenzoic acid dihydrochloride (3,4-DABA·2HCl) in a two-step procedure via the precursor polyamides, *pre*- PBO-*co*-PBI (Scheme 3.3). In this process, the molar compositions of 3, 4-AHBA.HCl and 3, 4-DABA.2HCl were varied in increments of 20 mol% to obtain a series of *pre*- PBO-*co*-PBI precursors. The resulting *pre*- PBO-*co*-PBI precursors were converted to PBO-*co*-PBI via a thermal ring closing reaction by gradual heating to 400 °C with a ramp rate of 10 °C/min in a muffle furnace. The thermal ring-closing temperature, T_{TR}, was determined by thermogravimetric analysis at a heating rate of 10 °C/min under a N_2 atmosphere. The complete ring-closing conversion to form the benzazole structure at 400 °C was characterized by FT-IR analysis.

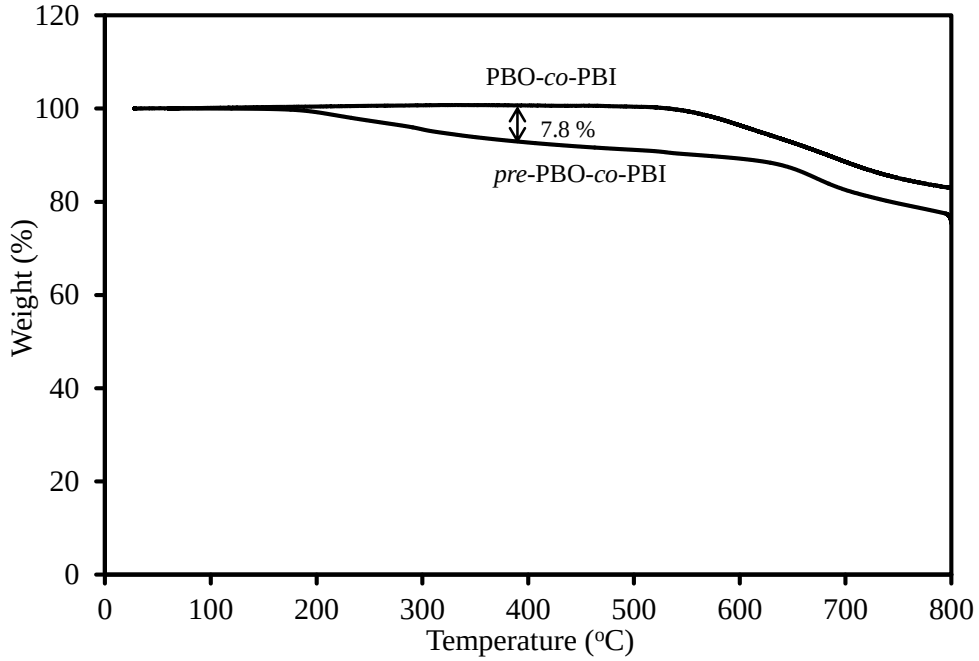

Figure 3.6 Thermogravimetric curves of PBO-*co*-PBI and its corresponding precursor

3.4 Results and discussions

3.4.1 *Thermal and mechanical performance of the copolymer* PBI-*co*-PA*:*

The effects of incorporating ABA into PBI on the thermal and mechanical properties of the resulting PBI films were investigated in detail. The copolymers of DABA with ABA were designated as amide-containing PBI (PBI-*co*-PA). The thermal degradation behavior of the PBI films was investigated by thermogravimetric analysis (TGA) (Figure 3.7-3.10). A mass loss was observed for the PBI films at >430 °C and at >370 °C for the aramid. Maximum char yields for the PBI-*co*-PA copolymers at 800 °C were 89% under nitrogen and 84% under air, which were much higher than those of conventional fully-aromatic polymers with high flame retardance (Kapton™, 53% [33]; poly(*p*-phenylenebenzobisoxazole), 61% [34]; both under nitrogen). The temperatures at which mass losses of 1% and 10% (T_{d1} and T_{d10}, respectively) under pyrolysis conditions were observed were plotted against the ABA content in PBI. The T_{d10} values for the PBI-*co*-PA films ranged from 640 to 745 °C with the maximum value obtained for PBI-*co*-PA of 15 mol% ABA. The T_{d1} values for the PBI-*co*-PA

films ranged from 430 to 575 °C, which is considerably higher than those of most conventional high-performance plastics. The T_{d10} and T_{d1} values for the PBI films in air (>495 °C and >420 °C, respectively) were also high, and varied depending on the ABA content. The PBI-*co*-PA of 15 mol% ABA showed the highest values (T_{d10}, 690 °C; T_{d1}, 495 °C). Because the ABA homopolymer is less thermostable than PBI, it is notable that incorporating relatively small amounts of ABA into the PBI backbone increased the thermal stability of the resulting PBI-*co*-PA films. This unique property may be explained by inter-chain hydrogen bonds in amorphous regions. The imidazole N–H groups of canonical PBI could bind with the –N= groups of adjacent PBI chains via hydrogen bonds, but the curved architecture of the PBI backbone likely decreases the occurrence of such hydrogen bonds in amorphous regions. Incorporating amide bonds into PBI can introduce straight sections into the PBI backbone, and therefore enhance the probability of forming imidazole–imidazole hydrogen bonds around the amide linkage. In addition, the H atom of an imidazole imine can form an inter-chain hydrogen bond with the O atom of the amide bond in PBI-*co*-PA. Thus, PBI-*co*-PA probably has more inter-chain hydrogen bonds than the DABA homopolymer (2, 5-PBI) in amorphous regions, resulting in its increased thermo-resistance.

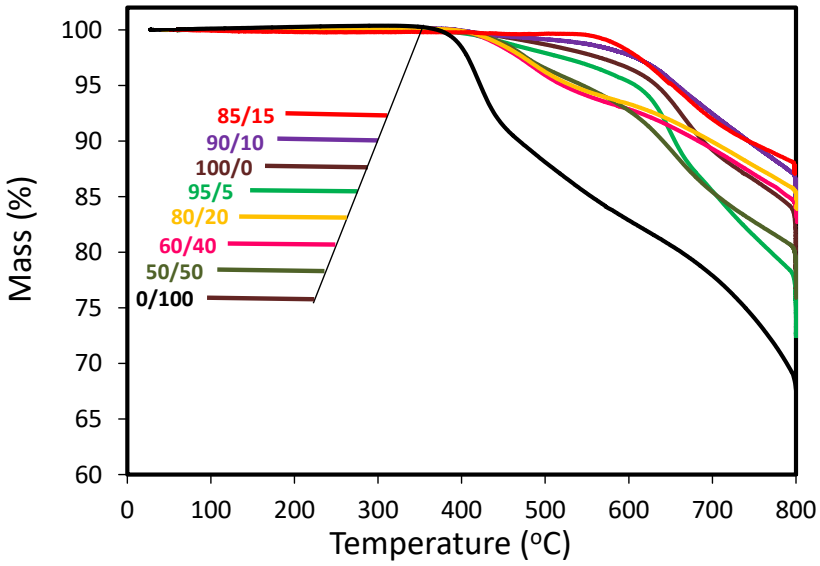

Figure 3.7 Thermogravimetric curves of 2, 5-PBI, PBI-*co*-PA with different copolymer compositions, and *para*-aramid measured under nitrogen

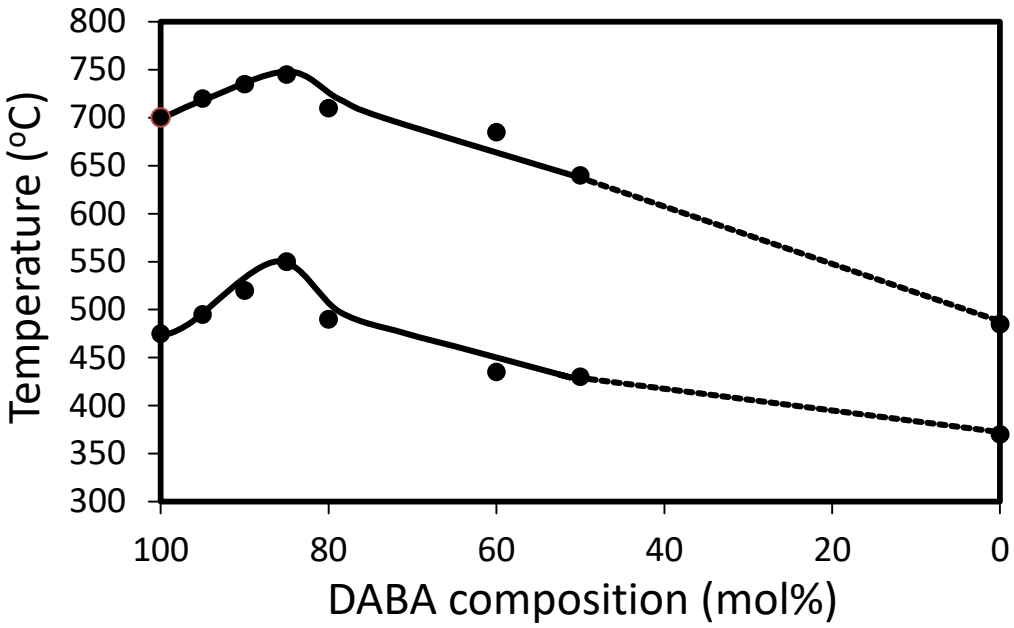

Figure 3.8 Plots of 1% (T_{d1}) and 10% (T_{d10}) mass-loss temperatures measured under nitrogen against DABA compositions

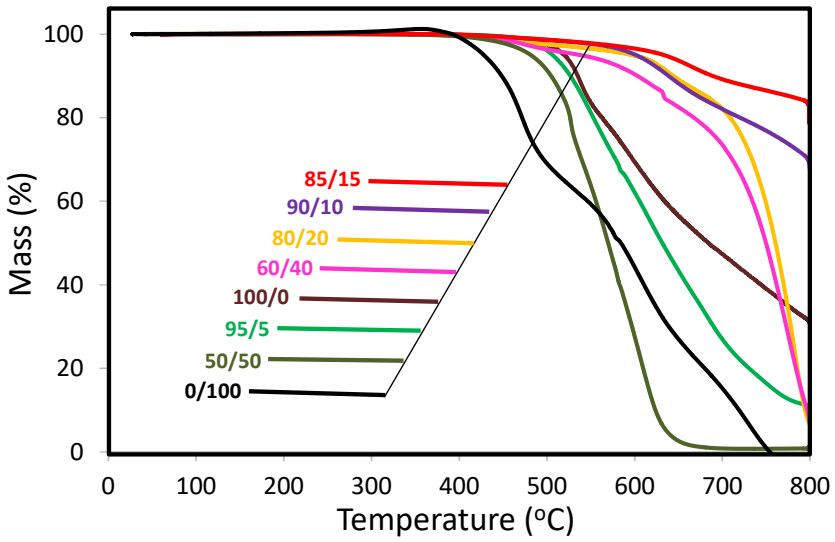

Figure 3.9 Thermogravimetric curves of 2, 5-PBI, PBI-*co*-PA with different copolymer compositions, and *para*-aramid measured under air

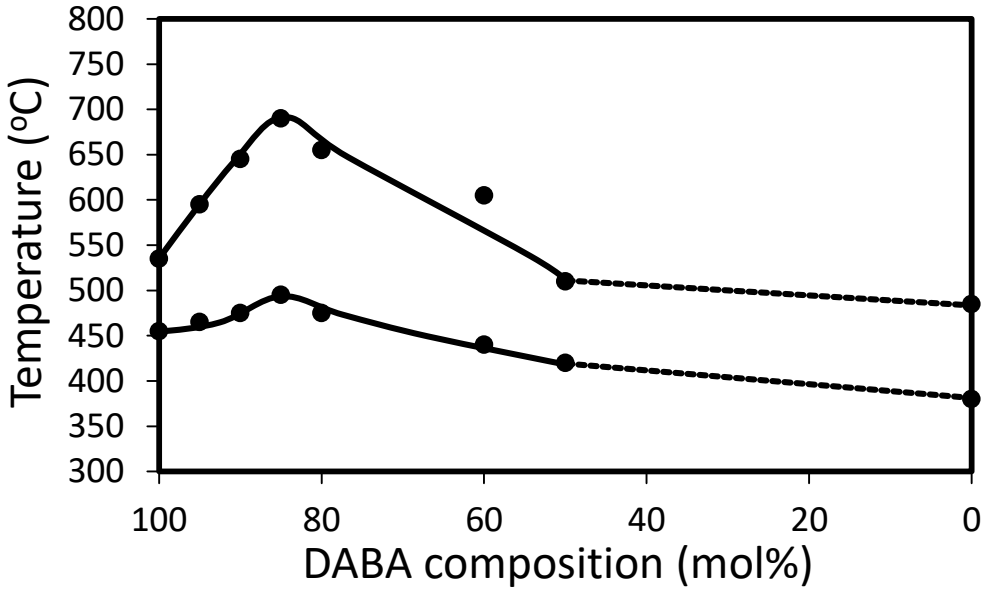

Figure 3.10 Plots of 1% (T_{d1}) and 10% (T_{d10}) mass-loss temperatures measured under air against DABA compositions

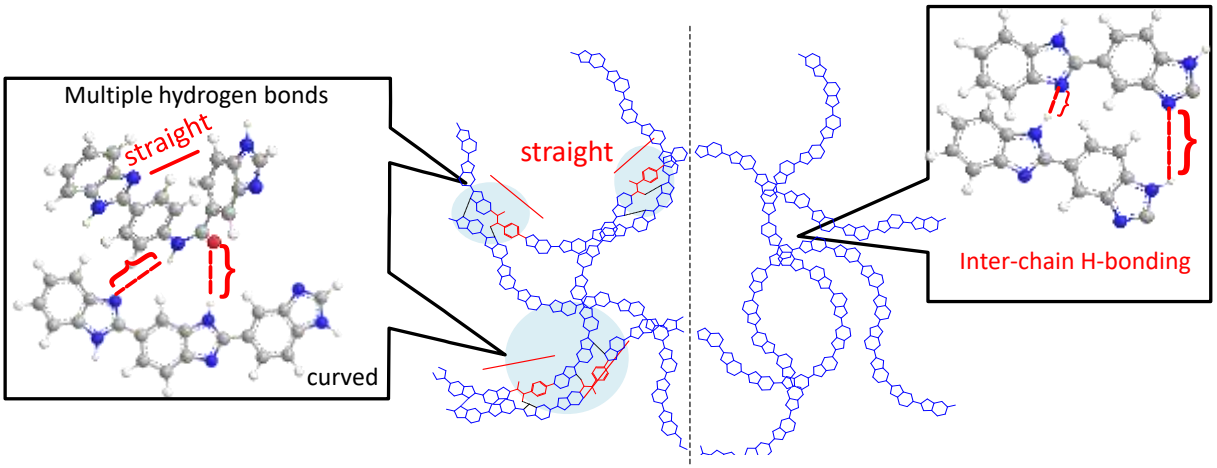

Scheme 3.4 Schematic illustration of copolymer PBI-*co*-PA structure and stability factor

Figure 3.11 PBI-*co*-PA (85/15) copolymer films obtained both in commercial and bio-based methods

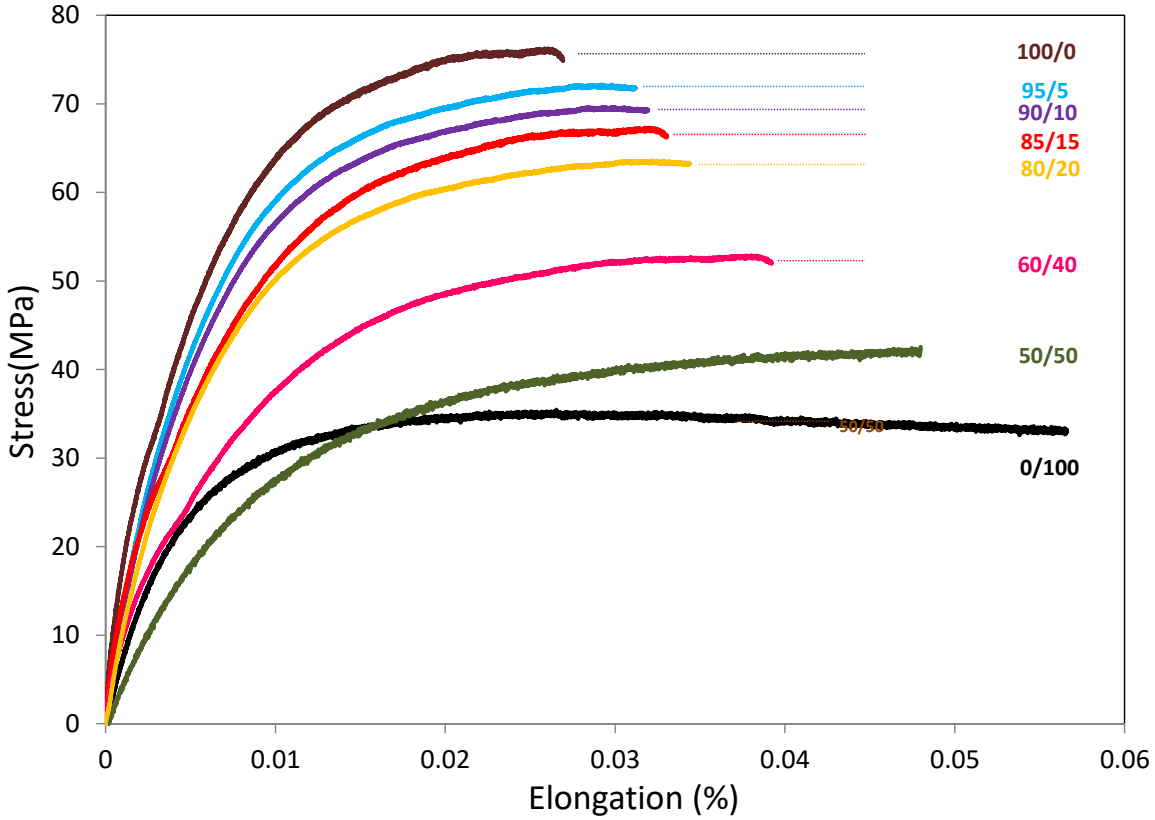

Figure 3.12 Stress-strain curve for various copolymer PBI-*co*-PA compositions

Tensile stress–strain curves of neat PBI and PBI-*co*-PA films are presented in (Figure 3.12). The neat PBI stress–strain curve exhibits an obvious nonlinear region starting at about 75 MPa, which likely corresponds to the primary damage of molecular chains during the large elongation, whereas, the nonlinear region of the stress-strain curve decreases with increasing amount of PA incorporation. Tensile strength value for neat PBI is 75 MPa, and PA incorporation to design the PBI-*co*-PA copolymer, tensile strength values fall in the decreasing range of 73-42 MPa with increasing PA amount. At the same time the Young's modulus shows highest value for the homopolymer PBI is around 3.6 GPa and for the copolymers (PBI-*co*-PA) this value falls in between the range of 3.4-1.8 GPa (table 3.2) as the PA incorporation increased as compared to PBI. Tensile at break (%) is lowest for the

homopolymer PBI 2.6% but increases gradually as the PA content increases up to 5.5 % in the copolymer composites. After evaluating the trend from the table 3.2, it can be assumed that highly rigid structure of PBI is responsible for highest mechanical strength but lowest value for tensile at break (%). During incorporation of the polyamide moiety increases the flexibility in the copolymer chain which is responsible for lower strength and Young's moduli but higher flexibility so film can successfully retain its structure after bending to a certain extent. The homopolymer ABPBI and most of the prepared copolymers are producing better mechanical properties as compared with conventional bio-pastic PLA (60 MPa) and most of other reported bio-plastics.

3.4.2 *Degree of crystallinity:*

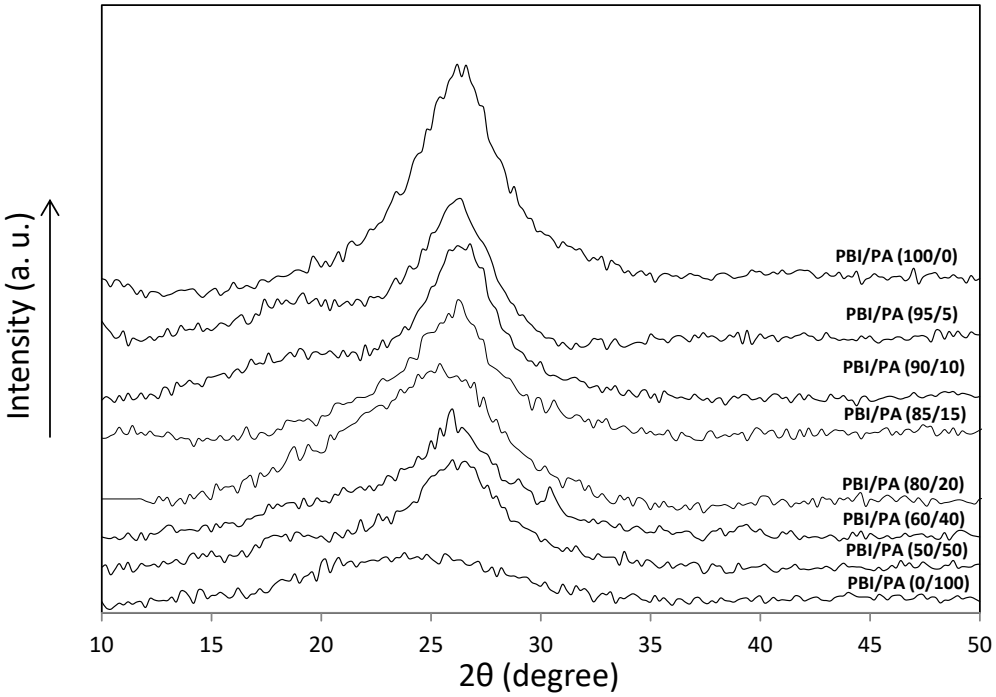

Figure 3.13 Wide angle X-ray diffraction (WAXD) diagrams of 2,5-PBI, PBI-*co*-PA with different copolymer compositions, and para-aramid

The crystalline structures of all the polymers (PBI and PBI-*co*-PA) were investigated by X-ray diffraction (XRD) (Figure 3.13) and corresponding degree of crystallinity values reported

in table 3.1 The XRD pattern of PBI homopolymer is showing sharp peak at 2θ= 26° whereas the copolymer PBI-*co*-PA was showing a small diffraction peak at 2θ = 18.2° along with the sharp PBI peak. The broad amorphous halo at 18.2° assumes to be responsible for the PA incorporation. Now for calculating degree of crystllinity we have followed the method of Nara & Komiya (1983) [46]. To minimize the calculation error baseline was drawn in each case by using Origin pro software and a smooth curve which connected peak baselines was plotted on the diffractograms. The area above the smooth curve was taken to correspond to the crystalline portion, and the lower area between the smooth curve and a linear baseline which connected the two points of intensity at 2θ of 45° and 15°. PBI shows highest crystallinity (27%) value and then there is gradual decrease in the range of 27% to 11% as we incorporate PA for all the compositions of PBI-*co*-PA and finally in case of homopolymer PABA there is only one broad peak in the PA region with no crystallinity at all. To explain this trend it can be described as most rigid structure PBI shows highest degree of crystallinity, but incorporation of different mole % of PA moieties in PBI-*co*-PA degree of crystallinity gradually decreases as flexible PA chain is amorphous and as compared with the sole PBI case.

Table 3.1 Degree of crystallinity for the prepared copolymers PBI-*co*-PA

Polymers DABA/PABA (mol/mol%)	Degree of crystallinity (%)
Homopolymer 100/0	27
PBI-*co*-PA 95/5	25
PBI-*co*-PA 90/10	23
PBI-*co*-PA 85/15	20
PBI-*co*-PA 80/20	18
PBI-*co*-PA 60/40	14
PBI-*co*-PA 50/50	11
*P*ara-Aramid 0/100	0

Table 3.2 **Thermal and mechanical properties for PBI-*co*-PA copolymers and other available high-performance polymers**

Polymers[a]	η_{inh}[b]	T_{d1}[c]	T_{d10}[c]	Maximal stress[d]	Young's moduli[d]	Elongations at break[d]
Polymer (DABA/ABA)	(dLg^{-1})	(°C)	(°C)	(MPa)	(GPa)	(%)
Homopolymer (100/0)	2.3	475	700	75±3.5	3.6±0.5	2.6
Biobased homopolymer (100/0)	–	470	716	68	3.3	2.6
PBI-*co*-PA (95/5)	2.4	495	720	71±2.9	3.1±0.7	3.1
PBI-*co*-PA (90/10)	2.5	520	735	69±3.4	3.1±1.2	3.3
PBI-*co*-PA (85/15)	2.6	575	745	68±1.7	3.2±0.3	3.4
Bio-PBI-*co*-PA (85/15)	–	580	743	66	3.2	3.0
PBI-*co*-PA (80/20)	2.4	440	697	63±2.4	2.8±0.9	3.6
PBI-*co*-PA (60/40)	2.2	435	683	52±2.7	2.1±0.6	3.8
PBI-*co*-PA (50/50)	2.1	430	640	42±3.2	1.8±1.1	4.7
para-Aramid (0/100)	1.9	370	485	33±1.4	1.4±0.2	5.5
Zylon™	–	565	715	5800	180	3.5
Kevlar49™	–	275	585	3000	112	2.4
Kapton™	–	500	580	231	2.5	72
Celazole™	–	165	570	100	5	2.2
PEEK	–	525	570	98	4	45
PPS	–	495	530	93	3.5	15
Nylon6™	–	390	415	75	2.4	15

a) Seven conventional high-performance plastics are presented for comparison: polybenzoxazole (PBO) Zylon™[34, 36]] para-aramide (PA) Kevlar 49™[19], polyimide (PI) Kapton™[33], PBI Celazole™[38,39] polyetheretherketone (PEEK)[40,41], polyphenylenesulfide (PPS) [42], and poly(ε-caprolactam) Nylon 6™[43, 44]. (b) Inherent viscosity of concentrated sulfuric acid solution of each PBI polymer. (c) Determined by thermogravimetry under a nitrogen atmosphere. (d) Obtained from stress–strain curves in elongation mode.

3.4.3 *Thermal and mechanical performance of the copolymer PBO-co-PBI:*

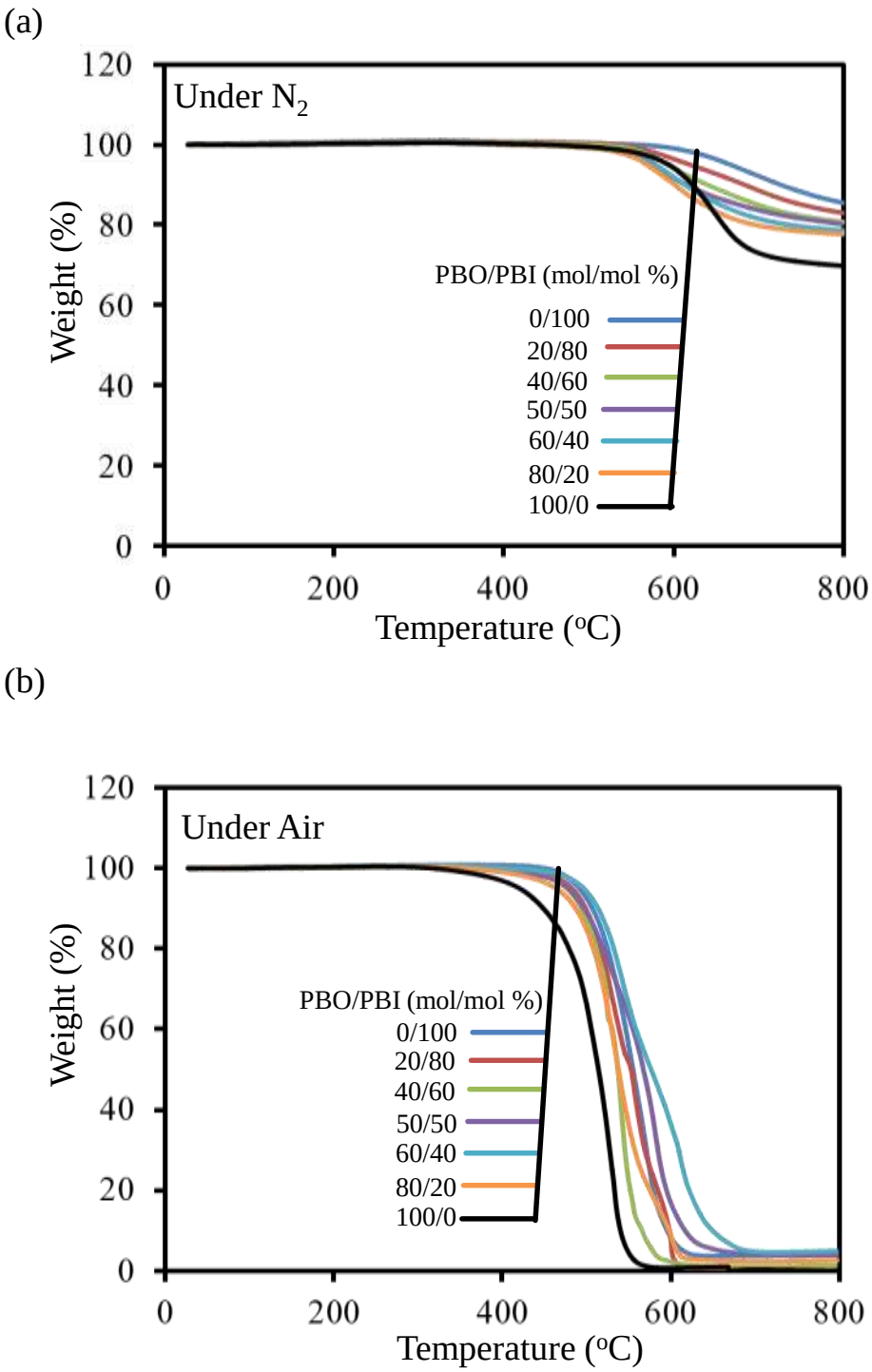

Figure 3.14 TGA curves for polymers with various PBO/PBI compositions under a) N_2 and b) air

The thermal stability of all the synthesized PBO-*co*-PBI copolymers was analyzed using TGA under nitrogen as well as an air atmosphere at a heating rate of 10 °C/min from room temperature to 800 °C. The TGA thermograms of all the prepared polymers showed no appreciable weight loss at temperatures up to 500 °C under N_2, indicating their high thermal stability.

The degradation temperatures T_{d5} and T_{d10} for the PBO-co-PBI copolymers were measured under N_2 and air atmospheres (Figure 3.14). Under N_2, the T_{d5} values ranged from 574 to 667 °C, while the T_{d10} values were between 601 and 716 °C. Under air, T_{d5} ranged from 421 to 491 °C, and the T_{d10} values were between 449 and 507 °C. These temperatures were 90-100 °C lower than those measured under N_2, presumably due to oxidative, thermal degradation [39, 40]. The copolymers with higher PBI compositions showed higher degradation temperatures due to the additional hydrogen bonding of the N-H group in benzazole [41-43]. All the prepared PBO-*co*-PBI copolymers showed higher T_{d10} values than conventional bio-based polymers. Their char yields (residual mass) at 800 °C under an N_2 atmosphere (between 83 and 77%) were also higher than those of several conventional plastics, such as Kapton™.

The stress-strain properties of the polymer films were investigated, and the maximal tensile strength, σ, Young's modulus, G, and strain at break, γ, were evaluated from the stress-strain curves (Figure 3.15). The averaged values (n=5) of all the polymers are summarized in Table 3.3. The σ and G values of the PBO-*co*-PBI copolymers ranged from 38-110 MPa and 2.4-3.9 GPa, respectively, while the elongation at break values showed a wide range of 2-28%. The mechanical strength of the PBO-*co*-PBI film with a 50/50 PBI/PBO composition was the best of all the prepared polymers, approaching the value of Kapton™. In contrast, Young's moduli of the copolymers did not change remarkably with the copolymer composition. The homopolymers PBI and PBO showed lower elongation at break (~2 and 7% respectively)

values, while those of the PBO-*co*-PBI copolymers with compositions of 40/60, 50/50, and 60/40 were increased to 23-28%. Copolymerization can affect the flexibility of polymer chains, presumably owing to the decreased regularity of the repeating units of the polymer backbone [43, 45]. The crystalline structures of copolymers PBI-*co*-PBO and homopolymer (ABPBI and ABPBO) were investigated by X-ray diffraction (XRD), which showed two broad peaks. Degree of crystallinity values were calculated quantitatively according to the method of Nara and Komiya [46]. Degree of crystallinity for all the synthesized polymers ranged between 30-40%. The copolymerization does not affect significantly on the crystallinity.

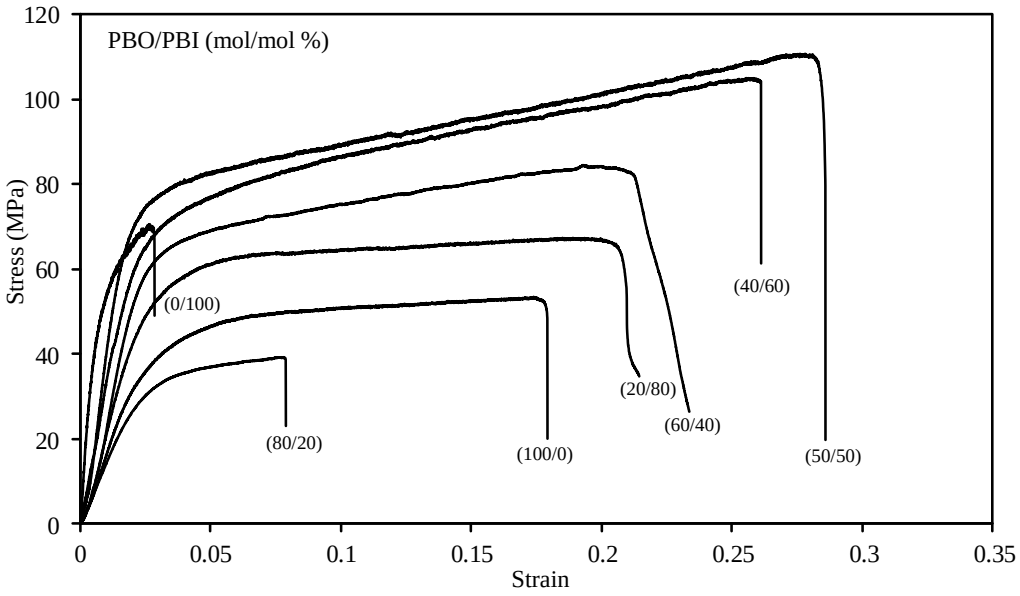

Figure 3.15 Stress-strain curves of various compositions of PBO-*co*-PBI

3.4.4 *Thermo-mechanical analysis (TMA):*

Determining glass transition temperature for the PBO-*co*-PBI films was difficult for machine limitation. Thermal mechanical analysis (TMA) was carried out using HITACHI TMA7100C (tensile mode) under nitrogen flow (flow rate, 200 mL min^{-1}) from 50 °C to 500 °C with a heating rate of 5 °C min^{-1} and an applied force of 100 mN to determine heat distortion temperature (HDT) and coefficient of thermal expansion (CTE) of the obtained polymers. Among all the available techniques, we have tried tension probe to measure as they will help to analyze the samples which are in the film form. Preheating of all the samples were done at 200 °C for 2 h to completely remove the solvents.

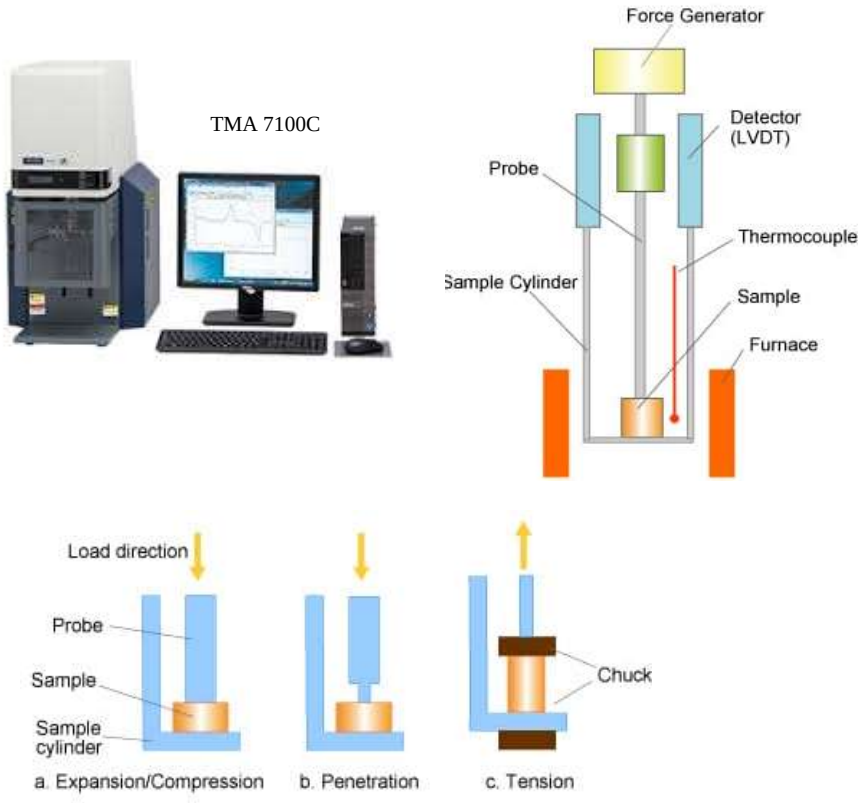

https://www.hitachi-hightech.com/global/products/science/tech/ana/thermal/descriptions/tma.html

Figure 3.16 Thermo-mechanical analysis instrumentation and mechanism

Table 3.3 Thermal and mechanical properties for polymers with various PBO/PBI compositions

Polymers [a]	T_{d5} [b] (°C)	T_{d10} [b] (°C)	T_{d5} [c] (°C)	T_{d10} [c] (°C)	CTE[d] (ppm/°C)	T_g [e] (°C)	σ [f] (MPa)	G [f] (GPa)	γ [f]	η_{inh} [g] (dL/g)
(PBO/PBI) 0/100	667	716	491	507	17.8	ND	76 ± 4.4	3.8 ± 0.15	0.02 ± 0.01	3.1
20/80	619	683	483	499	18.5	ND	66 ± 4.7	3.1 ± 0.20	0.21± 0.04	2.9
40/60	593	640	477	494	21.7	319	104 ± 3.9	3.8 ± 0.30	0.26± 0.06	3.4
50/50	574	614	478	497	22.4	303	110 ± 7.2	3.9 ± 0.38	0.28± 0.04	3.6
60/40	578	613	464	487	22.9	299	83 ± 6.4	2.7 ± 0.20	0.23± 0.02	3.0
80/20	568	601	455	481	25.1	289	38 ± 5.8	2.4 ± 0.25	0.07± 0.03	2.0
100/0	594	622	421	449	ND	ND	53 ± 7.4	2.8 ± 0.28	0.10± 0.05	1.8
Kapton™	450	590	390	430	32	360-410	135 ± 9.3	4.9 ± 0.62	0.13± 0.07	0.8

a) The polymers were prepared by a bio derived monomer 3,4-AHBA was utilized with varying the 3,4-DABA to prepared PBO-*co*-PBI with respect to PBO/PBI(mol %). (b,c) The thermal decomposition temperature at which 5 % and 10% weight-loss temperatures (T_{d5} and T_{d10}) of the PBO-*co*-PBI recorded by TGA at a heating rate of 10 °C min^{-1} under nitrogen b and air c atmosphere. (d) Coefficient of thermal expansion (CTE) were measured using thermo-mechanical analysis (TMA) method using a load of 100 mN/min. (e) T_g was determined as HDT by tangent intersection point drawn for above and below the transition curve of TMA. (f) The mechanical properties were measured by a stress-strain tensile test. Marks σ, *G*, and *g* refer to mechanical strength, Young's modulus, and strain at break, respectively, (g) Inherent viscosity were measured at 30 °C with identical concentration of polymer solution in H_2SO_4

HDT values of PBO-*co*-PBI and homopolymer films were measured by TMA (Table 3.3). In the present case, HDT corresponds to the glass transition temperature (T_g) because no distinct peaks were detected in DSC. As a result, HDT were not detected in PBI homopolymer and the copolymer with a PBO/PBI composition of 20/80, indicating too high T_g nearby limitation of TMA measurement. On the other hand, other copolymers with PBO/PBI composition of 40/60, 50/ 50, 60/40, and 80/20 showed HDT in the range of 289-319 °C, which increased with an increase in PBI content presumably due to strong intermolecular hydrogen bond bonds mediated NH of the imidazole ring. In PBO homopolymer, the film was too brittle to measure by TMA machine. Regarding CTE, the polymers showed very low values ranging in 17.8-25.1 ppm/K, which decreased with an increasing in PBI content. The result should be also attributed to strong interchain interaction of imidazole rings. Such a low CTE values ~ 20.0 ppm/K comparable to copper and aluminum foils can be very significant with research extension targeting to polymer/metal composite materials, similarly to Kapton™.

The product was insoluble in polar aprotic solvents such as NMP, DMF, and DMSO and partially soluble in TFA, and completely soluble in strong acids such as MSA and H_2SO_4. The inherent viscosities of the prepared PBO, PBI, and copolymers were measured using an Ubbelohde viscometer (0.5 g/dL polymer concentration in H_2SO_4 at 30 °C), as shown in Table 3.3. We found that the inherent viscosity increased with an increasing amount of PBI units, as shown in Table 3.3. The inherent viscosity of the PBO-*co*-PBI polymers was in the range of 1.8-3.6 dL/g, which was sufficient for the fabrication of fibers and flexible membranes.

3.4.5 *Dielectric properties comparison:*

Now as the main focus is establishment of rigid molecular design methodology which enhances the thermo-mechanical properties as well as electrical properties and maintains the minimal thermal resistivity focused so copolymerization has been considered. Also incorporation of PBO moiety with PBI moiety to get lower dielectric polymer materials than usual high-performance polymers such as: Kapton^{TM}. We have investigated dielectric properties with their structures by using following methods such as: determining dielectric constant, volume resistivity and dielectric breakdown voltage.

3.4.5.1 *Dielectric constant:*

The dielectric constant of the PBO-co-PBI films was measured using an LCR meter (HIOKI IM3536). The relative dielectric constant, ε_r, was calculated from the vacuum permittivity ε_0 (=8.85×10^{-12} F/m). The temperature was controlled at 20 °C, and the frequency range was 1 kHz-6 MHz. A constant pressure of 86 kPa was applied to the film during the measurement, and an electrical voltage of 1.0 V was applied by the two terminal method using brass electrodes. The measuring system was shielded from electromagnetic noise by a Faraday cage. The effect of 3 h of drying at 100 °C on the ρ_v and ε_r values of the films was also investigated.

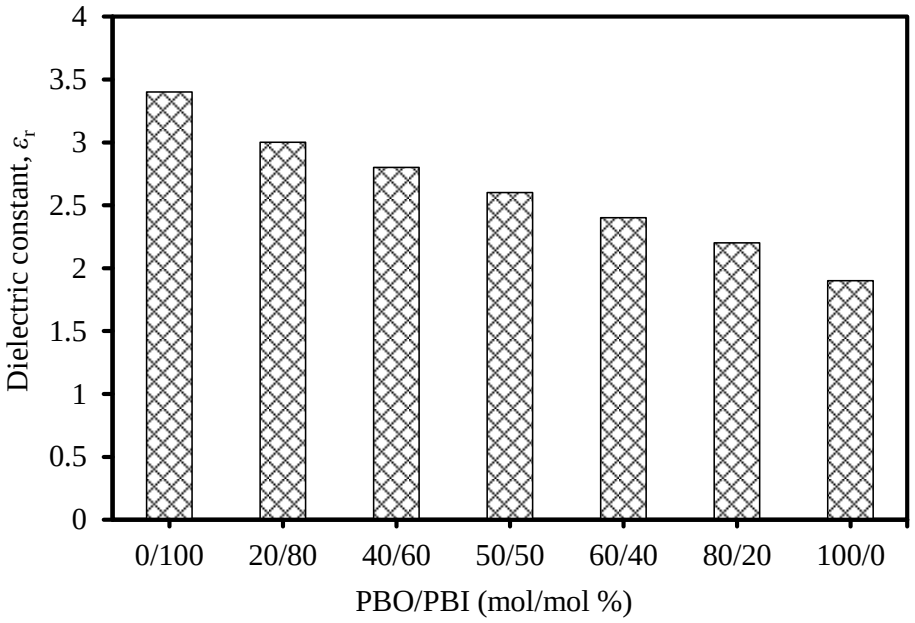

Figure 3.17 Dielectric constant of polymers with various PBO/PBI compositions

The dielectric constants, ε_r, of polymer films with very similar thicknesses were measured.

The value of ε_r was calculated using the formula (1)

$$\varepsilon_r = Cd/\varepsilon_0 A \qquad (1)$$

Where C is the capacitance, d is the film thickness, A is the cross-sectional area of the film and ε_0 is the free space permittivity of the films. The corresponding values for all the polymer films are presented in Figure 3.17 and Table 3.4. The dielectric constant for PBI and PBO homopolymer films recorded at 1 MHz was 3.9 and 1.9, respectively. The ε_r values of copolymers varies in a range from 3.0 to 2.2. We guess the low value might be attributed to very high rigidity and very low mobility responding to electric filed When PBO compositions were increased, the ε_r values have an tendency of decrease but not monotonously, which might be due to the reduced benz-azole polarity of PBO units and some unexpected structural effects in films. As a results, ε_r attained to the lowest value of 1.9 for PBO homopolymer. The copolymers with higher PBO composition showed lower ε_r values than commercial low ε_r materials, such as Celazole^{TM} (3.2), Kapton^{TM} (3.3), and UPILEX^{TM} (3.5), even comparable with PE (2.3-2.4) and PP (2.1), which suggests benz-azole structures including PBO and PBI are effective on reducing ε_r [47]. Furthermore, we have also checked the water absorption effect by drying experiment of all the polymer films as done in other measurements, and ε_r values became extremely low, but we did not get exact values due to measurement machine limitation. If ε_r values are recorded at 1 GHz, the ε_r value should be lower than that at 1 MHz. Eventually one can see that the poly(benz-azole)s can be used as an ultra-low k (~2.0) materials.

3.4.5.2 *Electrical resistivity:*

The electrical resistivity of the PBO-*co*-PBI films was carried out using a digital megohmmeter (DSM-8104 HIOKI) at room temperature. A DC electric voltage of 1 kV was applied by the two terminal method using conductive rubber electrodes with a guard electrode, and the measuring system was shielded from electromagnetic noise by a Faraday cage. The volume resistivity ρ_v (Ω cm) was calculated using the expression $\rho_v=(S/t) \times R_m$, where S is the area of the electrode and t is the thickness of the film, which had dimensions of 40×40 mm. The time evolution of the volume resistivity of the PBO-*co*-PBI films was measured.

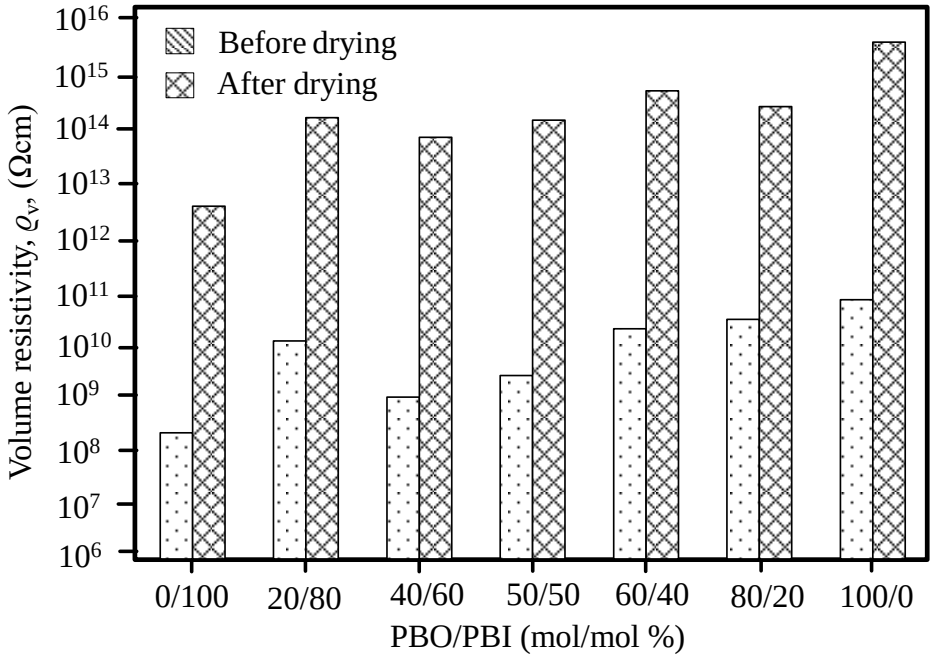

Figure 3.18 Volume resistivity for polymers with various PBO/PBI compositions before/after drying

The volume resistivity of all the PBO-*co*-PBI films changed with time and reached equilibrium at 60 s, demonstrating that the conductive ions moved to the electrodes and that the films were macroscopically polarized when the resistivity became constant. Figure 3.18 shows the relationship between the volume resistivity ρ_v at 20.0 °C and the PBO compositions for PBO-*co*-PBI films. The volume resistivities of the un-dried PBI-rich films were almost constant, with low values on the order of ~10^8 Ω cm, indicating their high ionic conductivity. The volume resistivity significantly increased when the PBO composition was higher than 60 mol%. The highest volume resistivity (1.7×10^{15} Ω cm) was observed for the 100 mol% PBO film with a thickness of 15 μm; this value was close to that of Kapton™ (5.1×10^{15} Ω cm, thickness = 13 μm). This behavior strongly indicates that the ionic conduction path was broken at 60 mol% PBO due to the percolation of insulating clusters of PBO. The percolation threshold for electric conductivity probably lies at approximately 60% PBO, indicating two-dimensional square lattice bond percolation behavior [48] via microscopic or molecular-level PBO clusters with low resistivity. On the other hand, the volume resistivities of the dried films were on the order of 10^{14}-10^{15} Ω cm, which are 7-8 orders of magnitude higher than their resistivity values without drying. Clearly, the volume resistivity of the PBI-rich films was strongly affected by the amount of water absorbed in the films. The volume resistivity for PBO contents greater than 50-60 mol% was relatively large, in accordance with the maximum tensile strength and strain at break results. However, it is difficult to discuss such small difference in the resistivity at high resistivity region over >10^{15} Ω cm. The dielectric constant for PBO-*co*-PBI films gradually decreased with the increasing molar ratio of PBO. Oppositely, the volume resistivity suddenly increased at a PBI molar ratio of 80 mol%, supporting the percolation behavior.

3.4.5.3 *Dielectric breakdown voltage:*

The dielectric breakdown voltage for the PBO-*co*-PBI films without any drying treatment was measured using an electrical safety analyzer (SE7430 Keisoku Giken) at room temperature. A DC electrical voltage of up to 6 kV was applied along the sample thickness using the two terminal method with a ramp-up time of 120 s at a rate of 1 kV s^{-1} using electrodes with a diameter of 20 mm; the maximum current limit was set as 10 mA.

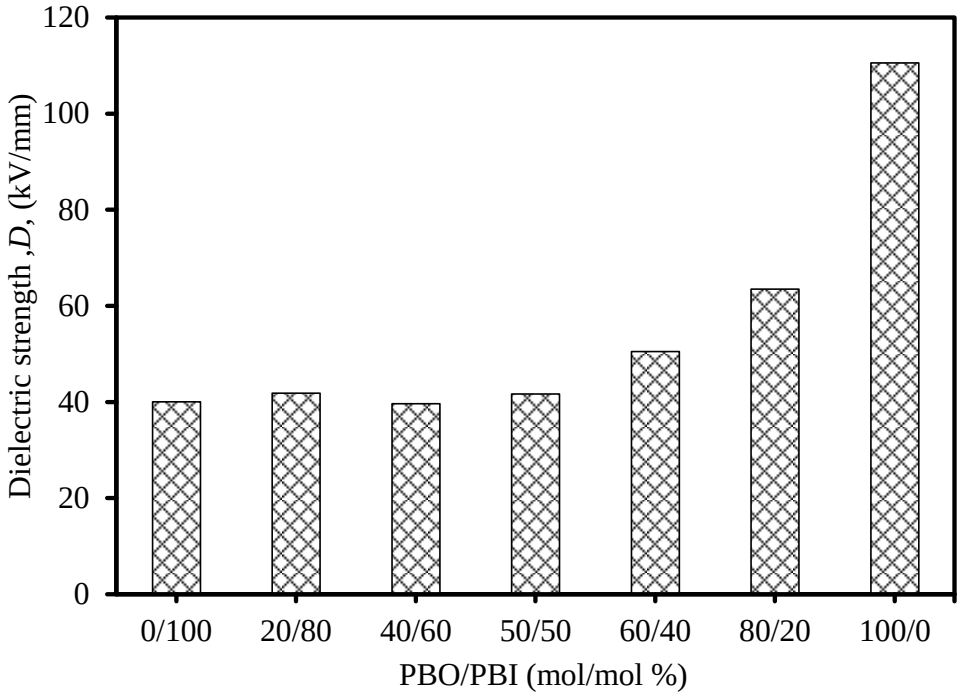

Figure 3.19 Dielectric strength of polymers with various PBO/PBI compositions

Moreover, there is a demand for materials with improved dielectric properties for future energy storage devices. The ability to withstand higher operating voltages ensures the reliability of such materials. The energy storage capacity of electrostatic capacitors is dependent on the permittivity and breakdown voltage of the insulating material. The insulating behavior of a material can be determined accurately from its dielectric strength, i.e.,

the maximum electrical field that can be applied to an insulating medium without causing a breakdown. The dielectric strength (D) is defined in equation (2),

$$D=V_{BD}/d \quad (2)$$

where V_{BD} is the breakdown voltage and d is the sample thickness, or in other words, the distance between the electrodes. The dielectric breakdown strengths of the undried PBO-*co*-PBI films are listed in Table3.4 The dielectric breakdown strength was almost independent of the PBO content for films with less than 60 mol% PBO; above this value, the dielectric breakdown strength significantly increased with the PBO content, which coincides with the volume resistivity ordielectric constant trend, as shown in figure 3.19.

Table 3.4 Dielectric properties for polymers with various PBO/PBI compositions

Polymers [a]	**Film Thickness (μm)**	ε [b]	ϱ_v [c] **(Ωcm) (before drying)**	ϱ_v [c] **(Ωcm) (after drying)**	D [d] **(kV/mm)**
(PBO/PBI) 0/100	19	3.5	1.8×10^{8}	2.0×10^{12}	40.0
20/80	22	3.0	7.9×10^{9}	7.6×10^{13}	41.8
40/60	25	2.8	7.8×10^{8}	3.4×10^{13}	39.6
50/50	24	2.6	1.9×10^{9}	6.9×10^{13}	41.6
60/40	21	2.4	1.3×10^{10}	2.3×10^{14}	50.5
80/20	23	2.2	1.9×10^{10}	1.2×10^{14}	63.5
100/0	19	1.9	4.3×10^{10}	1.7×10^{15}	110.5
Kapton™	25	3.3	5.1×10^{15}		116.0

(a)Polymer films with various (PBO/PBI) compositions were prepared maintaining film thickness 20±5 μm, (b) Dielectric constant, ε, measured at 1 MHz, (c) Resistivity, ϱ_v, of the films measured at 1 kV of DC electric voltage for 20 s application, (d) Dielectric strength, D, measured with increasing DC electric voltage up to 6 kV by two terminals method with a ramp-up time of 120s.

3.4.6 *Dielectric properties of various* PBI-*co*-PA *copolymer compositions:*

With extra-ordinary thermal stability PBI-*co*-PA can be superior polymeric dielectric materials for high-performance applications. Along with PBO-*co*-PBIs, dielectric properties were measured in case of PBI-*co*-PA copolymers as well. Dielectric constants were ranged between 3.5-2.4 as shown in table 3.5, and constantly decreasing with increase in PA content. PBI-*co*-PA with 50% PA content produced dielectric constant low enough and comparable with available low dielectric polymer materials. As compared with PBO homopolymer or PBO-*co*-PBIs, PBI-*co*-PA polymer structure is more polarizable as PBI moiety has conducting proton and PA moieties are more flexible in nature. As discussed before, polarizability induces higher conductivity in polymer structures. Volume resistivity data were observed much lower than Kapton^{TM} in the order of ~10^8 and almost 7 to 8 orders lower than the highest value observed in case of PBO homopolymer. Dielectric strength can be also observed to be much lower as compared with PBO-*co*-PBI or Kapton^{TM}.

Table 3.5 Dielectric properties for polymers with various PBI-*co*-PA compositions

Polymers	Film Thickness (μm)	Dielectric constant ε	Volume resistivity ϱ_v (Ωcm)	Dielectric strength D (kV/mm)
(PBI/PA) 100/0	14	3.4	$4.02.0\times10^{9}$	40.0
95/5	20	3.2	1.58×10^{13}	45.8
90/10	63	2.8	1.21×10^{9}	45.5
85/15	22	3.0	9.40×10^{8}	45.5
80/20	28	2.9	3.56×10^{8}	49.5
60/40	48	2.5	3.13×10^{8}	62.1
50/50	50	2.4	2.92×10^{8}	85.7
Kapton^{TM}	25	3.3	5.10×10^{15}	116.0

3.5 Conclusion:

Two aminobenzoic acid produced from biomolecules using genetic bio-engineering were used to prepare copolymer PBI-*co*-PA. The resulting bio-based PBI-*co*-PA of 15 mol% ABA showed the highest thermoresistance (T_{d10}, 743 °C) of any petroleum- or biomass-derived plastic. This finding represents a significant step forward in the global challenge to create heat-resistant high-performance plastics. For example, such a high thermo-resistance and good processability would enable the plastic to be hybridized with metals and/or inorganic compounds at a temperature above their melting points without thermally degrading the contacting plastics. If the PBI bioplastics are inserted as high-heat resistance insulator between conducting metals, high-performance electronic devices may be created such as super-integrated circuits, mass memories, high-power motors etc. opening the door to a new era of materials science for organic and light-metal composites.

On the other hand, PBO homopolymer and copolymer films with high PBO compositions showed very low ε_r values comparable with commercial PE and PP. If PBO units are partially replaced into PBI, O element of azole ring converted into NH group, to increase the polarity of backbones. The conversion elevated solubility in the solvent, thus processability is higher and thermal/mechanical performances as well as dielectric constant. As a result, polybenzoxazole homopolymer had the lowest ε_r with a superior thermal stability. The materials can be considered as high thermoresistance ultralow-*k* materials in microelectronic and electrical insulation.

3.6 References:

1. Philip, J. C., Ritchie, R. J., Allan, J. E. M. *Trends Biotechnol.* 2013, 31, 219.
2. Winnacker, M., Rieger, B. *Macromol. Rapid Commun.* 2016, 37, 1391.
3. Klemm, D., Heublein, B., Fink, H.-P., Bohn, A. *Angew. Chemie Int. Ed.* 2005, 44, 3358.
4. Kawaguchi, H., Hasunuma, T., Ogino, C., Kondo, A. *Curr. Opin. Biotechnol.* 2016, 42, 30.
5. Jin, X., Tateyama, S., Kaneko, T. *Polym. J.* 2015, 47, 727.
6. Tateyama, S., Masuo, S., Suvannasara, P., Oka, Y., Miyazato, A., Yasaki, K., Teerawatananond, T., Muangsin, M., Zhou, S., Kawasaki, Y., Zhu, L., Zhou, Z., Takaya, N., Kaneko, T. *Macromolecules* 2014, 49, 3336.
7. Suvannasara, P., Tateyama, S., Miyasato, A., Matsumura, K., Shimoda, T. Ito, T., Yamagata, Y., Fujita, T., Takaya, N., Kaneko, T. *Macromolecules* 2014, 47, 1586.
8. Lee, H. S., Lee, A. S., Baek, K. Y., Hwang, S. S. *InTech.*, (2012) 59.
9. Feig V. R., Tran, H., Bao, Z. *ACS Cent. Sci.*, 4 (2018) 337.
10. Kohl, P. A. *Annu. Rev. Chem. Biomol. Eng.*, 2 (2011) 379.
11. Ho, J. S., Greenbaum, S. G. *ACS Appl. Mater. Inter.*, 10 (2018) 29189.
12. Chen, Y., Zhang, S., Liu, X., Pei, Q., Qian, J., Zhuang, Q., Han, Z. *Macromolecules*, 48 (2015) 365.
13. Tao, L., Yang, H., Liu, J., Fan, L., Yang, S. *J. Polym. Sci. A*, 48 (21) (2010) 4668.
14. Wang, Y., Yang, S. Y., Huang, Y. L., Tien, H. W., Chin, W. K., Ma, C. C. M. *J. Mater. Chem.*, 21 (2011) 13569.
15. Diwedi, S., Sakamoto, S., Kato, S., Mitsumata, T., Kaneko, T. *RSC Adv.*, 8 (2018) 14009.
16. Zhang, X., Liu, J., Yang, S. *Rev. Adv. Mater. Sci.*, 46 (2016) 22.

17. Zhang, X. M., Liu, J. G., Yang, S. Y. *eXPRESS Polym Lett*., 10(10) (2016) 789.

18. Volksen, W., Miller, R. D., Dubois, G. *Chem. Rev*., 110 (1) (2010) 56.

19. Tsuge, Y., Kawaguchi, H., Sasaki, K., Kondo, A. *Microb Cell Fact.*, 15:19 (2016).

20. Noguchi, A., Kitamura, T., Onaka, H., Horinouchi, S., Ohnishi, Y., *Nat. Chem. Biol.*, 6 (2010) 641.

21. Kan, K., Kaneko, D., Kaneko, T. *Polymer*s, 3 (2011) 861.

22. Kan, K., Yamamoto, H., Kaneko, D., Tateyama, S., Kaneko, T. *Pure Appl. Chem*., 86(5) (2014) 685.

23. Ali, M. A., Shimosegawa, H., Nag, A., Takada, K., Kaneko, T. *J. Polym. Res.*, 24 (12) (2017) 1-7.

24. Kawasaki, Y., Nag, A., Minakawa, H., Kaneko, T., Takaya, N. *Appl. Microbiol. Biotechnol.*, 102(2) (2018) 631.

25. Eo, S. M., Oh, S. J., Tan, L. S., Baek, J. B. *Eur. Polym. J*., 44 (2008) 1603.

26. Kraytsberg, A., Eli, Y. E. *Energy Fuels*, 28 (12) (2014) 7303.

27. Tsuchiya, K., Ishii, H., Shibasaki, Y., Ando, S., Ueda, M. *Macromolecule*s, 37 (2004) 4794.

28. Suzuki, H., Ohnishi, Y., Furusho, Y., Sakuda, S., Horinouchi, S. *J. Biol. Chem*. 2006, 281, 36944.

29. Kawaguchi, H., Sasaki, K., Uematsu, K., Tsuge, Y., Teramura, H., Okai, N., Nakamura-Tsuruta, S., Katsuyama, Y., Sugai, Y., Ohnishi, Y., Hirano, K., Sazuka, T., Ogino, C., Kondo, A. *Bioresour. Technol*. 2015, 198, 410

30. Arnold, C. *J. Polym. Sci. Macromol. Rev*. 1979, 14, 265.

31. Koma, D., Yamanaka, H., Moriyoshi, K., Ohmoto, T. Sakai, K. *Appl. Environ. Microbiol.* 2012, 78, 6203.

32. Kubota, T., Watanabe, A., Suda, M., Kogure, T., Hiraga, K., Inui, M. *Metab. Eng.* 2016, 38, 322.

33. Dupont, DuPont TM Kapton ®, 2012.

34. Wu, G. M., Hung, C. H. *Achiev. Mater. Manuf. Eng*. 2006, 17, 27.

35. Carrasco, F., Pagès, P., Gámez-Pérez, J., Santana, O. O., Maspoch, M. L. *Polym. Degrad. Stab.* 2010, 95, 116.

36. Toyobo co. LTD. Zylon Technical Information. (2005).

37. DuPont. Kevlar aramid fiber. *Polym. Int.* 33, 438–439 (1994).

38. PBI Performance Products, I. Celazole® T-Series PBI (TU-60) properties.

39. Yang, J., Aili, D., Li, Q., Xu, Y., Liu, P., Che, Q., Jensen, J. O., Bjerrum, N. J., He, R. *Polym. Chem.* 2013, 4, 4768.

40. M. Properties, PEEK 450G Data Sheet, Victrex 2014.

41. Patel, P. Hull, T. R., Lyon, R. E., Stoliarov, S. I., Walters, R. N., Crowley, S., Safronava, N. *Polym. Degrad. Stab*. 2011, 96, 12.

42. Seo, K. H., Park, L. S., Baek, J. B., Brostow, W. *Polymer (Guildf).*1993, 34, 2524.

43. Li, J.-J., Song, G.-J., She, X.-L. Han, P., Peng, Z., Chen, D. *Polym. J.* 2006, 38, 554.

44. Matweb, Overview of Materials for Nylon 6/66, 2011.

45. Kawaguchi, H., Uematsu, K., Ogino, C., Teramura, H., Nimi-Nakamura, S., Tsuge, Y., Hasunuma, T., Oinuma, K., Takaya, N., Kondo, A. *Biochem. Eng. J.* 88, 188–194 (2014).

46. Nara, S., Komiya, T. *Starch - Stärke*. 35, (1983) 407.

47. Professional plastics: Electrical Properties of Plastic Materials. https://www.professionalplastics.com/professionalplastics/ElectricalPropertiesofPlastics.pdf

48. Zeff, M. *Phys. Rev. Lett.,* 69 (1992) 2670.

Chapter 4:

Modification of bio-based polybenzimidazole structure to prepare pseudo-solid polymer electrolyte to apply in lithium ion batteries

4.1 Abstract:

In this chapter we have described about preparation of high ion-conducting polymer electrolyte with high lithium transference number (t_{Li}^{+}) using organoborane-modified polybenzimidazole (B-PBI) and ionic liquid (IL), 1-butyl-3-methylimidazolium bis(trifluoromethanesulfonyl)imide (BMImTFSI). The structural characteristics of these electrolytes were examined by nuclear magnetic resonance and Fourier-transform infrared spectroscopy. Thermo-gravimetric analysis and dynamic viscosity measurements were used to investigate the thermal and rheological properties of the electrolytes. Unlike other solid polymer electrolyte systems, the addition of lithium salt was not required in the case of the electrolytes prepared in this study as the molecular designing already incorporates lithium. The amount of BMImTFSI (w/w %) affected the ion transport behavior of the composite polymer electrolytes. The ionic conductivity of the electrolytes increased with an increase in the IL content. The electrolyte with B-PBI/BMImTFSI (w/w %) (25/75) showed the highest conductivity of 8.8×10^{-3} S cm^{-1} at 51 °C. It has also showed the highest t_{Li}^{+} value of 0.63 at room temperature with wider electrochemical potential window of 5.45 V. The composite electrolytes were employed in anodic half-cells (Si/electrolyte/Li) and they showed high reversible capacity up to 1300 $mAhg^{-1}$ and retained it even at high charging rate. Electrochemical impedance spectroscopy and dynamic electrochemical impedance spectroscopy were performed before and after the charge-discharge measurements to confirm the formation of stable solid electrolyte interface with B-PBI/BMImTFSI (w/w %).

Keywords: lithium-ion battery, polybenzimidazole, boronation, ion conductivity, charge-discharge, interface etc.

4.2 Introduction:

With increasing demand for portable electronic devices in our daily life requirement of stable, durable energy source also increases. Lithium ion-battery (LiB) is already well-known as energy storage device for past few decades due to their high energy density as compared to conventional Ni-Cd or Ni-H_2 batteries and perfect to be used in electronic appliances such as: laptop, mobiles etc. However, safety issues and performance abilities for high energy requirements are always been an issue with the conventional liquid electrolytes used (e.g.: ethylene carbonate and propylene carbonate) in conventional LiBs. Retention of capacity and longevity of LiBs are prime concern for the research in this field, which is dependent both on electrode and electrolyte used which support diffusion of lithium-ions through the matrices. Batteries with non-liquid electrolytes are considered to be safer and stable in this regard and developing solid or semi-solid, polymer gel electrolytes are various in this kind which seeks researcher's keen attention. Ionic liquids (ILs) have also gained considerable popularity for their non-volatile, inflammable and low viscous nature (1-7).

One of the recent advancements in lithium ion secondary batteries is on solid polymer electrolytes which will potentially enable much higher energy density when compared with liquid electrolyte based batteries. Traditional solid polymer electrolytes (SPEs) such as poly(ethylene oxide) (PEO) suffered very low lithium transference number due to strong binding of ether oxygen to lithium ion [8]. To enhance the lithium transference number, valuable approach has been either 1) covalent introduction of highly dissociable lithium salt structure (polymer salt hybrids) [9] or 2) incorporation of anion receptor to bind anion for selective Li ion transport [10-11]. In both approaches, utilization of boron chemistry [12-13] has been very useful both in designing highly dissociable lithium salt structure and efficient anion receptor. These led to remarkably high lithium transference number of resulting solid polymer electrolytes. Zhou *et al.* reported preparation of single lithium ion conducting

polymer electrolyte by dissolving lithium salts in super-delocalized polyanions, and could attain high t_{Li}^{+} with moderately high ionic conductivity [23-24]. Novel molecular design of solid-state electrolytes must induce better conductivity, which would enable high rate battery performance and also chemical and electrochemical compatibility with the electrode material [25]. To achieve high ionic conductivity in addition to satisfactory lithium transference number, promising approach is preparation of polymer ion gel electrolytes including ionic liquids [14]. Till now versatile types of polymer ion gel electrolytes have been already reported, however, few of them exhibit both high ionic conductivity and high lithium transference number at the same time. Design of solid polymer-salt hybrid electrolytes with highly dissociable lithium salt structure and their plasticization with ionic liquid will offer a valuable approach to produce high performance pseudo solid electrolytes [15-17]. Furthermore, close observation and understanding of the potential profile across electrode/electrolyte interface is indispensible to check solid-state battery stability [18].

Due to structural advantages and thermo-mechanical stability polybenzmidazole group of polymers are well established in terms of energy applications as well as side-chain functionalization for several other possible applications [24-27]. In this study, we developed novel high-performance poly (2, 5-benzimidazole) type polymer electrolytes using 3, 4-diaminobenzoic acid (3, 4-DABA) as the starting material. The imidazole ring was modified to introduce lithium boroimidazolate to prepare SPE. An IL was added to the prepared SPEs while maintaining their solidity. The composition of the electrolytes was optimized to tailor ionic conductivity, potential window and t_{Li}^{+} for the fabrication of anodic half-cells [19]. Dynamic electrochemical impedance spectroscopy (DEIS) was used for the real-time examination of the interfacial structure during the charging and discharging processes [20-22]. The composite polymer electrolytes showed maximum ionic conductivity of 8.8 $x10^{-3}$ Scm^{-1} and maximum t_{Li}^{+} of 0.63. They were carefully designed for application in secondary

batteries. The Li/electrolyte/Si anodic half-cell showed a maximum discharging capacity of 1300 mAh g^{-1} at 0.1 C and could retain a capacity of 800 mAh g^{-1} even at a higher current rate of 2 C with Coulombic efficiency of 92%.

4.3 Experimental Section:

4.3.1 *Synthesis of low molecular weight Poly (2, 5-benzimidazole) (ABPBI):*

As described in chapter 2, Poly (2, 5-benzimidazole) (ABPBI) can be synthesized by the homo-polycondensation of 3, 4-diaminobenzoic acid (3, 4-DABA) (Scheme 4.1). Poly(phosphoric acid) (PPA, $H_{n+2}P_nO_{3n+1}$) (13-15 g. approx.) was purged with nitrogen gas in a 200 mL three-neck round-bottomed flask, which was maintained at 120 °C for 1 h to remove moisture completely. 3, 4-DABA.2HCl (0.58 g, 2.6 mmol) was then added to this flask and the mixture was maintained at 120 °C for 1 h. After homogenization, the temperature was increased to 180 °C and maintained for 2 h before increasing it further to 200 °C, which was maintained for 3 h. The reaction mixture turned dark brown from yellow with time, and the viscosity of the mixture increased gradually with time. The resulting solution was precipitated over water to obtain threads. These threads were then crushed, washed with water and dried at 100 °C under vacuum. ABPBI powder was immersed in a 10% KOH solution overnight, and was then washed on a filter paper repeatedly with deionized water until the filtrate showed neutral pH. The resulting powder was then soaked in acetone and dried at 100 °C under vacuum for two days to finally obtain pure ABPBI polymer (yield 95%).

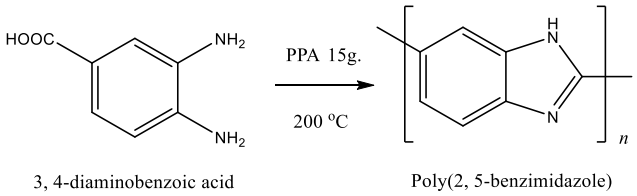

Scheme 4.1 Polybenzimidazole preparation scheme using 3, 4-DABA monomer

4.3.2 *Synthesis of boronated polybenzimidazole (B-PBI):*

A three-necked flask was charged with 15 mL super anhydrous DMSO. To this flask 0.520 g (51 mmol, 1 eq.) of ABPBI was added. The flask was settled under vacuum for 1 h at 80°C to completely remove moisture. The temperature was then decreased gradually to room temperature. LiH (1.22 g) (153 mmol, 3 eq.) was transferred to another flask in a glove box under Ar atmosphere and was then dispersed in 8-10 mL of anhydrous DMSO. This dispersion was transferred by a syringe to the flask containing the ABPBI solution at room temperature while maintaining the anhydrous condition. The resulting mixture was stirred at room temperature for 24 h (the first step in Scheme 4.2). The reaction mixture was then stirred at 80 °C for another 1 h, after which it turned red indicating the formation of N-Li linkage due to its reaction with ABPBI. The reaction mixture was then cooled to ambient and

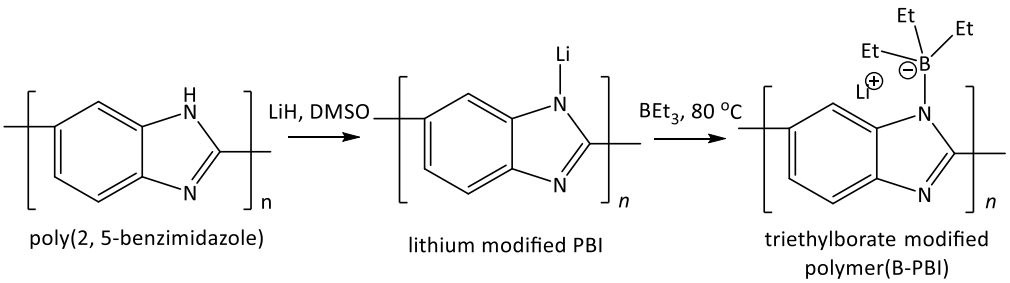

Scheme 4.2 Modification scheme of poly(2, 5-benzimidazole) by LiH and BEt_3 to obtain boronated polybenzimidazole (B-PBI)

44 mL (94 mmol, 6 eq.) of triethylborane (BEt_3) (1mol/L) was added slowly over the period of 30 min while stirring on the ice bath. A yellow precipitate appeared which was dissolved when the mixture was hated to 80 °C. The reaction mixture was stirred for 24 h at this temperature (the second step in scheme 4.2). After cooling the crude brown product was precipitated over toluene-acetone (1:1) repeatedly. The product was dried in a vacuum oven for three days at 80 °C to finally obtain boronated polybenzimidazole (B-PBI).The final product was weighed 0.80 g (yield 84%).

4.3.3 *Preparation of the B-PBI/BMImTFSI composite polymer electrolyte:*

The typical procedure for preparing the composite polymer electrolytes is as follows: 0.1 g ($4x10^{-6}$ mol) of B-PBI was taken in five different bottles to which BMImTFSI was added in different volumes (35 µL ($1.2x10^{-4}$ mol), 70 µL ($2.3x10^{-4}$ mol), 140 µL ($4.8x10^{-4}$ mol), 210 µL ($7.1x10^{-4}$mol), and 280 µL ($9.5x10^{-4}$ mol)) to prepare electrolyte mixtures with various weight compositions (66/33, 50/50, 33/66, 25/75, 20/80, respectively) (Figure 4. 1(a)) [28]. The electrolytes were sonicated at 40°C for 30 min to prepare homogeneous composite polymer electrolytes. The physical state of the prepared electrolytes changed from powder to paste like gel with an increase in the BMImTFSI amount as shown in Figure 4.1(b).

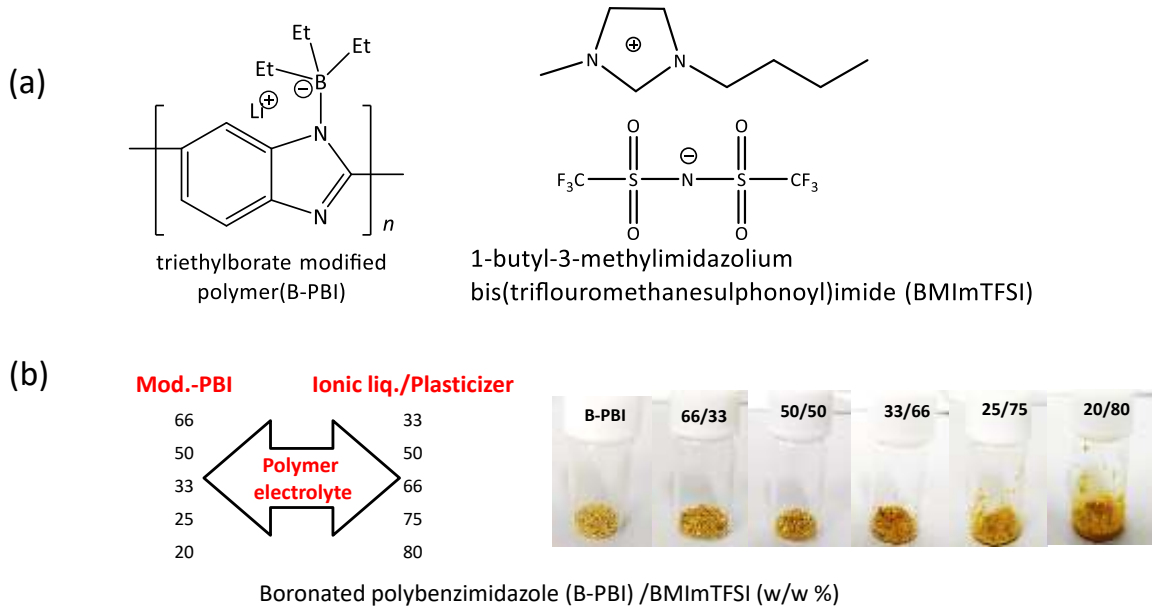

Figure 4.1 (a) Structure of the ionic liquid BMImTFSI and B-PBI **(b)** pictures of the B-PBI/BMImTFSI composite polymer electrolyte

4.3.4 *Measurements:*

The ^{11}B NMR spectra were recorded on a Bruker NMR spectrometer model AVANCE III 400 with BBFO plus ATMA probe operating at 400.13 MHz and DMSO-d_6 was used as the NMR solvent. The ^{13}C solid-state NMR (cross polarizationtotal sideband suppression/CPTOSS) spectra were recorded at 500 MHz on a Bruker Avance III spectrometer at a spinning speed of 8 kHz, using a standard cross-polarization pulse sequence. The samples were packed in a 7 mm-diameter zirconia rotor with a Kel-F cap and were spun at 10 kHz. A contact time of 2 ms was used and the period between the successive accumulations was 5 s. The number of scans was 10000. The FT-IR spectra of the polymers were recorded on a PerkinElmer Spectrum One spectrometer using a diamond- attenuated total reflection (ATR) mode. Thermo-gravimetric analysis (TGA) was conducted using a Hitachi STA7200. The samples (< 5 mg) were placed in a platinum crucible and were heated to a maximum temperature of 800 °C at a heating rate of 5 °C/min. The samples were tested

under nitrogen atmosphere. The 5% (T_{d5}) and 10% (T_{d10}) degradation temperatures of the samples were also investigated along with their temperatures at the onset of degradation (T_{onset}). The ionic conductivity measurement has been done using a complex-impedance gain-phase analyzer (Solartron model 1260; Schlumberger, Germany) over the frequency range of 0.1 Hz–1 MHz. Lithium ion transference number of the samples was measured by the method described by Evans *et al*. [23]. The measurements were carried out under an Ar atmosphere using identical Li electrodes and a potentiostat coupled with a frequency response analyzer (Versastat-3; Princeton Applied Research Co. Ltd.). The impedance measurements were carried out over the frequency range of 100 kHz–10 mHz. A DC potential of 0.03 V (vs. Li/Li^+) was used during the polarization studies.

Evans-Vincent-Bruce equation was used to calculate the t_{Li}^+ of the samples:

$t_{Li}^+ = [Is\ (\Delta V\text{-}I_oR_o)]\ /[I_o\ (\Delta V\text{-}IsRs)]$, where I_o and I_s are the initial and steady state current respectively, R_0 and R_s refer to the charge transfer resistance for the initial and steady states, respectively, ΔV is the DC potential applied across the cell and current determined by the DC polarization.

Linear sweep voltammetry (LSV) measurements were performed in a sandwich cell with a Li/binary mixture electrolyte/Pt configuration. The measurements were performed at a scan rate of 10 mV s^{-1}, over the potential range of 0–6 V vs. Li/Li^+ using a biologic VSP s/n 1190 set-up. The charge-discharge analytical studies were carried out using a silicon-based anodic half-cell was prepared having CR2025 type coin cells with silicon as the working electrode (ϕ 15 mm, Kindly donated by NISSAN Co.), lithium metal as the counter electrode (ϕ 15 mm, Honjo metals, Japan) and a disc-shaped polypropylene based membrane (Celgard) as the separator (16 mm). The prepared silicon-based anodic half-cell was charged and discharged in a galvanostatic mode with a cut off potentials limit (1.5 V-0.01 V) at various current rate

ranging between 0.1-2 C using compact charge and discharge system (EC Frontier; ECAD-1000). DEIS measurements were carried out on a VSP potentiostat (BioLogic) electrochemical analyzer/workstation over a frequency range of 100 kHz-10 mHz with a sinus amplitude of 10 mV. The DEIS measurements were carried out at the open circuit potentials (OCP) of 1.650 V–0.01 V during charging and in the reverse direction during discharging. The step potential divided equally into 16 steps. Rheological measurements were carried out using a rheometer (MCR301, Anton Paar) with a stainless steel cone plate having a diameter of 25 mm (CP25, Anton Paar). The minimum torque which could be detected by the rheometer was 0.1 μN m. During the viscoelastic measurements, the temperature was maintained at 25.0 ± 0.1 °C using a Peltier plate. The samples were directly loaded in a nitrogen atmosphere. At first, a strain sweep test was carried out to determine the linear viscoelastic (LVE) region from the initial strain value of 0.01 to the final strain value of 10 with a constant frequency of 1 rad/s. The frequency sweep test was carried out in the LVE region ($\gamma = 0.01\%$) over the frequency range of 0.01–60 rad/s.

4.4 Results and discussion:

4.4.1 *Structural characterization:*

The FT-IR spectrum of B-PBI (Figure 4.2(a)) showed the peak corresponding to B-N stretching at 875 cm-1, C=N and aromatic C=C peaks were also observed. The broad –NH peak on the iother hand disappeared as the imidazole proton was substituted by triethylborane. Furthermore, the 11B-NMR spectrum (Figure 4.2 (b)) of B-PBI showed a single sharp peak at 2.73 ppm, confirming the sole presence of the quaternary borate B-PBI and the removal of the residual starting material.

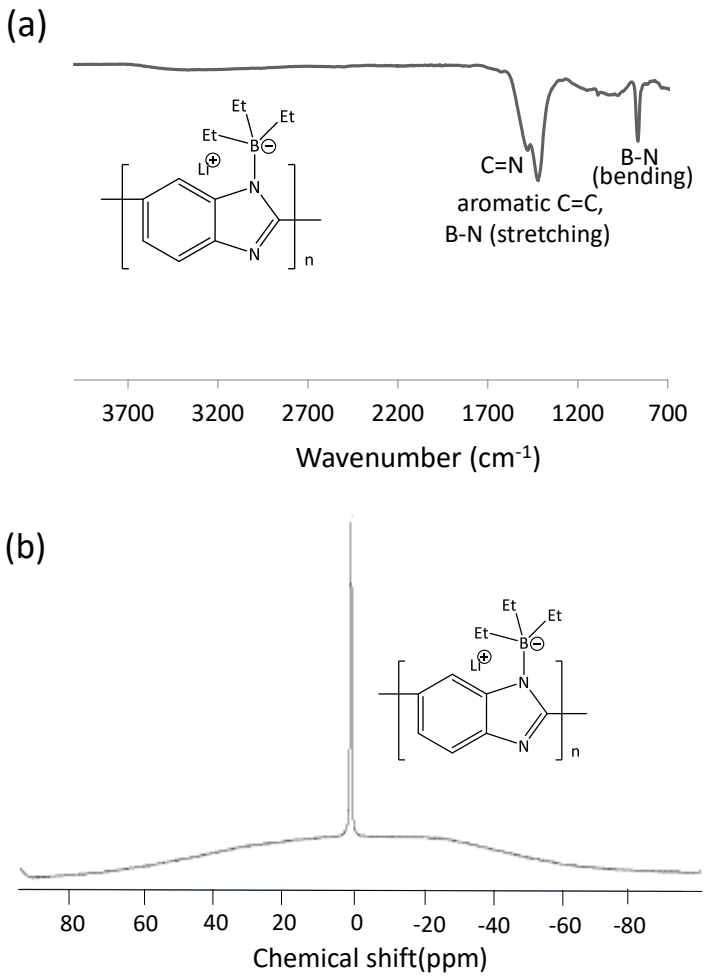

Figure 4.2 Spectra of boronated polybenzimidazole (a) FT-IR spectrum, (b) ^{11}B-NMR showing single borate peak

4.4.2 *Thermal stability of the polymer electrolyte composites:*

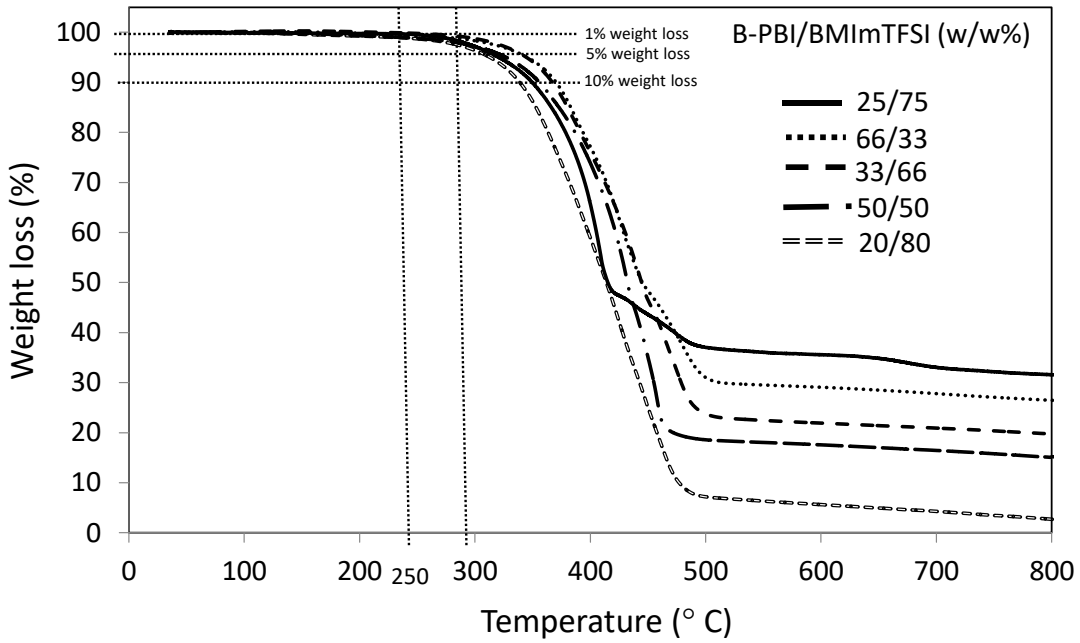

Figure 4.3 Thermo-gravimetric analysis curves of various composite mixtures between boronated polybenzimidazole (B-PBI) and BMImTFSI

Table 4.1 Thermal decomposition temperatures of various polymer electrolytes

B-PBI/BMImTFSI (W/W%)	B-PBI(mol%)[(b)]	BMImTFSI(mol%) [(c)]	T_{d5}[(d)](°C)	T_{d10}[(e)] (°C)
66/33	100 mg ($4x10^{-6}$)	35 µL ($1.2x10^{-4}$)	340	375
50/50	100 mg ($4x10^{-6}$)	70 µL ($2.3x10^{-4}$)	345	370
33/66	100 mg ($4x10^{-6}$)	140 µL ($4.8x10^{-4}$)	335	368
25/75	100 mg ($4x10^{-6}$)	210 µL ($7.1x10^{-4}$)	325	355
20/80	100 mg ($4x10^{-6}$)	280 µL ($9.5x10^{-4}$)	310	340

(a)Thermal decomposition temperatures were determined by thermo-gravimetric analysis under N2, (b) B-PBI: boronated polybenzimidazole; (c) BMImTFSI: 1-Butyl-3-methylimidazolium bis(trifluoromethanesulfonyl)imide which is used as the plasticizing agent ; (d) Td5 : 5% weight loss temperature measured by thermo-gravimetric analysis ; (e) Td10 : 10% weight loss temperature measured by thermo-gravimetric analysis

Figure 4.3 shows the thermal weight loss curves of the electrolyte composites. The onset degradation temperatures of the composites were found to be within the range of 250–300 °C. The 5% (T_{d5}) and 10% (T_{d10}) decomposition temperatures of these composites are given in Table 4.1. These temperatures were high enough for solid-state Li-ion battery applications.

From the viewpoint of safety, thermally stable polymer electrolytes are in great demand for Li-ion batteries. In electric vehicles, the local temperature of batteries may approach 120 °C, which is near or higher than the boiling point of commercial liquid electrolytes. All the composite electrolytes maintain their residual weight in between 15-31 % of their primary weight even at 800 °C except B-PBI/BMImTFSI (w/w %) (20/80), it shows only 2 % residual mass at 800 °C. With increasing amount of added BMImTFSI, residual mass decreases except in the case of (25/75), which shows highest residual mass i.e. 31 %.

4.4.3 *Rheological studies:*

Rheological study is a well-known physical technique to study the flow and deformation properties of materials. In this study at first dynamic shear strain sweep test is most important to determine the viscoelastic region. Dynamic shear strain sweep test is most important to determine the viscoelastic region [29-30]. Storage modulus (G') is representative energy storage in the materials and depends upon the material deformation during the oscillation which is the detrimental factor for the elastic behavior of a certain material. Loss modulus (G'') on the other hand measures the energy lost per capita of sinusoidal deformation and detrimental factor for the viscous behavior of a certain material. The dependence of storage and loss moduli (G', G'') on the shear strain (ϒ) and angular frequency (ω) of the composite polymer electrolyte B-PBI/BMImTFSI (w/w %) (25/75) composition which was solely used as electrolyte (electrochemical studies already performed support its selection for battery application) to prepare anodic half-cells to check battery performance is presented in figure 4.4 (a, b). The electrolyte sample showed linear region (Newtonian plateau) at lower shear strain and become nonlinear at higher strain percentage but *G'* and *G''* doesn't crossover each other even over 10% of shear strain which proves predominate elastic nature of the

composite polymer electrolyte over the viscous nature. The dependence of *G'* and *G''* on the angular frequency (ω) measures the flow behavior of the electrolyte material while the shear strain has been kept as constant at 0.01% and sharp increase of *G'* with ω supports better elasticity nature whereas *G''* also increases monotonously along with ω. Clearly, with lesser amount of added BMImTFSI, other electrolytes like B-PBI/BMImTFSI (w/w %) (66/33), (50/50) and (33/66) shows better solidity. On the other hand, in case of (20/80) solidity decreases further but keeps enough high value to use as composite solid electrolyte.

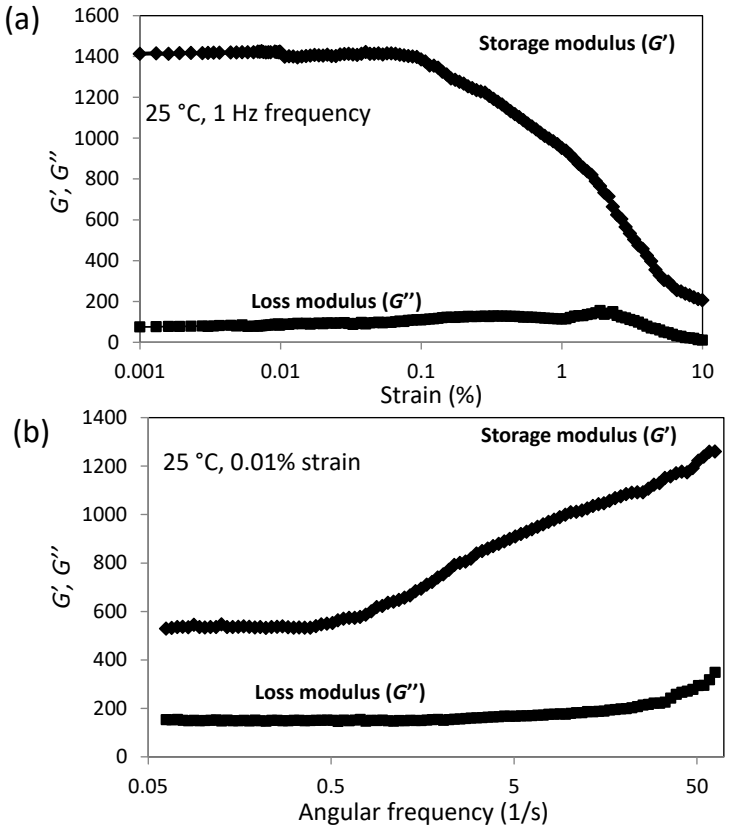

Figure 4.4 Storage moduli, *G'* and loss moduli, *G''* of the polymer electrolyte (25/75) measured with varying (a) shear strain, (b) shear frequency

4.4.4 Electrochemical properties:

4.4.4.1 *Ionic conductivity measurements:*

Ionic conductivity of 66/33, 50/50, 33/66, 25/75 and 20/80 B-PBI/BMImTFSI (w/w%) composites measured at several temperatures using AC impedance method. Since these composite electrolytes already contained lithium salts in the form of lithium borate in the side chain of B-PBI, the addition of any lithium source was not required unlike in the case of most of the commercial polymer electrolytes [31-34]. Prior to the measurements, the samples were dried thoroughly for 24 h at 100 °C under vacuum. The ionic conductivity of the samples increased constantly with temperature (Fig. 4.5). At 51 °C, the composite electrolytes showed an ionic conductivity in the range of 3.0–8.8x10^{-3} S cm^{-1} (Table 4.2). The ionic conductivity of the electrolytes increased with an increase in their IL content. The 25/75 electrolyte showed the highest ionic conductivity of 8.8x10^{-3} S cm^{-1} at 51 °C. The ionic conductivities of the electrolytes developed in this study were at least 10 times higher than those of the electrolytes reported previously, which required externally added lithium salts (Table 4.2). The 66/33 electrolyte had the highest B-PBI content was mainly solid in nature. The liquid nature of the electrolytes was induced by the addition of BMImTFSI. As the BMImTFSI content increased, the number of carrier ions increased, which in turn increased the ionic conductivity of the electrolytes. The Arrhenius plots of the electrolytes showed linear profiles with an increase in temperature, indicating that no decomposition or phase change occurred over the measured temperature range (Figure 4.5(a)). The Vogel-Fulcher-Tammann [35] (VFT) plots (Figure 4.5(b)) of the electrolytes were fitted according to the linear regression equation and the parameters so obtained are listed in Table 4.2.

$$\sigma_{(t)} = A/\sqrt{T}\exp[-B/(T-T_0)]$$

In the above equation $\sigma_{(t)}$ is the ionic conductivity at temperature *T*, whereas T_0 is the ideal glass transition temperature which was optimized to obtain linear VFT plot. '*A*' and '*B*' refer to the number of carrier ions and activation energy for ion transport respectively. With an increase in the BMImTFSI amount, the number of carrier ions increased, while the activation energy decreased.

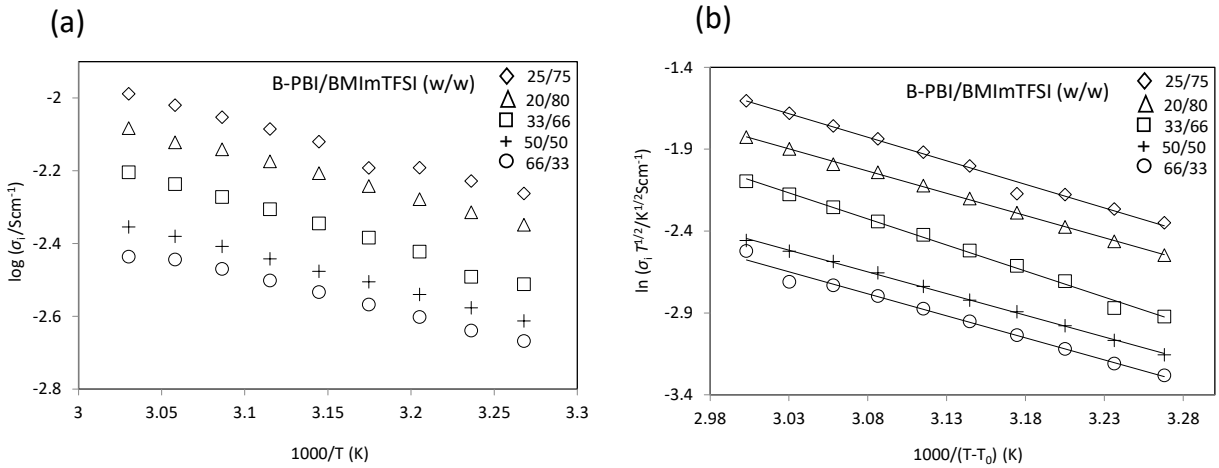

Figure 4.5 Ionic conductivity measurements of various composite polymer electrolytes (a) Arrhenius plots and (b) Vogel-Fulcher-Tammann (VFT) plots

4.4.4.2 *Lithium-ion transference number:*

The contribution of lithium cation migration under the ionic conduction of various ionic species was denoted by t_{Li}^{+}. It was estimated using the method reported by Evans *et al*., which combined the DC polarization and AC impedance techniques [23]. All the measurements were carried out by chronoamperometry and impedance analysis, and the error margin was less than ± 1%. The highest t_{Li}^{+} was observed to be 0.63 at room temperature for

(25/75) B-PBI/BMImTFSI (w/w %) among all the composite polymer electrolytes (Table 4.2) while lithium ion conductivity of the same is in the order of 10^{-3} S cm^{-1}. With an increase in the IL content, the t_{Li}^{+} of the polymer ion gels increased monotonously till it reached the value of 0.63 for the (25/75) B-PBI/BMImTFSI (w/ w %) composite electrolyte. This was unexpected observation; however, it can be attributed to the fact that the efficient plasticization of solid polymer-salt hybrid electrolytes makes them highly dissociable. The lithium transference numbers of the composite electrolytes developed in this study and those reported previously are compared in Table 4.2, which clearly demonstrates the superior characteristics of the electrolytes developed in this study.

Table 4.2 VFT parameters, lithium transference number (t_{Li}^{+}) and working potential window of various composite polymer electrolytes

B-PBI: BMImTFSI	Ionic conductivity (Scm^{-1}) at 51°C[a]	Carrier ion number, *A* ($K^{1/2}Scm^{-1}$) [b]	Activation energy, *B* (K) [c]	R^2 [d]	Lithium Transference number at r.t.[e]	Li-ion conductivity (Scm^{-1}) [f]	Working potential window(V)[g]
66/33	$3.4X10^{-3}$	159	2850.2	0.997	0.27	$9.2X10^{-4}$	ND
50/50	$3.9X10^{-3}$	239	2666.3	0.998	0.42	$1.6X10^{-3}$	4.85
33/66	$5.3X10^{-3}$	1128	2545.7	0.999	0.51	$2.7X10^{-3}$	5.45
25/75	$8.8X10^{-3}$	1356	2433.2	0.999	0.63	$5.5X10^{-3}$	5.22
20/80	$7.2X10^{-3}$	1297	2531.6	0.999	0.57	$4.1X10^{-3}$	ND
$(PEO)_8LiClO_4$	$2.4X10^{-4}$ (at 70°C)	-	-	-	0.20	$4.8X10^{-5}$	4.2
PEG-borate ester $LiClO_4$	$1.0X10^{-3}$ (at 70°C)	-	-	-	0.24	$2.4X10^{-4}$	4.2
PVDF-HFP/$LiClO_4$	$1.06X10^{-3}$ (at r.t.)	-	-	-	0.36	$3.8X10^{-4}$	4.5
Nafion (Li^+)	$2.05X10^{-4}$ (at r.t.)	-	-	-	0.89	$1.8X10^{-4}$	4.2

(a) Temperature varying ionic conductivity measured by using AC impedance method, (b) Carrier ion number resemblance total number of charge carrier ions, (c) activation energy must be lower to make ion conduction easier, (d) R2 : Regression co-efficient, (e) Li- transference number was determined by using DC polarization and AC impedance method, (f) ionic conductivity contributed by cationic (Li+-ion) conduction, (g) Determined using linear sweep voltammetry technique

4.4.4.3 *DC Polarization:*

Chronoamperometry experiments were performed to check Li-ion diffusion in the composite electrolyte matrix. DC voltage of 0.03 V applied across Li/electrolyte/Li type cell for infinite time limit. After certain time, steady state current profiles obtained in the DC polarization method (Figure 4.6), contributed only by Li ion conduction implies that Li ions were successfully incorporated into the polymer during modification [36].

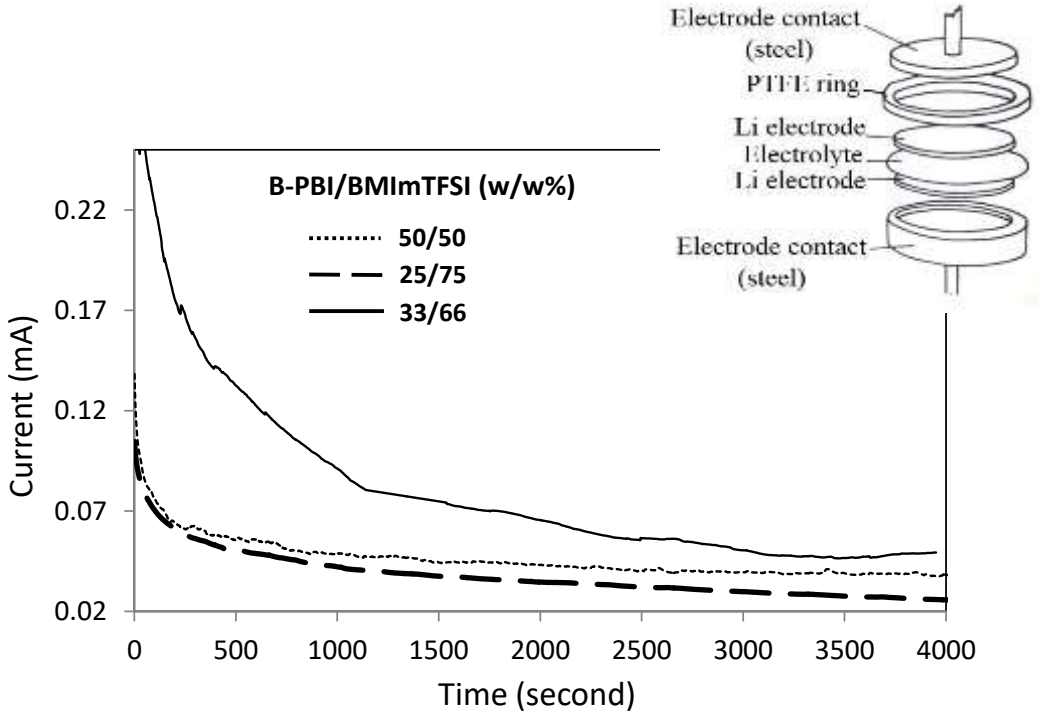

Figure 4.6 DC Polarization profiles of various composites of boronated polybenzimidaozole with BMImTFSi (B-PBI/BMImTFSI)

Inset: Cell set-up for DC polarization

4.4.4.4 *Plausible mechanism responsible for high ionic conductivity:*

Polybenzimidazole (PBI) itself is basically a non-conjugated polymer. However, the imidazolate anion formed after the lithiation and boronation of its imidazole moiety, has six π-electrons, which induce aromaticity. Therefore B-PBI with lithiated and boronated imidazole moiety can be regarded as a unique type of π-conjugated polymer (Scheme 4.3). In the case of the electrolytes developed in this study, anionic charge was delocalized on the PBI-derived conjugated polymer, which reduced the site hopping energy of lithium ions. This specific situation will be responsible for markedly high ionic conductivity and lithium transference number of the resulting polymer ion gel electrolyte. This phenomenon is conceptually novel. Boron atom also receives a considerable number of electrons; however, the boronation of imidazole unit should not be quantitative. In spite of the efficient delocalization of anionic charge, long range electronic conduction occurs along the conjugated chains, which can prevent lithium ion transport. However non-quantitative boronation breaks the π-conjugation to inhibit the electronic conduction, thus increasing the high lithium transference number significantly.

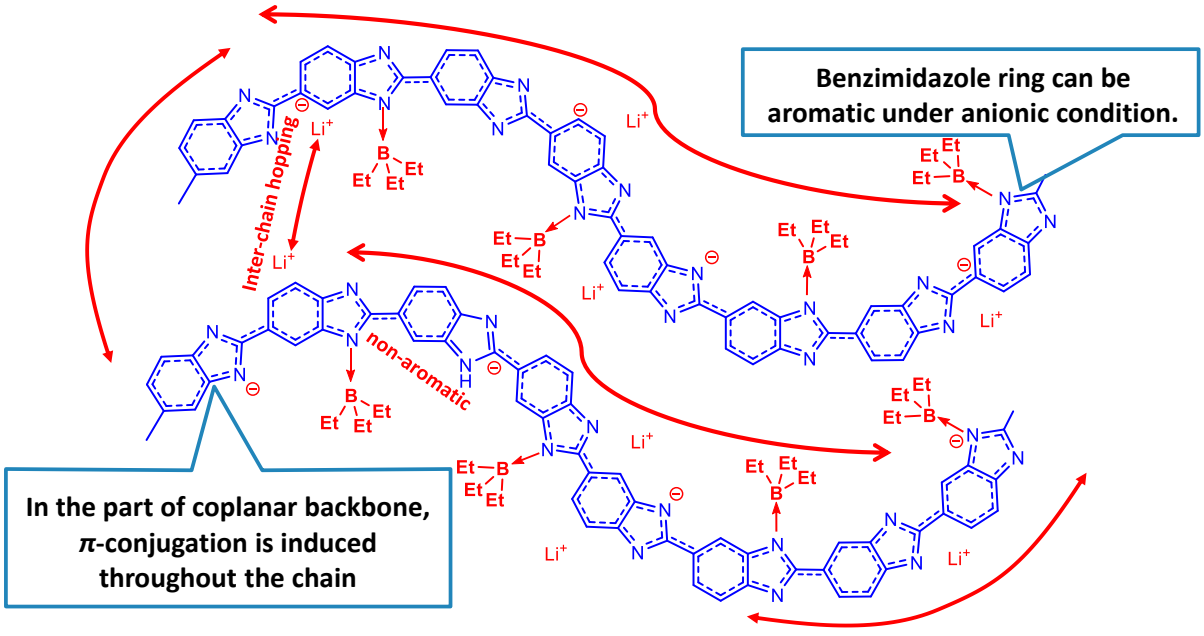

Scheme 4.3 Speculated mechanism of lithium ion conduction through the system

4.4.4.5 *Linear sweep voltammetry (LSV):*

Apart from thermal stability the electrochemical stability is also measured by linear sweep voltammetry (LSV) measurement which is another significant property of the electrolytes for its safe use in lithium ion battery. LSV measurement was performed with various composite polymer electrolytes in Li/electrolyte/Pt cell configuration at a scan rate of 10 mV s^{-1} within 0 to 6 V range of potential. For three composite polymer electrolytes B-PBI/BMImTFSI (w/w %) 50/50, 33/66 and 25/75 we have obtained working potential window in between 4.85 to 5.45 V (Table 4.2). After a linear voltammogram (Figure 4.7) in up to a certain voltage in each case there is a sudden increase of the current which confirms the occurrence of electrochemical reaction and thus provide electrochemical window wide enough to be applied in most of the Li-ion batteries.

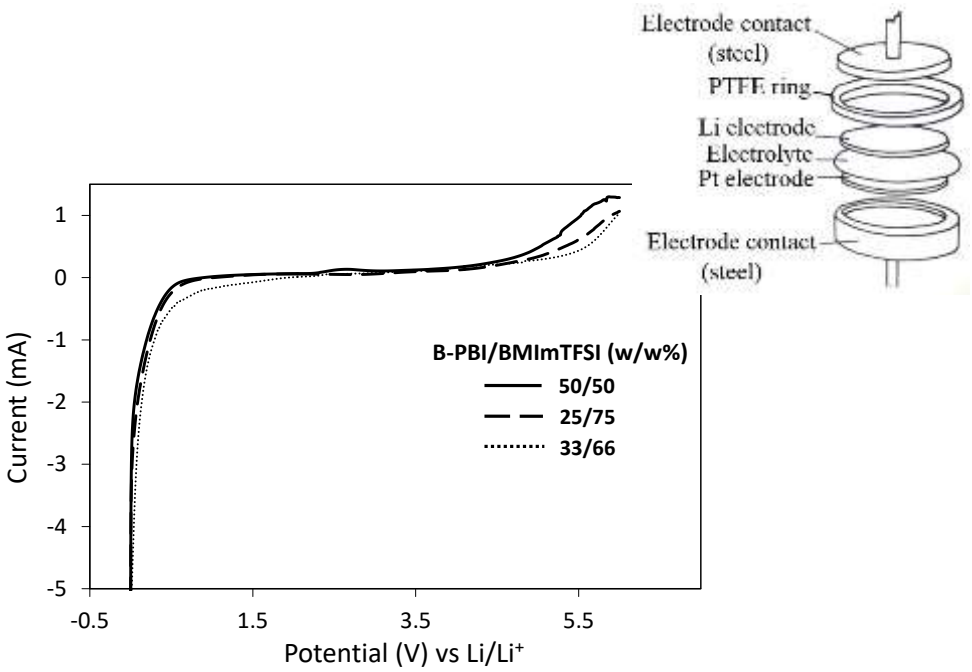

Figure 4.7 Linear sweep voltammetry curves of various composites of boronated polybenzimidaozle and BMImTFSI (B-PBI/BMImTFSI)

Inset: Cell set-up for linear sweep voltammetry measurements

4.4.4.6 *Anodic half-cell fabrication:*

Anodic half-cells were fabricated using CR2025 type cells, with silicon as working electrode (12 ϕ, NISSAN) and lithium metal as counter electrode (15 ϕ, Honjo metals) and prepared composite polymer electrolyte (~ 30 mg) separated by ring shaped Celgard® based separator (15 ϕ) following a format as shown in Figure 4.8, appropriate quantity of ethylene carbonate: diethyl carbonate (EC: DEC) (1:1) (~20 µl) was added to wet the electrolyte for stable SEI formation. Cells assembly was carried out in a glove box maintained under Ar atmosphere. Considerable time was given the cell to allow the cell to get stabilized.

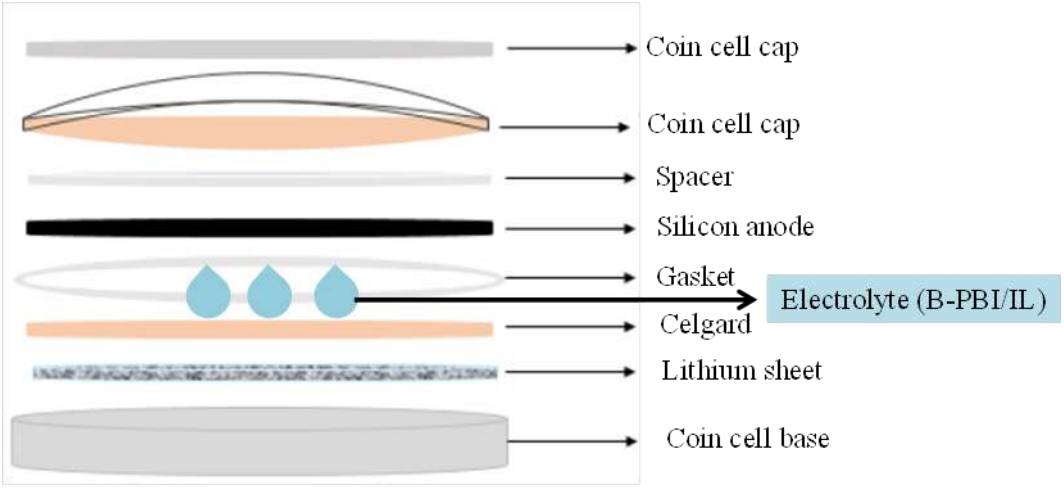

Figure 4.8 Anodic half-cell set-up for charge-discharge

4.4.4.7 *SEI layer formation in solid polymer electrolyte:*

Solid electrolyte interphase (SEI) layer formation is a common phenomenon of layer formed between electrode (mainly on the anode surface and primarily during the first cycle) and solid polymer electrolyte. As they are well-known for high electrochemical safety at high energy density SEI layer must also be stable to make the device function properly [38]. As shown in

below schematic diagram 4.4 (a, b) the components that are usually products from salt degradation and solvent reduction in the electrolytes [41-42]. Performance of LiBs specially rate capability, cyclability, reversible capacity depends on stabilization of the passivation layer such as: SEI layer. Stable passivating SEI layer usually prevents the corrosion of the electrode from reaction with the electrolyte by inhibiting undesired electrolyte consumption, but also limits the kinetics of the ion transport processes [43]. Most of the compounds in the SEI layer contain Li, which associates with an irreversible capacity loss. Understanding the formation mechanism as well as the chemical composition of the SEI is necessary to improve battery performance. Analysis of pristine SEI layer formation and its stability is considered to be very difficult task for electrochemists as they are highly sensitive to air, moisture etc. and varieties of techniques were developed. Photoelectron spectroscopy is very widely popular technique for surface analysis of the electrodes. Le Granvalet-Mancini *et al.* [39] studied the passivation layer formed on the lithium metal which is in contact with PEO-triflate SPE using Atomic Force Microscopy (AFM) and concluded that the layer has low conductivity. Ismail *et al.* [40] used XPS to investigate the surface layer on lithium metal after contact with lithium salt doped SPEs.

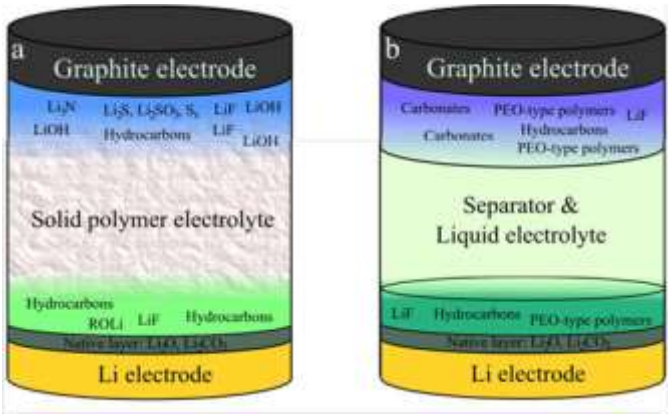

Scheme 4.4 Schematic representation of compositions of the SEI layers formed in (a) polymer electrolyte based, (b) conventional liquid electrolyte based

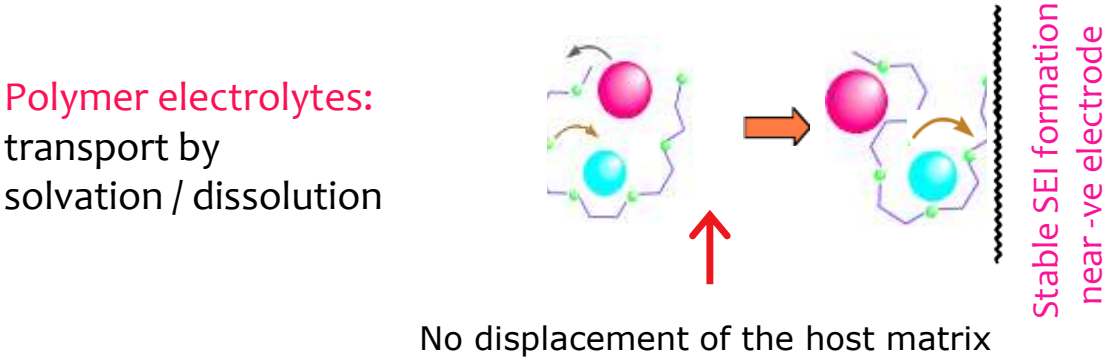

Scheme 4.5 Lithium ion transport mechanism comparing between liquid electrolytes and solid electrolytes followed by SEI formation

In this chapter, we will introduce a comparatively novel technique of understanding real-time SEI formation, optimization of the potential window; stability of the formed SEI layer etc. based on dynamic electrochemical impedance spectroscopy (DEIS) which is different than conventional electrochemical impedance spectroscopy (EIS) method.

4.4.4.8 *Charge-discharge studies:*

The prepared silicon based anodic half-cell was charged and discharged using ECAD 1000 single channel system. The charge-discharge study were done at various charging rates, during charging process, lithium ions travel towards silicon anode, while during discharging in the opposite direction.

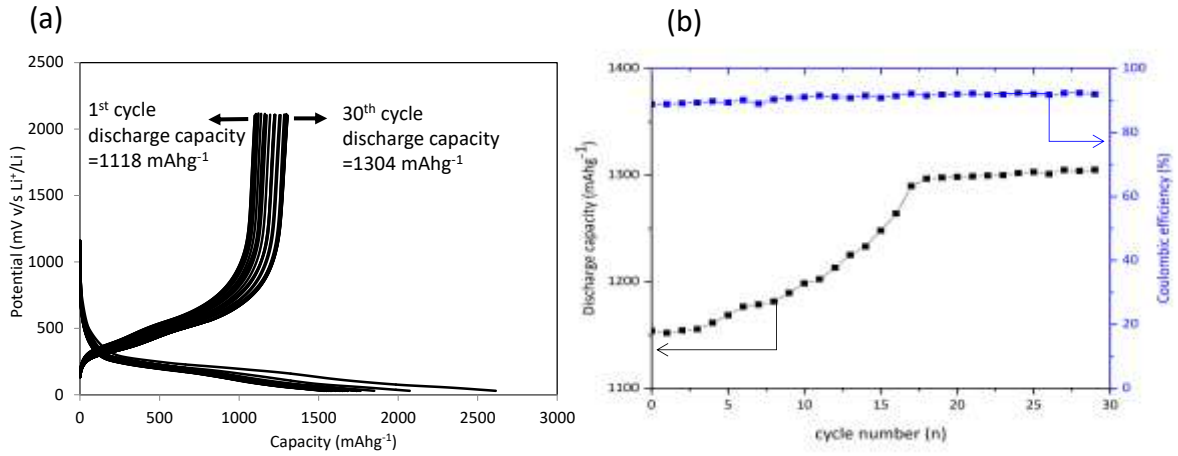

Figure 4.9 Charge-discharge measurements of the Li/electrolyte/Si cell fabricated using (25/75) B-PBI/BMImTFSI (w/w %) polymer electrolyte at 0.1C (a) Charge-discharge profile (b) Discharge capacity and Coulombic efficiency

4.4.4.9 *Battery performance:*

Because of its high ionic conductivity and t_{Li}^{+}, (25/75) B-PBI/BMImTFSI (w/w %) was further subjected to electrochemical studies. Charge-discharge characteristics were studied for the composition B-PBI/BMImTFSI 25/75 (w/w %) in a coin type anodic half-cell. The CR2025 coin-type anodic half-cell consisted of silicon as the working electrode, Li metal as the counter electrode, a polypropylene separator, and the composite polymer as the electrolyte (ca. 30 mg). Ethylene carbonate: diethylene carbonate (EC: DEC) solution (25-30 µL) was used to wet the electrode surface. The application of the EC: DEC accelerated the formation of the solid electrolyte interface (SEI) layer through the interaction with the

electrode. The cell was assembled in a glove box under an argon atmosphere (UNICO UN-650F, H_2O and O_2 content <0.1 ppm). The assembled cell was kept undisturbed overnight for stabilization. First, the anodic half-cell was subjected to two cycles at 0.05 C rate. Highly irreversible capacity was observed during these cycles because of the formation of the SEI layer. It was then subjected to 30 more cycles at 0.1 C rate, the result of charge-discharge is shown in Figure 4.9 (a), (b) shows the cycling performance (the discharge capacity and Coulombic efficiency) of the composite electrolyte at 0.1 C rates. The discharge capacity increased with an increase in the number of cycles, indicating that a stable conductive SEI layer was formed during this period. After 18 cycles of increasing values, discharge capacity got stabilized for the next 12 cycles at the same charging rate. The Coulombic efficiency of

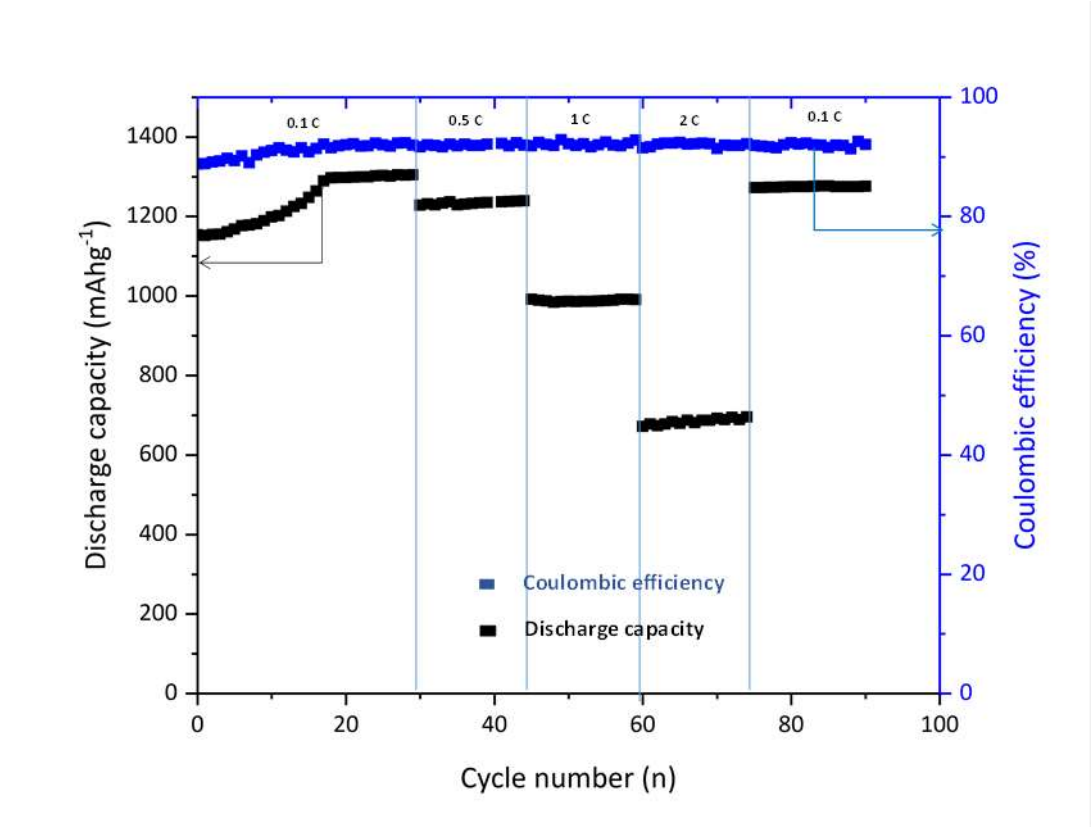

Figure 4.10 Rate cycling performance of the Li/electrolyte/Si cell fabricated using the (25/75) B-PBI/BMImTFSI (w/ w%) polymer electrolyte for 90 cycles at various rates (cycle 0-29 at 0.1 C, 30-44 at 0.5 C, 45-59 at 1 C and 60-74 at 2 C and again 75-89 at 0.1

the electrolyte increased with an increase in the number of cycles because of the formation of a good SEI layer. Figure 4.10 shows the cycling performance of the cell at variable charging rates of 0.1 C–2 C. The discharge capacity and Coulombic efficiency values were plotted as a function of the number of cycles. When the current rate was increased by five times i.e., from 0.1 C to 0.5 C (30^{th}–44^{th} cycle), discharge capacity decreased as expected. However, the discharge capacity stabilized with an increase in the number of cycles at 0.5 C. At the current rate of 1 C (45^{th}–59^{th} cycle), discharge capacity decreased, while the Coulombic efficiency showed constant values. When the current rate was further increased to 2 C (60^{th}–74^{th} cycles), the discharge capacity decreased further, whereas the Coulombic efficiency remained constant for almost all the current rates. Most importantly when it reverts to lower charging rates of 0.1 C (75^{th}–89^{th} cycles), cell produced discharge capacity of 1275 mAh g^{-1} with constant coulombic efficiency. It exhibits the structural stability of the prepared anodic half-cell. These results indicate that the formation of the SEI layer occurred via a reaction between the EC: DEC solvent and the electrode. The SEI layer stabilized with time at both the lower and higher rates. Furthermore, cathodic half-cell was also prepared using $LiNi_{0.33}Co_{0.33}Mn_{0.33}O_2$ (Li-MNC)/electrolyte/Li cell to perform charge-discharge at high potential (~4.5 V). Similar to the anodic half-cells, we have performed charge-discharge for 30 cycles at 0.1 C as shown in Figure 4.11(a, b). Stable SEI layer formation was depicted from increasing trend of discharge capacity even at higher potential range, which in the other way exhibits electrochemical stability of the prepared electrolyte.

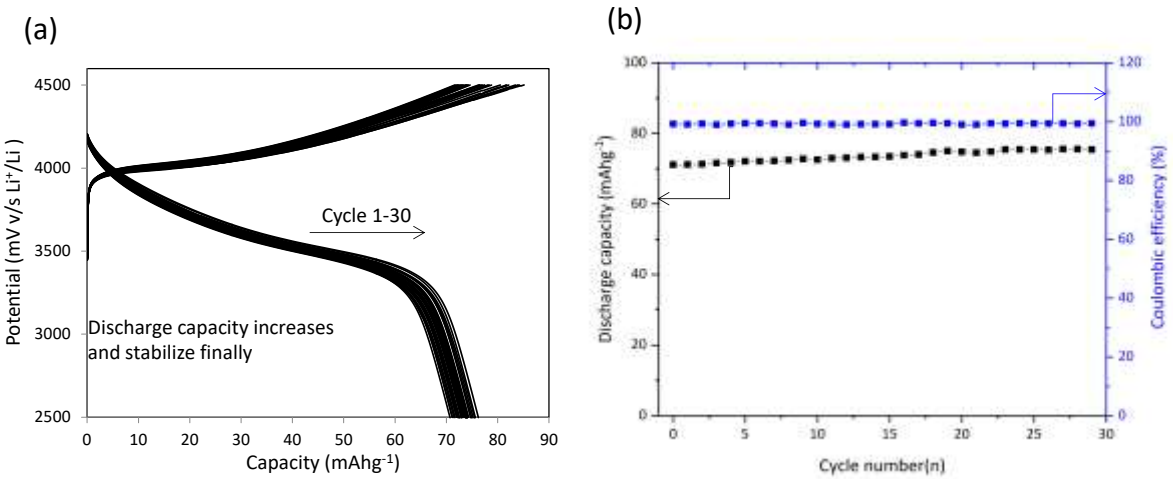

Figure 4.11 Charge-discharge measurements of the Li-MNC/electrolyte/Li cell fabricated using (25/75) B-PBI/BMImTFSI (w/w %) polymer electrolyte at 0.1C (a) Charge-discharge profile (b) Discharge capacity and Coulombic efficiency

4.4.4.10 *Impedance analysis:*

Impedance analysis is a non-destructive, deeper study of the interfacial properties inside the battery before and after charge-discharge cycling. To further confirm the formation of a better interface during charge-discharge process electrochemical impedance spectroscopy (EIS) measurements of the anodic half-cell were performed during before and after charge-discharge conditions. Initially the measurement was carried out for a freshly prepared anodic half-cell at its OCP and then after 10 cycles of charge-discharge at 0.5 C rate to check the effect of cycling on the impedance plots. Figure 4.12 shows the impedance profiles for before and after cycling with the same half-cell and it can be easily concluded that during cycling charge-transfer resistance (R_{CT}) decreased as compared to the freshly prepared half-cell. Upon equivalent circuit fitting (Table. 3) all the parameters including R_{CT} (R_2) are lower in value after charge-discharge as compared with the corresponding parameters of the freshly prepared cell which infers that the overall impedance of the anodic half-cell is reduced as charge-discharge proceeds.

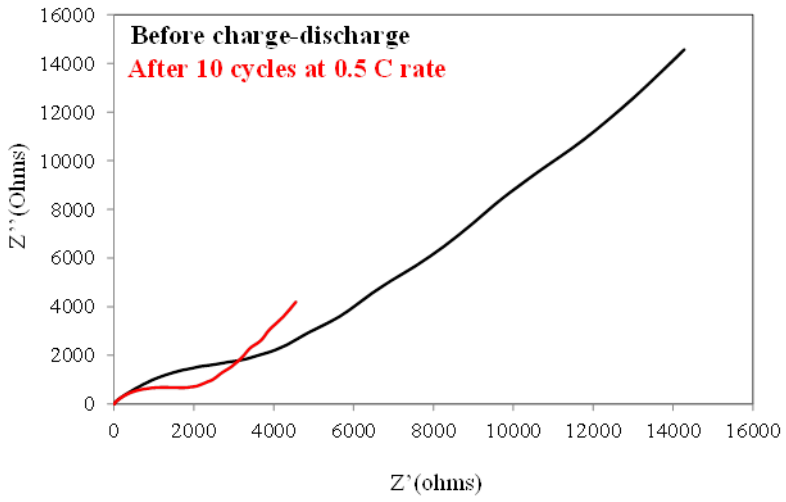

Figure 4.12 Comparative Nyquist plots of the anodic half-cell using polymer electrolyte (25/75) measured immediately after fabrication and after charge-discharge

Table 4.3 Circuit fitting of impedance measurements immediately after fabrication and after charge-discharge

	Circuit	R_1	$R_2(R_{CT})$	R_3	R_4	x^2
Before cycling	R(QR)(CR)(Q(RW))	8.95	98.31	3428	$5.25\text{x}10^{4}$	$2.73\text{x}10^{-4}$
After cycling	R(QR)(CR)(Q(RW))	4.89	91.91	1661	$2.68\text{x}10^{4}$	$4.11\text{x}10^{-4}$

(a)Circuit fitting to quantitatively extract physical values from impedance data, (b)Chi-square values correspond to equivalent electric circuit models (EECMs) circuit fitting accuracy

After charge-discharge cycling, the R_{CT} of the cell decreased significantly, indicating the formation of a stable SEI layer, which improved the interfacial properties [37]. To further investigate the interfacial changes during the charge-discharge process DEIS measurements were carried out. The DEIS approach is superior to EIS as it produces impedance spectra at regular potential intervals, which mimics the actual charge-discharge process between cut-off potentials.

4.4.4.11 *Dynamic Electrochemical Impedance Spectroscopy (DEIS):*

It was deemed requirement to understand the internal parameters of the cell, which could probably improve cycle-life, stability etc. Estimation of working potential range can be determined using cyclic voltammetry and potential window experiments. However, those methods are insufficient to optimize the range within the available electrochemical window. Also, in classic electrochemical impedance spectroscopy (EIS) method, impedance measurements are performed after the battery reaches at a steady state, for which there is no direct current (DC). Hence, during the equilibrium state of the battery experiencing zero DC potential, the real picture of the interfacial process cannot be depicted using EIS. Recently, DEIS has been introduced as characterization technique to determine the electrochemical responses of interfacial phenomenon. This technique provides variable frequency response of an AC signal superimposed with a potentiodynamic DC voltage during potential scan of anodic half-cells. In a nut-shell following are the advantages of DEIS over conventional EIS method [20, 21]:

a) Differences between charging and discharging process (i.e. intercalation and de-intercalation of lithium ions over the electrode) can be easily determined while obtaining the real time information from batteries.

b) Electrochemical reactions result in the formation of the SEI and depending upon the electrolytes and electrodes SEI layer can be stabilized or decayed which can be determined using DEIS technique.

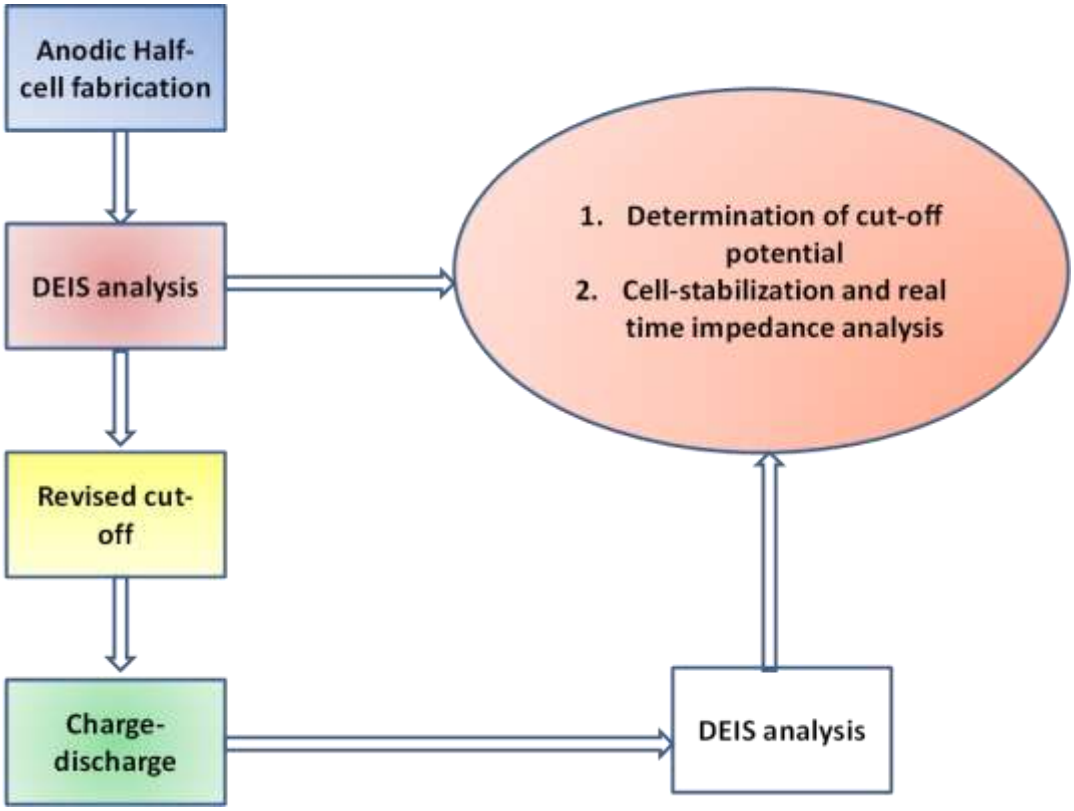

Figure 4.13 Protocol employed for DEIS analysis of the prepared anodic half-cells using composite polymer electrolyte

Fresh anodic half-cell was fabricated using polymer electrolyte (25/75) and after overnight stabilization DEIS measurement was performed i.e. charging and discharging at various potentials were measured. From the charge-discharge study at various rates (fig. 4.10) it was found that after first few cycles at the current rate of 0.5 C reversible capacities got steady and increased with increasing cycle number which may be the result of the formation of SEI layer and lithium intercalation as discussed in the previous section. We cycled the same cell at the rate of 0.5 C for 10 cycles, followed by charge-discharge DEIS was performed in the similar fashion to study the effect of cycling on the interface and formation of the SEI layer if any. Fig. 4.14(a, b) shows the DEIS profiles during charging comparing the variation of R_{SEI} (representing Li^+ transport resistance through the SEI layer) with respect to the potential for both the cases of freshly prepared and already pre-cycled anodic half-cell. Now, close look at

fig. 4.14 (a and b) i.e. comparing between the DEIS charging profiles before and after cycling it is clearly observed that semicircle radii i.e. R_{SEI} at higher frequency were restrained in case of pre-cycled cell as compared with that of the freshly prepared cell. Similar observations were found for the DEIS discharging profiles as well [fig. 4.15 (a, b)] i.e. overall radii of the semicircles are getting diminished in case of pre-cycled cell as compared with the freshly prepared cell. For quantitative analysis we performed fitting of the impedance data to equivalent electric circuit models (EECMs) from the corresponding Nyquist and Bode plots [22]. R_{SEI} corresponding impedance values during charging and discharging process obtained from DEIS were plotted against various potentials for both the cases of freshly prepared and pre-cycled half-cells as shown in fig. 4.16 (a, b). Quantitative data also supports the formation of the stable interface which results in the decrease of the R_{SEI} leading to improved reversible capacity in the case of pre-cycled cell as compared with the freshly prepared cell. Closely reproducible plots of R_{SEI} with respect to the potential values during both charging and discharging infer indirect evidence for the stability of the electrode-electrolyte interface even after several cycles.

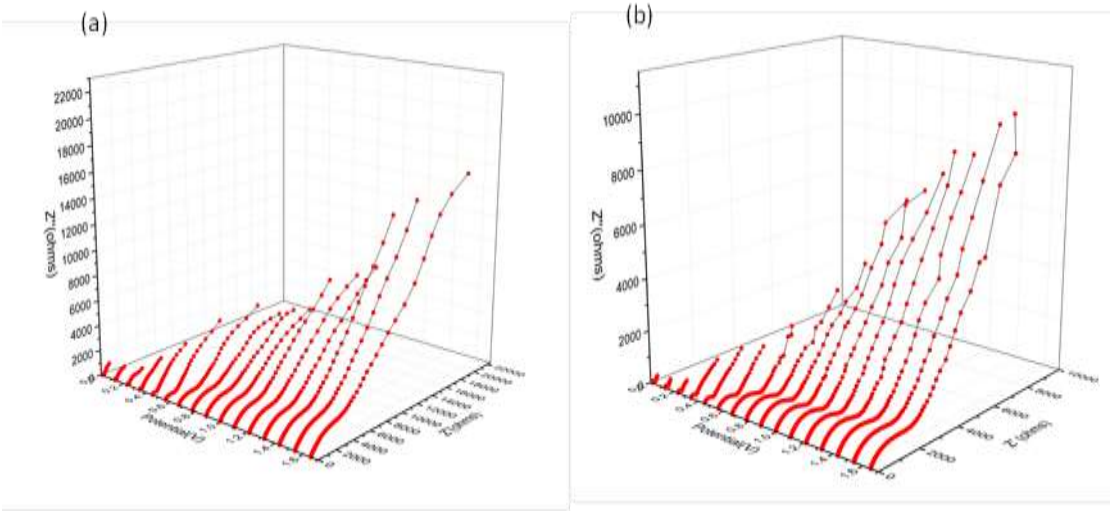

Figure 4.14 DEIS profile during charging of an anodic half-cell fabricated using polymer electrolyte (25/75), (a) freshly prepared cell, (b) after 10 cycles at charging rate of 0.5 C

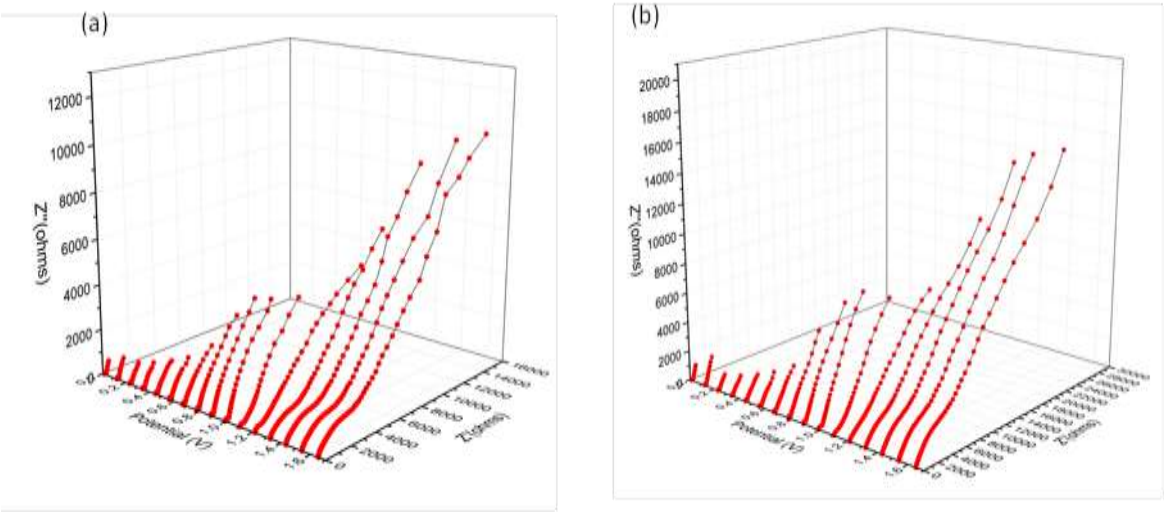

Figure 4.15 DEIS profile during discharging of an anodic half-cell using polymer electrolyte (25/75), (a) freshly prepared cell, (b) after 10 cycles at charging rate of 0.5 C

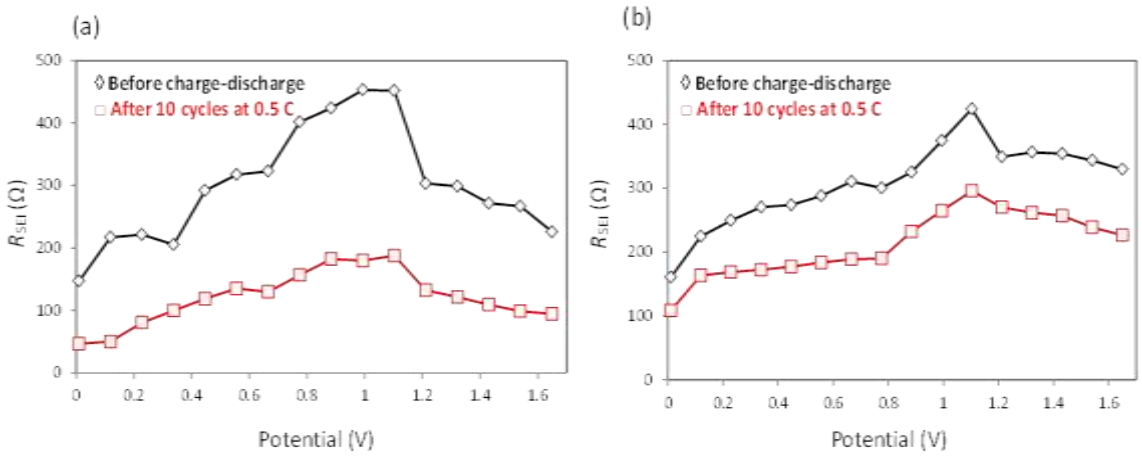

Figure 4.16 Variation of R_{SEI} with potential of the anodic half-cell fabricated using polymer electrolyte (25/75) and comparison between freshly prepared and pre-cycled cell, (a) during charging of DEIS measurements and (b) during discharging of DEIS measurement.

4.5 Conclusion:

Poly (2, 5-benzimidazole) (ABPBI) was modified by the formation of lithium imidazolate formation by complex formation with triethylborane to design ionic B-PBI. Further, it was mixed with BMImTFSI to prepare various composite polymer electrolytes (B-PBI/BMImTFSI (w/w %)) exhibiting single ion conductivity. All these composites showed thermal stability at temperatures in the range of 250–300 °C and an average 10% weight loss temperature (T_{d10}) as high as 350 °C The solidity of the composites was evaluated by rheological measurements, which revealed that their storage modulus was higher than the loss modulus. Ionic conductivity and Li-ion transference number t_{Li}^{+} were measured for the composite series and better properties were observed as BMImTFSI content increase relative to B-PBI. The (25/75) B-PBI/BMImTFSI (w/ w %) composite showed the highest ionic conductivity and t_{Li}^{+} of 8.8×10^{-3} S cm^{-1} and 0.63, respectively. The LSV measurements revealed that the composites showed a wide potential window of 4.85–5.45 V, which is high enough for high-energy battery applications. Battery performance was evaluated using the (25/75) B-PBI/BMImTFSI (w/ w %) composite and discharge capacity showed stable profiles at different charge-discharge rates and even at a high current rate of 2 C more than 53% of reversible capacity remains as compared with the rate of 0.1 C. The composite showed a Coulombic efficiency of >90% irrespective of the current rate. EIS and DEIS studies were carried out to investigate the interfacial properties of the composite electrolyte-based anodic half-cell before and after charge-discharge cycling. The R_{SEI} of the cell decreased after cycling, indicating that cycling resulted in the formation of a stable SEI layer.

4.6 References:

1. Bruce, P. G., Scrosati, B., Tarascon, J-M. *Angew. Chem. Int. Ed.*, 2008, 47, 2930.
2. Tarascon, J. M., Armand, M. *Nature*, 2001, 414, 359.
3. Quartarone, E., Mustarelli, P. *Chem. Soc. Rev.*, 2011, 40, 2525.
4. Deng, K., Wang, S., Ren, S., Han, D., Xiao, M., Meng, Y. *ACS Appl. Mater. Inter.*, 2016, 8, 33642.
5. Porcarelli, L., Shaplov, A. S., Salsamendi, M., Nair, J. R., Vyogdskii, Y. S., Mecerreyes, D., Gerbaldi, C. *ACS Appl. Mater. Inter.*, 2016, 8, 10350.
6. Zhang, Y., Lai, J., Gong, Y., Hu, Y., Liu, J., Sun, C., Wang, Z. L. *ACS Appl. Mater. Inter.*, 2016, 8, 34309.
7. Hou, H., Xu, Q., Pang, Y., Li, L., Wang, J., Zhang, C. Sun, C., *Adv. Sci.*, 2017, 4, 1700072.
8. Wakihara, M. *Mater. Sci. Eng.*, 2001, R33, 109.
9. Matsumi, N., Nakashiba, M., Mizumo, T., Ohno, H. *Macromolecules*, 2005, 38, 2040.
10. Zhang, H., Li, C., Piszcz, M., Coya, E., Rojo, T., Rodriguez-Martinez, L. M., Armand, M., Zhou, Z. *Chem. Soc. Rev.*, 2017, 46, 797.
11. Matsumi, N., Sugai, K., Ohno, H. *Macromolecules*, 2002, 35, 5731.
12. Matsumi, N., Mizumo, T., Ohno, H. *Chem. Lett.*, 2004, 33(4), 372.
13. Qin, B., Liu, Z., Zheng, J., Hu, P., Ding, G., Zhang, C., Zhao, J., Kong, D., Cui, G., *J. Mater. Chem. A*, 2015, 3, 7773.
14. Gupta, H., Shalu, Balo, L., Singh, V. K., Singh, S. K., Tripathi, A. K., Verma, Y. L. Singh, R. K. *Solid State Ionics*, 2017, 309, 192.
15. Tiruye, G. A., Munoz-Torrero, D., Palma, J., Anderson, M., Mercilla, R. *J. Power Sources*, 2015, 279, 472.

16. Liao, K. S., Sutto, T., Andreoli, E., Ajayan, P., McGrady, K. A., Curran, S. A. *J. Power Sources*, 2010, 195, 867.

17. Ye, H., Huang, J., Xu, J. J., Khalfan, A., Greenbaum, S. G. *J. Electrochem. Soc.*, 2007, 154(11), A1048.

18. Sun, C., Liu, J., Gong, Y., Wilkinson, D. P., Zhang, J. *Nano Energy*, 2017, 33, 363.

19. Ye, Y-S., Rick, J., Hwang, B-J. *J. Mater. Chem. A*, 2013, 1, 2719.

20. Smaran, K. S., Joshi, P., Vedarajan, R., Matsumi, N. *ChemElectroChem*, 2015, 2(12), 1913.

21. Patnaik, S. G., Vedarajan, R., Matsumi, N. *J. Mater. Chem. A*, 2017, 5(5), 17909.

22. Huang, J., Li, Z., Zhang, J. *J. Power Sources*, 2015, 273, 1098.

23. Evans, J., Vincent, C. A., Bruce, P. G. *Polymer*, 1987, *28*(13), 2324.

24. Bhavsar, R. S., Kumbharkar, S. C., Rewar, A. S., Kharul, U. K. *Polym. Chem.*, 2014, 5, 4083.

25. Jung, M., Lee, W., Krishnan, N. N., Kim, S., Gupta, G., Komsiyska, L., Harms, C., Kown, Y., Henkensmeier, D. *Appl. Surf. Sci.*, 2018, 450, 301.

26. Nawn, G., Pace, G., Lavina, S., Vezzu, K., Negro, E., Bertasi, F., Polizzi, S., Notto, V. D. *Macromolecules*, 2015, 48, 15.

27. Nawn, G., Vezzu, K. Bertasi, F., Pagot, G. Pace, G., Conti, F., Negro, E., Notto, V. D. *Electrochim. Acta*, 2017, 228, 562.

28. Shalu, V. K. Singh, R. K. Singh, *J. Mater. Chem. C*, 2015, 3, 7305.

29. Mitsumata, T. Miura, T., Takahashi, N., Kawai, M. Okajima, M. K. Kaneko, T. *Phys. Rev. E*, 2013, 87, 042607.

30. Schaefer, J. L., Moganty, S. S., Yanga, D. A., Archer, L. A. *J. Mater. Chem. A*, 2011, 21, 10094.

31. Wang, M., Zhao, F., Dong, S. *J. Phys. Chem. B*, 2004, 108, 1365.

32. Kato, Y., Yokoyama, S., Yabe, T., Ikuta, H., Uchimoto, Y., Wakihara, M. *Electrochim. Acta*, 2004, 50, 281.

33. Liu, W., Zhang, X. K., Wu, F., Xiang, Y. *IOP Conf. Ser.: Mater. Sci. Eng*., 2017, 213, 012036.

34. Sun, H. Y., Sohn, H. J., Yamamoto, O., Takeda, Y., Imanishi, N. *J. Electrochem. Soc*, 1999, 146 (5), 1672.

35. Perez-Madrid, A. *J. Chem. Phys*., 2005, 122, 214914.

36. Singh, A., Vedarajan, R., Matsumi, N. *J. Electrochem. Soc.*, 2017, 164 (8), H5169.

37. Joshi, P., Iwai, K., Patnaik, S. G., Vedarajan R., Matsumi, N. *J. Electrochem. Soc.*, 2018, 165 (3), A493.

38. Xu, C., Sun, B., Gustafsson, T., Edstrom K., Brandell, D., Hahlin, M. *J. Mater. Chem. A*, 2014, 2, 7256.

39. Granvalet-Mancini, L. M., Hanrath, T., Teeters, D. *Solid State Ionics*, 2000, 135, 283.

40. Ismail, I., Noda, A. Nishimoto, A., Watanabe, M. *Electrochim. Acta*, 2001, 46, 1595.

41. Aurbach, D. *J. Power Sources*, 2000, 89, 206.

42. Andersson, A. M., Henningson, A., Siegbahn, H., Jansson, U., Edström, K. *J. Power Sources*, 2003, 119-121, 522.

43. Verma, P. Maire, P., Novák, P. *Electrochim. Acta*, 2010, 55, 6332.

Chapter 5:

General Conclusion

General Conclusion:

Aromatic rigid chain polymers are well-known for their superior thermo-mechanical and other properties as high-performance plastics over aliphatic backbone polymers. Recently, bio-based polymers developed and commercialized are mainly aliphatic ring polymers. Bio-based high-performance polybenzimidazoles were prepared in this research using bio-derived monomers starting from various natural sources. All the aromatic monomers used in this research are either directly nature-derived through white biotechnological pathway or chemically modified the bio-available starting molecules. Also, apart from extra-ordinary physical properties of these polymers were employed for various applications through structure modification, copolymerization etc.

In the **Chapter 2**, detail descriptions on various monomer syntheses were given to prepare polybenzimidazole, polybenzoxazole and polyamide. Novel route to prepare 3, 4-diamino benzoic acid (3, 4-DABA) starting from biomolecule 3-amino-4-hydroxybenzoic acid (3, 4-AHBA) was established. Smiles rearrangement was employed as the main step for this conversion, each steps were optimized and characterized using ^{1}H-NMR and ^{13}C-NMR. Homopolymers PBI and PBO were prepared using bio-based monomers and were characterized using FT-IR, solid state ^{13}C-NMR, TGA etc. Membrane casting method of these bio-based polymers was described as well and mechanical properties such as; strength, flexibility was also determined in both cases.

In the **Chapter 3**, PABA was introduced as comonomer with PBI to obtain novel copolymer structure PBI-*co*-PA with ultra-high thermal stability. Due to rigidity in PBI polymer chains and insolubility, incorporating polyamide (PA) units can be introduced to increase processibility of the copolymer. But, we observed very interestingly, that small composition of PA (15%) along with 85% DABA composition can produce highest thermal stability (T_{d10}, 743°C) among all the existed petroleum or bio-derived polymers. Now, this

super-high heat resistance and good processibility can be important to enable the plastic to be hybridized with metals/inorganic compounds to prepare organic-inorganic hybrids and can be applied as super-integrated circuits, high-power motors etc. On the other hand, PBO moiety was introduced with PBI moiety to synthesize another novel copolymer structure PBO-*co*-PBI. High PBO composition copolymers showed very low dielectric constant (ultra-low *k*) along with high thermal and mechanical stability which is prerequisite to be used as insulating agent in microelectronics.

In the **Chapter 4,** PBI polymer backbone was modified by substituting the imidazole proton with lithium hydride followed by triethylborane to prepare ionic B-PBI. This modified B-PBI was formed with loosely bound lithium ions and can be lithium ion conducting solid polymer. Next, composite formation took place by mixing with ionic liquids BMImTFSI (B-PBI/BMImTFSI) (w/w %) which exhibits single ionic conductivity. All these composites showed high thermal stabilities at the temperature range of 250-300 °C with T_{d10} around 350 °C and solidity was checked quantitatively using dynamic shear strain sweep test. Ultra-high ionic conductivity of 8.8×10^{-3} S cm^{-1} at 51 °C, much higher as compared with other reported composite solid polymer electrolytes such as: PEO-based or PEG-based electrolytes. LSV measurements revealed wide electrochemical window of all the composite polymer electrolytes ranged between 4.85-5.45 V, to apply for high energy battery applications. Charge-discharge study at various rates shows stable discharge capacity and high coulombic efficiency. Also, we have introduced comparatively newer technique of DEIS to examine interfacial properties during charge-discharge.

Research achievements:

Main publications:

1. **Aniruddha Nag**, Md. Asif Ali, Ankit Singh, Raman Vedarajan, Noriyoshi Matsmi, Tatsuo Kaneko, "N-boronated polybenzimidazole for composite electrolyte design of highly ion conductive pseudo solid-state ion gel electrolytes with high Li-transference number" *J. Mater. Chem. A*, 2019, 7, 4459–4468.

2. **Aniruddha Nag**, Md. Asif Ali, Makoto Watanabe, Maninder Singh, Kittima Amornwachirabodee, Shunsuke Kato, Tetsu Mitsumata, Kenji Takada, Tatsuo Kaneko, "High-performance poly(benzoxazole/benzimidazole) bio-based plastics with ultra-low dielectric constant from 3-amino-4-hydroxybenzoic acid" *Polym. Degrad. Stab.*, 2019, 162, 29-35.

3. **Aniruddha Nag**, Md. Asif Ali, Makoto Watanabe, Maninder Singh, Kittima Amornwachirabodee, Shunsuke Kato, Tetsu Mitsumata, Kenji Takada, Tatsuo Kaneko, "Dataset of various characterizations for novel bio-based plastic poly (benzoxazole-co-benzimidazole) with ultra-low dielectric constant" *Data in Brief* (2019) (submitted).

4. **Aniruddha Nag *et al.*** "Ultrahigh heat-resistant bioplastics developed from cellulosic feedstock" to be submitted in Advanced Functional Materials.

5. **Aniruddha Nag *et al.*** "Synthesis of high-performance novel structure bio-based copolymer poly(benzimidazole-*co*-benzamide) using bioderived monomers" (*in preparation*).

Related publications:

1. Mohammad Asif Ali, Nupur Tandon, **Aniruddha Nag**, Kenji Takada, "Molecular Orientation of Bio-Polyamides After Cryogenic Nanohybridization with Montmorillonites" *Arab. J. Sci. Eng.*, 2018, 44(1), 153-158.

2. Yukie Kawasaki, **Aniruddha Nag**, Hajime Minakawa, Shunsuke Masuo, Tatsuo Kaneko, Naoki Takaya, "Novel polycondensed biopolyamide generated from biomass-derived 4-aminohydrocinnamic acid" *Appl. Microbiol. Biotechnol.*, 2018, 102(2), 631-639.

3. Mohammad Asif Ali, Hiroshi Shimosegawa, **Aniruddha Nag**, Kenji Takada, Tatsuo Kaneko, "Synthesis of thermotropic polybenzoxazole using 3-amino-4-hydroxybenzoic acid" *J. Polym. Res.*, 2017, 214(24).

Patents:

Japanese patent applied (Patent application reference number: **18-0628**)

Conferences:

Oral presentations:

1. "Novel Molecular Designing of High-Performance Bio-Based Polybenzimidazole to Prepare Single-Ion Conducting Solid Polymer Electrolyte." **Aniruddha Nag**, Mohammad Asif Ali, Raman Vedarajan, Noriyoshi Matsumi, Tatsuo Kaneko. Materials Research Society spring meeting, 2019, Phoenix, Arizona, USA. April 22-26, 2019.
2. "Novel molecular modification of bio-based polybenzimidazole to obtain single ion conducting polyelectrolyte." **Aniruddha Nag**, Md. Asif Ali, Raman Vedarajan, Noriyoshi

Matsumi, Tatsuo Kaneko. 67th Symposium on Macromolecules, University of Hokkaido, Sapporo campus, Japan. September 12-14, 2018.

3. "Novel bio-based solid polymer electrolyte with stable interfacial properties." **Aniruddha Nag**, Mohammad Asif Ali, Raman Vedarajan, Noriyoshi Matsumi, Tatsuo Kaneko. 10th international conference on modification, degradation and stability of polymer (MoDeSt 2018) at University of Tokyo, Tokyo, Japan. September 2-6, 2018.
4. "Solid electrolytes for next generation Li batteries." Tatsuo Kaneko, **Aniruddha Nag**, Raman Vedarajan, Noriyoshi Matsumi. Invited talk at ARCI and IIT Madras, Chennai, India, July 18-19, 2018.
5. "Novel bio-molecular design of N-boronated polybenzimidazole with single ion conductivity." **Aniruddha Nag**, Mohammad Asif Ali, Raman Vedarajan, Noriyoshi Matsumi, Tatsuo Kaneko. 255th ACS National meeting, New Orleans, Louisiana, USA, March 18-22, 2018.
6. "Syntheses of bio-derived polybenzimidazoles using renewable starting material 3-amino-4-hydroxybenzoic acid." **Aniruddha Nag**, Md. Asif Ali, Seiji Tateyama, Tatsuo Kaneko. 66th SPSJ annual meeting, May 29-31, 2017, Makuhari Messe, Chiba, Japan.
7. "Synthesis of high performance polybenzimidazoles and their application for polymeric ionic conductor". **Aniruddha Nag**, Md. Asif Ali, Seiji Tateyama, Tatsuo Kaneko. EcoDePS 2016, Dec 7, University of Tokyo, Japan.

Poster presentations:

1. "Syntheses of high-performance bio-based plastics from 3-amino-4-hydroxybenzoic acid and their applications." **Aniruddha Nag**, Md. Asif Ali, Maninder Singh, Tatsuo Kaneko. JAIST Japan-India symposium, JAIST, Japan, 7th March, 2019.
2. "Novel molecular designing of high-performance bio-based polybenzimidazole to prepare single-ion conducting solid polymer electrolyte." **Aniruddha Nag**, Mohammad Asif Ali,

Raman Vedarajan, Noriyoshi Matsumi, Tatsuo Kaneko 14th IUPAC International Conference on Novel Materials and their Synthesis (NMS-XIV), Guangzhou, China, 21-26 October, 2018.

3. "Molecular modification and application of bio-based polybenzimidazole as stable polymer electrolyte." **Aniruddha Na**g, Mohammad Asif Ali, Raman Vedarajan, Noriyoshi Matsumi, Tatsuo Kaneko. 10th international conference on modification, degradation and stability of polymer (MoDeSt 2018) at University of Tokyo, Tokyo, Japan. September 2-6, 2018.
4. "Preparation of various polybenzimidazole copolymer plastics using renewable 3-amino-4-hydroxybenzoic acid." **Aniruddha Nag**, Mohammad Asif Ali, Makoto Watanabe and Tatsuo Kaneko. JSPS symposium Universiti Sains Malaysia, Penang, Malaysia. July 8-11, 2018.
5. "Novel synthetic pathway for polybenzimidazole electrolytes with single ion conductivity". **Aniruddha Nag,** Mohammad Asif Ali, Raman Vedarajan, Noriyoshi Matsumi, Tatsuo Kaneko. 16th International Symposium on polymer electrolyte (ISPE-16). Yokohama, Japan, June 24-29, 2018.
6. "Ultrahigh heat-resistance polybenzimidazole/polyamide from Streptomyces-derived biomonomers." **Aniruddha Nag**, Mohammad Asif Ali, Tatsuo Kaneko. 255th ACS National meeting, New Orleans, Louisiana, USA, March 18-22, 2018.
7. "Ultrahigh heat-resistance polybenzimidazole/polyamide derived from *Streptomyces sp.*" **Aniruddha Nag**, Mohammad Asif Ali, Kenji Takada, Tatsuo Kaneko. Eocmaterials symposium, March 1, 2018, Tokyo, Japan.
8. "Preparation of polybenzimidazoles (PBI) using bio-based starting material and its modification to prepare ionic conductive material." **Aniruddha Nag**, Mohammad Asif

Ali, Noriyoshi Matsumi, Raman Vedarajan, Tatsuo Kaneko. 66th SPSJ annual meeting, May 29-31, 2017, Makuhari Messe, Chiba, Japan.

9. "Preparation of polybenzimidazoles (PBI) using bio-based starting material and its modification to prepare ionic conductive material." **Aniruddha Nag**, Mohammad Asif Ali, Noriyoshi Matsumi, Raman Vedarajan, Tatsuo Kaneko. 6th International Conference on Bio-based polymer (ICBP), May 14-17, 2017, Yuan-Ze University, Taiwan.
10. "Syntheses of bio-based polybenzimidazoles with ionic side groups and their ion-gel preparation." **Aniruddha Nag**, Md Asif Ali, Seiji Tateyama, Raman Vedarajan, Noriyoshi Matsumi, Tatsuo Kaneko.11th International gel symposium. March 7-9, 2017, Nihon University, Chiba, Japan.
11. "Synthesis of High-performance polybenzimidazoles from bio-based starting materials and preparation of ion-gel". **Aniruddha Nag**, Md. Asif Ali, Seiji Tateyama, Noriyoshi Matsumi, Tatsuo Kaneko. 11th SPSJ International Polymer Conference 2016. Dec 13-16, 2016, Fukuoka international convention center, Fukuoka, Japan.
12. "Synthesis of high performance polybenzimidazoles and their application for polymeric ionic conductor". **Aniruddha Nag**, Md. Asif Ali, Seiji Tateyama, Tatsuo Kaneko. EcoDePS 2016, Dec 7, University of Tokyo, Japan.

Awards:

1. **Doctoral Research Fellowship (DRF)** (full time researcher) from July 2016-June 2019 in Japan advance institute of science and technology.
2. **Outstanding performance award** on behalf of the oral and poster presentation in Eco Design · Products & Services Symposium (EcoDePS) 2016.
3. **JAIST foundation research grant** for conference presentation (ICBP, 2017, Taiwan).

4. **"The 10th international conference on modification, degradation and stabilization of polymers (MoDeSt 2018)"** selected the presentation as the winner of "**MoDeSt grant"** and waive off the registration fees.
5. **Excellent Poster Prize** in 14th IUPAC international conference on Novel Materials and their synthesis (NMS-XIV), Guangzhao, China 2018.
6. **JAIST President Award** *for the social service* activities and others in 2018.
7. "Ionic modification of polybenzimidazole" research was show-cased on the **front cover page in J. Mater. Chem. A (2019).**

Acknowledgement

This research entitled “Syntheses of high performance bio-based polybenzimidazoles and their electrical applications” was performed at Energy and Environment area, Graduate School of Advanced Science and Technology, Japan Advanced Institute of Science and Technology (JAIST), in the time period of July 2016 to June 2019. The research was financially supported by Japan Science and Technology, under the project: CREST (JPMJCR13B3), Japan Science and Technology (JST).

I would like to express my sincere gratitude to ***Professor Tatsuo Kaneko*** of JAIST for his continuous guidance, suggestions, constructive criticism and kind support throughout my doctoral course. His motivating and Co-operative nature helped me to work freely and broaden the research scope in various fields. The accomplishments during my Ph. D study would not be possible without his encouragement and valuable suggestions.

I would like to convey my grateful acknowledgement to ***Professor Noriyoshi Matsumi*** for giving me an opportunity to carry out the experiments in his laboratory and his valuable research guidance without that this study wouldn’t be completed.

I am also thankful to ***Professor Tetsu Mitsumata*** in Niigata University for letting me to do research in his laboratory and performing some of the valuable measurements, which were included in this thesis and minor research dissertation.

I am also grateful to ***Professor Kohki Ebitani*** and ***Professor Toshiake Taniike*** for their valuable guidance as my second research supervisor in JAIST. Discussions and suggestions from them helped me a lot throughout the pathway of completing my thesis.

I would like to express my appreciation to the reviewers ***Professor Noriyoshi Matsumi***, ***Professor Toshiake Taniike*** and ***Professor Hideyuki Murata*** of JAIST and ***Professor Tetsu Mitsumata*** of Niigata University for their assistance to complete my thesis.

My special thanks to ***Dr. Maiko Okajima*** for her kindness and her efforts and concerns, which helped me to complete my academic research and leading healthy and smooth life in JAIST.

I would also like to thank our previous ***Asst. Professor Seiji Tateyama*** and presently ***Asst. Professor Kosuke Okeyoshi*** and ***Asst. Professor Kenji Takada*** for their valuable suggestions time to time.

I would like to give my sincere thanks to Dr. Mohammad Asif Ali, Dr. Sumant Dwivedi, Dr. Maninder Singh and Dr. Amit Kumar for their support and help. Moreover, I am grateful to my other lab mates both present and previous, Dr. Siqian Wang, Dr. Kittima Amornwachirabodee, Mrs. Thawinda Kongprathet, Mr. Yin Hongrong, Ms. Kulisara Budpud, Mr. Zhong Xianzhu, Mr. Noda Takumi, Mr. Yasuyoshi Funahashi, Mr. Han Qiang, Mr. Yuki Kawashita, Mr. Takuya Kobayashi, Mr. Hiromasa Shinagawa, Ms. Miki Yamashita, Mr. Zhang Shuo, Ms. Miwa Ochi, Mr. Takuma Iwasaki, Mr. Takuya Kumakura, Mr. Yoshiya Tonomura, Mr. Toyochiro Harimoto and previous students, Mr. Yusuke Mori, Mr. Makoto Watanabe, Mr. Masaki Inagaki and Yohei Yoshinaka for sharing and helping me throughout my doctoral study. My special thanks to Ms. Gargi Joshi for all her help, and I wish her all the best for her doctoral degree at the same time with me. Apart from all of my Indian friends who are also students and researchers in JAIST, I am also thankful to Ms. Sonali Bhakta and Dr. Iffat Tasnim Haque Awreen for being there beside me during all the time in JAIST.

Also, in my family, I am thankful to my elder sister *Mrs. Susmita Nag Dutta*, Brother-in-law *Mr. Debkumar Dutta* and nephew *Samadrita Dutta* for all of your support and love to me.

Finally, I am grateful to my mother *Mrs. Suktara Nag* for showing ultimate mental strength and support to me alone after passing away of my father *Late Sreemanta Kumar Nag*. I believe in the strength of my parents blessings and without that, this research wouldn't be possible.

March 2019 **Aniruddha Nag**

Japan Advanced Institute of Science and Technology